UNDERSTANDING METAL NANOCLUSTERS THROUGH ULTRAFAST AND NONLINEAR SPECTROSCOPY

by

Sung-Hei Yau

A dissertation submitted in partial fulfillment
of the requirements for the degree of
Doctor of Philosophy
(Chemisty)
in the University of Michigan
2013

Doctoral Committee:

Professor Theodore Goodson III, Co-Chair
Professor Eitan Geva, Co-Chair
Professor Raoul Kopelman
Associate Professor Angela Violi

DEDICATION

To my family and Fangting Yu, for providing everything I need to reach this day.

ACKNOWLEDGEMENTS

My PhD was an unexpected journey, with countless individuals who have impacted me in profound ways along the way. This has been one of the most exciting adventure in my life and I feel truly blessed to have come this far. I want to thank my parents for providing the opportunity for me to study in the US. This opportunity was sought with great sacrifices and compromises. Being in different cultures, my education was built upon many different schools and teachers. In particular, my days at St. Francis Xavior College (Middle School under United Kingdom system) and Plainview-Old Bethpage John F. Kennedy High school have been the most rewarding. Special thanks to Ms. Bess Eliav, who was my chemistry teacher in high school. She encouraged me to challenge myself in chemistry and provided the support I needed to excel. I would also like to also thank all the teachers that have supported me on the various subjects; it is through the accumulation of knowledge from the various disciplines that defines who I am today. I have spend close to a decade at the University of Michigan, both in my undergraduate and gradate study. I will always be a wolverine. During my undergraduate days, I was fortunate enough to meet Professor Theodore Goodson III, who later became my advisor. It was Prof. Goodson's enthusiasm that attracted me to physical chemistry and it was his encouragement that inspired me to work on this project, and it was his wisdom and support that propelled me to accomplish my work. In addition my committee Prof. Eitan Geva, Prof. Raoul Kopelman and Prof. Angela Violi have provided excellent insights along the way. Additionally, Prof. Ramakrishna Guda and Dr. Oleg Varnavski have been essential in providing the training and guidance I needed for this study. I would like to thank my good friends Jason Chen and Jonathan Chang and their families for helping me getting adjusted to the US. Finally I would like to thank Fangting Yu for giving me love and support for the past 3 years and beyond.

TABLE OF CONTENTS

LIST OF FIGURES

Chapter 1

Introduction

1.1 A Brief History of Metal Nanosystem Physics

Metal nanomaterials (colloids) have been the interest of material scientists and physicists since the introduction of Mie theory more than 100 years ago. The advancement in the synthesis and characterization of metal nanosystems in the past 20 years lead to a rapid expansion in the understanding and application of these materials. [1–6] The intense interest in nanosystems is further fueled by the numberous applications of theses materials, such as their catalytic properties, their application in cancer diagnostics, molecular electronics and photonics.[1–5,7–13] Additionally, metal nanosystems offer new insight into different areas of chemistry and physics, such as the size-induced metal-insulator transition (quantum size effect).[4,14,15] Metal nanosystems presents a unique opportunities to investigate fundamental laws of science that have yet to be understood.[4,14–18]

In order to fully present the properties of metal nanosystems, it is important to extract principles from both bulk metal and molecular systems. Quantum size effect is well known in semi-conductor physics. Figure 1 presents the electronic properties of different systems and their relations to size.[14,19] Bulk metals are very common in everyday life, and they can be defined as systems with sizes that are larger than the wavelength of the external electromagnetic field.[20] Bulk metals can be described electronically by classical electronics.[6,14,19] The electron distribution and their energy levels can be described in Figure 1 (left side) by the occupied (black color) and unoccupied (white) states. The occupied electronic levels are very closely packed whcih allows for electronic transitions

between levels freely, known as the "sea of electrons" or bands. The outer most energy level for metal is known as the Fermi energy (E_F), which has an energy value that corresponds to the ejection of an electron at zero Kelvin. At the very small sizes are insulators or molecular systems, which have very quantized energy levels. The electrons in a molecular system are confined to a particular energy level, and can be described by quantum mechanics.[14,15]

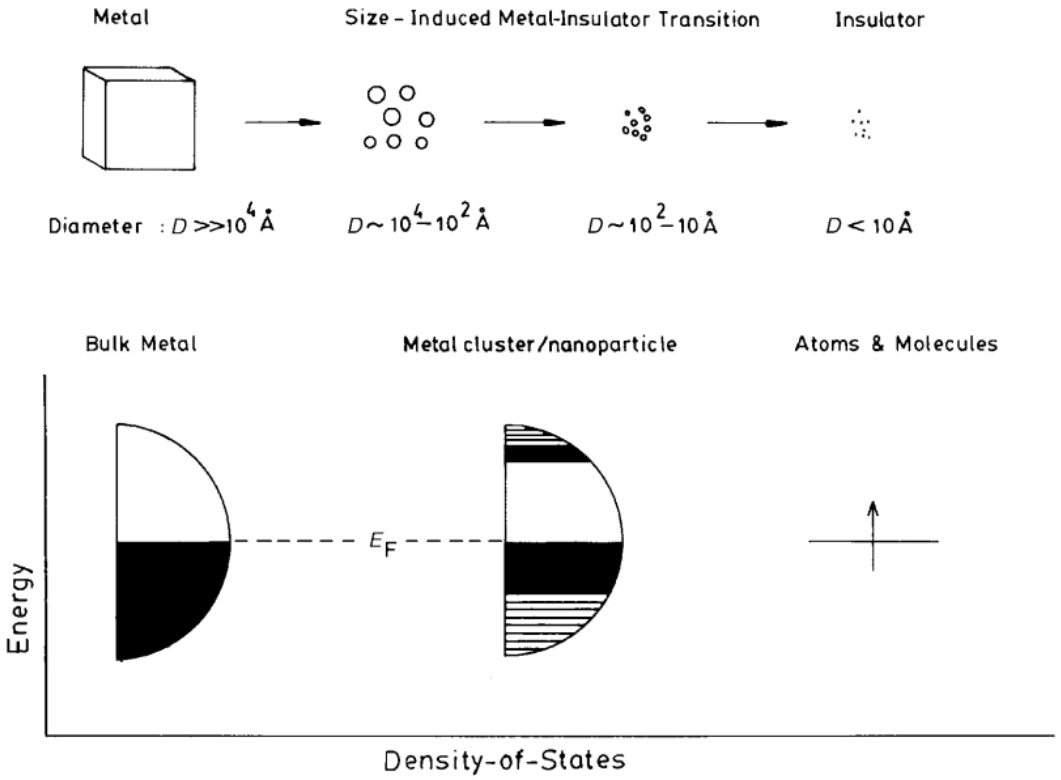

Figure 1.1 General overview of the size-induced metal-insulator transition[14]

Metal nanosystem research started with investigations into metal colloids in the 1900's. Research emphasis was placed on their optical properties.[23,32–36] It was not until later that these colloids were identified as nanoparticles. The work by Gustov Mie started modeling nanoparticles by solving the Maxwell equation for light interaction with gold nanoparticles.[23] Later work on the band theory for metals further explained the physical nature of the optical excitation of gold nanoparticles.[36] In the earlier stages of metal nanosystem research, nanoparticles (sizes up to 100 nm) are the major focus.[2,7,8,37–41] There are many different types of metal nanoparticles, with gold based systems being the

focus of many investigations. [1,3,6,12,25,42] Gold nanoparticles offer a few advantages, namely their higher stability and their application in catalysis.[6,8,42–44] It is interesting to note that for metal nanoparticles, the electronic properties are dictated by their sizes and shapes.[1,18,24,25,45–47] The tunable size of metal nanosystems offers the possibility of a wide range of applications, including molecular electronics,[2,11,25–27] image markers[9,29] and catalysts[7]. One of the major differences between nanoparticles and bulk metal is the emergence of a strong dipolar surface plasmon resonance (SPR) in the visible region.[7,14,28,31,48,49] The SPR is caused by the collative oscillation of the metal valence electrons, unique for nanoparticles. Mie theory and its extensions can predict with good agreement the wavelength of the SPR in the absorption spectrum (detailed in sec 1.2 and chapter 3, 4). SPR offers strong electric field localized in an area (known as the lighting rod effect) and can be used to enhance the fluorescence of organic dyes.[49] The use of SPR is the major driving force in the field of plasmonics and has many applications in bio-imaging.[9,19,31,50–52]

1.2 Metal Systems in the Gas Phase

Investigations into smaller metal systems started in the gas phase which focused on metals like aluminum, sodium, gallium and others.[31–38] Gas phase metal systems are produced by heating the bulk metal to produce atomic vapor, which contains metal dimmer, trimer and larger particles.[31,38] Mass spectrometry of these metal systems reveal that the electronic structure of clusters appeared to reflect that of a spherical potential well.[31,38] For metal ions with a single electron (i.e Na+), clutters are formed at 2, 8, 20, etc which follows the same trend as electron shell closings (also known as the spherical potential well). The spherical potential well explains the specific system sizes and the higher stability. These metal nanosystems were later named “magic clusters”, due to their high stability and specific sizes.[31,38] At the time, there were many different models that describe the stability and electronic properties of the magic clusters. One of these models is the jellium model,[39,40] which assumes a uniformly positively charged sphere filled with an electron gas. However, the theoretical treatment of the electron gas is not trivial. The Jellium model suggests a confined electron gas for nanosystems, and predicts electronic properties of clusters, such as the Mie Plasmon.[6,31,39] To provide a simpler model to

explain many experimental results, the close shell model was developed.[31,41,42] The close shell model considers the valence electrons in clusters as being independent from the atom but the electrons are confined in a spherically symmetric potential well. The use of a spherical potential well is a good assumption, because the nanoclusters appear to be spherical at the cluster sizes. The symmetry of the system assumes that the valence electrons successively fill the degenerate levels, and the stability of the magic clusters comes from the systematic shell closing. The idea is reflected directly in the case of sodium clusters with its one valence electron and shell closing at 8, 20, 40 and others.[31] Larger stable systems were found experimentally but they do not follow the shell closing trend.[43] The development of a new model is necessary. Using basic idea from Clemenger and Nilsson, a new model was developed based on the simple close shell model.[31,42] The Ellipsoidal Shell Model (or the Clemenger-Nilsson Model) takes the same basic assumption as the close shell model but treats the electrons using basic quantum chemistry.[31,42] The model assumes a simple Hamiltonian for a electron in a single-particle three-dimensional harmonic oscillator (equation 1.1).

Equation 1.1 $$H = \frac{p^2}{2m} + \frac{m\omega_0^2 q^2}{2} - Uh\omega_0\left[l^2 - n(n+3)/6\right]$$

The p and q term in the Hamiltonian are single-electron momentums and coordinate operators respectively. l is the angular momentum. n is the shell number and the third term of the Hamiltonian is the anharmonic correction for larger systems, which is mostly ignored for clusters. Equation 1.4 shows the form of the potential U.

Equation 1.2 $$U(r) = -\frac{U_o}{\exp[(r - r_o)/\varepsilon] + 1}$$

U_0 is the sum of the Fermi energy and the work function. r_0 is the effective radius. ε determines the variation of the potential at the edge of the sphere. The eigenvalue for the ellipsoidal model can be solved (equation 1.3).

$$\textbf{Equation 1.3}\quad E_n = h\omega_o\left\{\left(n+\frac{3}{2}\right)-U\left[l^2-n(n+3)/6\right]\right\}$$

In order to account for non-spherical systems, the ellipsoidal shell model factors in a fixed volume, with the cluster shape adjusted to minimize the total electronic energy. The shape consideration can be represented by equation 1.4 where the R_x,R_y and R_z are the semiaxes of the ellipsoid. n_x, n_y, and n_z are the harmonic-oscillator quantum number.

$$\textbf{Equation 1.4}\quad E(n_x,n_y,n_z)=h\omega_0\left\{(n_x+\frac{1}{2}\}\frac{R_0}{R_x}+(n_y+\frac{1}{2}\}\frac{R_0}{R_y}+(n_z+\frac{1}{2}\}\frac{R_0}{R_z}\right\}$$

The ellipsoid model has been used for metal clusters in the gas phase and is consistent with experimental results.[41] For larger nanoparticle systems, Mie theory can predict SPR with a high accuracy (see section 1.3). Even though these gas phase studies provided interesting insight the interactions of metal atoms, these systems only exist in a vacuumed environment, which limits their applications. The various models used for these gas phase systems can be directly used in condensed phase systems, and provided a strong theoretical frame work.

1.3 Metal Nanoparticles and Nanoclusters in the Condensed Phase

The synthesis of metal nanosystems in the condensed phase (solutions) produced different sets of materials compared to the gas phase. Condensed phase synthesis produces larger systems such as nanoparticles before the discovery clusters. Nanoparticles offer many interesting properties and it is where the majority of the previous optical and detailed electronic characterization has been focused on. [10,12,28,44–48] Studies on nanoparticles in the condensed phase can be well explained by the Mie theory (and its extensions).[20,41,42,49] The models assume that electrons can be confined in a area, similar to the Jellium model. An external field can be applied to the system which causes the separation of its charges. When the field is removed, the system will return to equilibrium which causes an oscillation of its electric field. The frequency of this

oscillation is known as the Mie resonance frequency (ω_M^2), which is a function of the total charge (Q) and the valence electron mass (M_N)(equation 1.1). α is the polarizability of the system. The frequency which the Mie oscillation is self sustaining is the Surface Plasmon Resonance (SPR) which is widely used in the field of plasmonics..[31,41,42,49–52]

$$\textbf{Equation 1.5}\ \omega_M^2 = \frac{Q^2}{M_n \alpha}$$

Using the Mie theory model, the absorption cross section can be calculated with equation 1.2 where N is the number of electrons (a substitute of Q) and the mass of the electron m_e (a substitute of M_N), and introduces a damping factor Γ. This model is an extension on the work by Mie[20,41] and produces absorption spectrum with an excellent agreement to the observed results, especially the intensity and the λ_{max} of the SPR. [41]

$$\textbf{Equation 1.6}\ \sigma = \frac{4\pi {N_e}^2}{3 m_e c} \frac{\omega^2 \Gamma}{(\omega^2 - \omega_M^2)^2 + (\omega\Gamma)^2}$$

While the SPR from nanoparticles are interesting, we are more interested in extending the nano-tool box to an even smaller scale, where the system sizes are smaller than 2 nm. What are the motivations to study these ultra small systems? At 2 nm, the system size approaches the Fermi wavelength of an electron (~2nm), which is the De Broglie wavelength of an electron at the Fermi-level. This size limited is similar to the size-induced metal insulator transition.[14,19,53,54] Using a basic particle-in-a box model to exaime nanoclusters, this special wavelength limit can be derived from the free electron mode,[1] which is analogous to the close shell model for gas phased clusters (see pervious section). While the close shell model focuses on explaining the stability of the "magic" nanoclusters, the free electron model investigates the HOMO-LUMO gap for spherical systems at room temperature.[1,19] For bulk metal, their electronic structure can be characterized by a continuous density of states through the Fermi energy, and electrons are freely transported between the valence band and the conduction band, the lack of a HOMO-LUMO gap give rise to the electronic properties in bulk metals.[14,19,53,54].

The free electron model uses the simple particle in a box model to calculate the energy of the 6s (valence) electrons for gold and silver. Supposing there are N electrons in a volume a^3, the Schrödinger equation can be simplified into the general form in equation 1.7 which can be solved into three dimensions in the Cartesian coordinates, with eigenvalues En in equation 1.8. $n^2 = n_x^2 + n_y^2 + n_z^2$.

Equation 1.7 $$\mathrm{H}\Psi = \left(-\frac{h^2}{2m}\nabla^2 + V \right)\Psi = E\Psi$$

Equation 1.8 $$E_n = \frac{\pi^2\hbar^2}{2ma^2}n^2$$

The principle quantum numbers n_x, n_y and n_z are integers, and assuming a sphere with radius n, the energy states should be distributed on the spherical surface. This treatment of the electron in a spherical surface is the same as the close shell model used for sodium nanoclusters.[1,31] The number of energy states (N') can be represented by the volume of the sphere. Since the principle quantum numbers are only positive, only 1/8of the n-space is considered and equation 1.8 can then be rewritten as equation 1.9.

Equation 1.9 $$N' = \frac{\pi}{6}\left(\frac{2ma^2}{\pi^2\hbar^2} \right)^{\frac{3}{2}} E^{\frac{3}{2}}$$

The spacing of the electron energy levels (δ) can be represented by the reciprocal of the density of state (the derivative of equation 1.9). The spacing of the electron energy level is shown in equation 1.10.

Equation 1.10 $$\delta = \frac{4\pi^2}{a^3}\left(\frac{\hbar^2}{2m} \right)^{\frac{3}{2}} E^{-\frac{1}{2}}$$

The energy spacing between the electron energy level can be related to conductivity (or the transport of electrons) in three different cases, which is the SIMIT parameters, known as the Kubo criterion.[19,54] For energy spacing (δ) that is much smaller than the thermal energy (k_BT, 0.0256eV) at room temperature, the material is a metal. While insulating particles have δ that is larger than the thermal energy, and molecules have δ that is much larger than the thermal energy. Applied to the case of nanoclusters, the critical size of electronic energy quantization can be calculated when δ is equal to k_BT, and using a Fermi level of 5.5 eV for gold. The resulting size is a ~1.7 nm sphere, very close to the experimental observation of 2 nm size of nanoclusters. The significance of this result is that using a very simple quantum model, we can estimate the size when the energy levels of the system are quantized under room temperature conditions. The quantization of the energy levels is characteristic of nanoclusters, thus the 2 nm size also defines the separation of nanocluster and nanoparticles. The quantization of energy level would predict that energy levels are sufficiently spaced to allow visible energy transition and non-radiative dissipative pathways between the closely-spaced energy levels are mostly eliminated.

It is worth mentioning that nanoclusters are very different than metal networks, where usually only 2-3 metals atoms are connected. Metal networks have been extensively studied in inorganic chemistry, but metal networks are atomic in nature and they are different then metal clusters, where the system can be as big as 144-309 metal atoms.[24]

Small metal "magic" clusters have been studied in the gas phase extensively (section 1.2). It was not until the discovery of these smaller systems (figure 1.2) in the condensed phase that leads to the expansion of current studies. There many different ways to achieve metal systems on the nanocluster scale. Tomalia et. al. first reported the synthesis of smaller metal particles in the context of making dendrimer metal nanocomposites where the size of the nanoparticles and nanoclusters are controlled by the dendrimer opening.[55–57] It was later found that dendrimer-captured nanoclusters have interesting optical limiting and time-resolved optical properties, as well as their

applications in catalysis.[11,44,55,58] Building on the promising work of Tomalia, the search for even smaller metal particles made utilizing the dendrimer PAMAM were reported by Crooks et. al. and Chandler et. al.[58–61] Bauer et. al. at NIST utilized a G9 dendrimer and reported a nanocluster of ~1 nm.[62,63] Dendrimer-captured nanoclusters represent a highly stable system with clear size control, but the complete characterization of the metal core was not available, due to the stability of the core without the dendrimer is poor. Optical studies conducted on these dendrimer nanoclusters suggested for the first time that the emission (fluorescence) mechanism might vary depending on the size of the metal nanosystems. Major differences between nanoparticles and nanoclusters were also reported for the first time.[44,55] Besides dendrimer capture, another major synthetic approach uses ligand protection to produce a stable metal-ligand system. This ligand protected approach was demonstrated by the Schmid group, yielding nanoclusters approaching the 1 nm size.[7,64] Subsequent progress in the synthetic methods by the Burst group has lead to well-isolated gold nanoparticles and nanoclusters of various distinct sizes.[8,65–67] The Brust approach also allows nanoclusters to be made in large quantities in the condensed phase,[8,65–67] and the Brust synthesis has since beome the foundation for synthetic development of nanoclusters. In brief, the synthesis uses a ligand (usually alkanethioltes, arylthiolate or glutathione) and metal salt in a strong reducing environment, by adding $NaBH_4$. The ligand serves to regular and stabilize cluster formation from metal salt in solution.[1,32,68–71] Because of the self-assembly nature of nanoclusters, single size metal nanoclusters can be made in large quantities, under optimized conditions.[1,71–75]

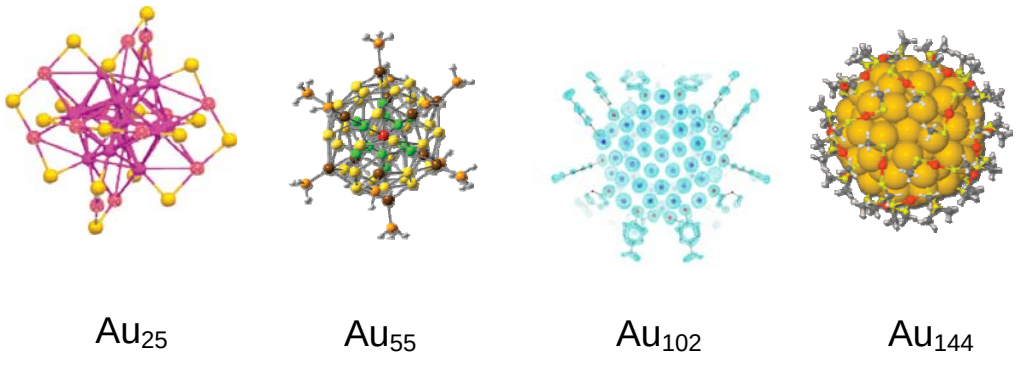

Figure 1.2 Gold nanoclusters of various sizes. [6,30,93,94]

One of the biggest hurdles in the advancement of nanomaterials research is the identification of the exact metal core composition and the fine details in the ligand binding.[78–81] Unlike metal networks, where 1-2 metal atoms are connect to an organic frame work, nanoclusters cannot be conventional techniques such as nuclear magnetic resonance (NMR) or Infrared (IR) spectroscopy.[78–81] Various characterization techniques will be discussed in chapter 2. Overall, it has been identified that nanoclusters synthesized through Brust synthesis contain one single layer of ligand shell, and was later named Mono-layered Protected Clusters (MPC).[79,80,82,83] MPCs are generally considered to have two separate parts: a metal core and a single layer ligand shell. As mentioned before, gold is the major candidate for nanocluster studies because it can be synthesized in large scale with high purity and stability.[72,80,84] Crystallography of gold nanoclusters leads to the total characterization of $Au_{25}(SG)_{18}$ and $Au_{102}(SR)_{44}$. [27,76]

It is critical to understand the metal-thiolate bond and the metal core packing, which will provide important structural details to further the understanding and model of nanoclusters. In particular, the modeling of the electronic state from structural information is essential to understanding the optical properties observed. The structure of gold nanoclusters was first proposed by Schmidt.[7] At that point, the spherical potential well of clusters was not yet developed, so Schmidt's model focused on basic packing and the geometry of the nanoclusters. This idea (or the full shell model) was adopted from Xe in the gas phase, and did not consider the electronic effects due to the lack of valence electrons from Xe.[7,64,85] The full shell model is based on the idea that there is a basic core unit of gold nanocluster and the stable sizes are the result of expansion of the existing shell motif. In the case of gold nanoclusters, twelve atoms surround a central atom, forming a 13 atom cluster The shell is packed with the icosahedra motif, and face center cubic motif for nanoparticles (figure 1.5).[7] The calculations of atom numbers of the cluster with subsequent additional shell is shown in equation 1.9, where n is the shell number (equation 1.9). This model predicted many observed core sizes, such as Au_{13} and Au_{55} and Au_{147}. However this model does not give direct evidence of the origin of the packing beside physical compactness nor does it predict any physical or optical behavior.

The large numbers of electrons from gold systems are also ignored, but it is quickly addressed in following models.

$$\textbf{Equation 1.9}\ Core\_atom\_number = 10 * n^2 + 2$$

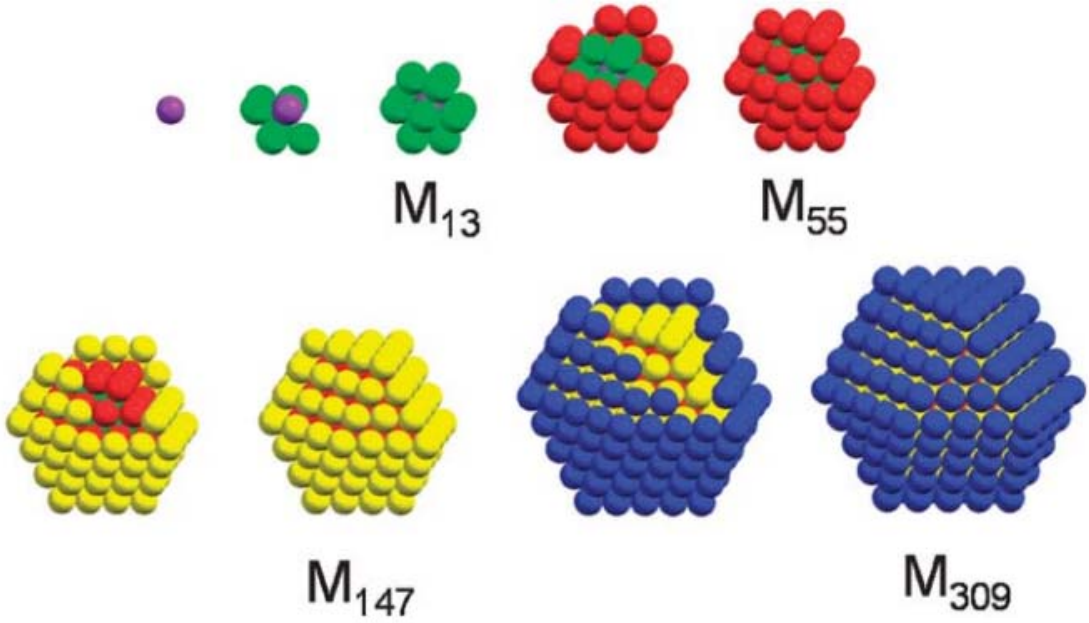

Figure 1.3 *The* Full shell model of gold nanoclusters, with a 13 metal core in an icosahedra packing. The subsequent shell closing gives 55, 147 and 309 metal cores.[7]

Since the full shell model cannot explain the photo-physical observations of nanoclusters, the community at large turn to the Jelliem model (or the Kubo model) to explain nanoclusters.[19,41] The Jellium model treats the nanoclusters as a uniformly positively charged sphere filled with an electron gas. Although this is a good assumption for nanoparticles, it was clear that nanoclusters lack SPR. The lack of SPR is a strong evidence that these nanoclusters are molecular-like, an exact analog to the clusters in the gas phases (section 1.2). It was not until the total structural characterization of $Au_{25}(SG)_{18}$ and $Au_{102}(p\text{-}MBA)_{44}$ using x-ray diffraction crystallography that a more complete modeling of the nanoclusters was developed.[27] Jin and Aikens groups used the crystal structure to model $Au_{25,}$[18,27] whose the metal core is consisted of thirteen atoms surround by a metal-ligand shell (figure 1.6). The 13 atom metal core has the same packing as the one in the full shell model, an icosahedra core. The ligand binds to the outer "shell" gold atoms, leading to the formation of sulfide-gold-sulfide-gold-sulfide

bonds, known as the "staple" motif. Currently, the growth of the staple motif and the nanocluster core is not yet understood.

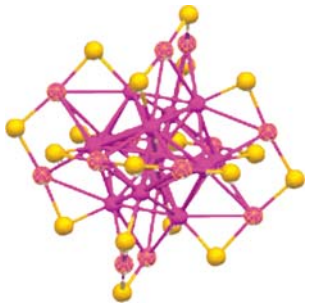

Figure 1.4 Crystal Structure of $Au_{25}(SR)_{18}$[27]

Besides Au_{25}, Au_{102} is also characterized using x-ray crystallography. The structure of Au_{102} is similar to that of Au_{25}, but the center core is not of icosahedra packing, rather it is a D_{5h} Au79 core, surrounded by 23 gold atomes bound to 44 ligands. Although the binding motif is different, the principle of "divide and protect" is realized.[86] The core is charge neutral and is divided from the oxidized metal bound ligand, $Au_{79}[Au_{23}(p\text{-}MBA)_{44}]$. Although the exact structural details of Au_{25} and Au_{102} are different, they share the same core-and-shell structure and they are both considered as a super atom.

While the full shell model can be used to explain the size of some nanoclusters, the crystal structure provides additional information to expand on the models, such as the ellipsoid model.[41] The nanocluster metal core can be treated as one single atom, separated from the ligand-metal outer shell, and the stability achieved for the specific size is not the function of the physical packing or rather the electron shell closing. This model recapitulates the behavior of an atom, thus the meatl core is called a "super atom" The super atom theory takes the Julleium / Kubo model along with the ellipsoid model and applied it directly to the nanocluster.[16] Shell closing can be represented mathematically by equation 1.10 where the shell closing number (n*) is equal to the valence number of the atom ($_{VA}$), multiply by the number of atoms (N) and subtracted by the number of ligand-bonded metal (M) and the overall charge (Z). The shell closing number follows

that of noble gas configuration (2, 8, 18, 34, 58, 92, 138, …). The super atom theory is base largely on the Au_{102} structure but can also be used to explain Au_{13}, and Au_{25}. Based on the crystal structure, density function theory calculation was carried out which revealed that the stability is associated with the creation of a 0.5 eV HOMO-LUMO gap in the case of Au_{102}. It is interesting to note the full shell model and the super atom theory explains the same set of clusters, where one considers the physical packing and the other also considers the electron shell closing. Currently, the super atom theory has not yet been used to explain the non-symmetric systems which leave room for the further development of the theory to include all deformations, like the ellipsoid model.

One of the major differences of MPCs from gas phase system is the use of ligand protection. The success (or the accuracy) of the super atom theory introduces an important for nanoclusters: the metal core is a super atom which is separated from the ligand shell (divide and protect).[16,86]

Equation 1.10 $n^* = Nv_A - M - Z$

When the core is treated as a super atom, many interesting questions arise. One of the most important questions is the division between the super atom and the nanoparticles, which was addressed in detail by our group in the past 10 years. [4,17,26,29,44,55,87,88] In the pervious sections, we highlighted the interest in nanosystems with sizes that approach the Fermi wavelength of an electron.

From the various systems and models presented, it should be clear that MPCs provide a unique opportunity to study metal nanosystems. Where previous gas phase studies provided much useful insight into the fundamental science of metal clusters, MPCs offers a chance to directly study the metal core in the condensed phase. Because of the range of available sizes, quantum confinement effects can be studied. Total characterization of gold nanoclusters provided a good platform for developing more sophisticated models. At the present time, we think that the ellipsoid model provides a very simple and straight-forward approach to explain the stability of nanoclusters and

should be incorporated into the super atom theory. Nevertheless, the super atom theory has explained many of the optical effect observed for gold nanoclusters, and can be extended to include other metal systems. Overall, the advantages of MPCs allow very detailed optical studies on the electronic states. In the following chapters, three different metal nanoclusters are investigated using steady state and ultrafast techniques with a few major focuses: quantum size effect, emission and its mechanism, and comparing systems of different metals. The major aim of this thesis is to uncover the fundamental science of metal nanoclusters through the use of spectroscopy, and to extend the current understanding of these small metal topologies.

1.4 Optical Investigation and Applications

We introduce herein the justification of using various optical techniques to understand MPCs. Detail descriptions of the individual techniques can be found in chapter 3. The treatment of nanoclusters as a super atom suggests that the energy levels for nanoclusters are discrete, which indicates that the nanoclusters should have distinct molecular-like optical properties. Molecular systems have discrete transitions, such as absorption and emission with distinct features, which are not usually observed for bulk metals. The absorption spectrum reveals the major energy transitions and SPR.

Beside absorption, the super atom could possibility emit when excited, due to the discrete energy levels. A major focus on the native emission from metal nanoclusters has been placed on the application of using nanocluster in imaging without the aid of organic dyes, which can theoretically improve the resolution of biological imaging.[10,11,89,90] Demonstrated by many publication (detail in chapter 4 and 5) gold and silver nanosystems are emissive, with fluorescence efficiency 5-6 orders of magnitude higher than their bulk metal counterparts. Moreover, published results have shown that for a series of MPCs, the emission wavelength is size-dependent.[11,24,26,80]

Two-photon absorption is a type of nonlinear optical spectroscopy and it is a third order optical process with a quadratic dependence on the incident radiation. [11,24,26,80]

Detailed description of this process can be found in chapter 3. Briefly, the sample absorbs two photons simultaneously; whose total energy promotes the system to an excited state. For example, two-photons of 800 nm is absorbed simultaneously, which is excited to an excited state with an energy gap corresponding to 400 nm. In my work I measure the emission from the excited state directly. An absorption cross section of the two-photon process can be calculated (chapter 3). The application of fluorescence from gold (or any other metal) particles for medical and imaging applications is immense. The use of one-photon or two-photon excited emission can further improve the resolution in nano (bio) photonics.[8,11,90]

In addition to the techniques described above, I also utilize ultrafast techniques to investigate the electronic properties of nanoclusters. Time resolved fluorescence up-conversion can provide details about the emission process. Additionally, fluorescence up-conversion can detect the polarity dependence of the emission which is often associated with the rotation and flexibility of the molecule. Since MPCs are spherical (symmetric), the fluorescence anisotropy was not investigated. Besides the emission process, excited state dynamics can be investigated by transient absorption, where the excited state dynamics can be resolved by both time and wavelength.

Transient absorption can often resolve energy transfer in the system and other processes such as the electron-electron scattering and electron-phonon relaxation for some nanosystems (detailed in chapter 4).[4,44,47,48] Steady state and ultrafast optical experiments provide a detailed picture of the electronic states and their transitions for metal nanoclusters. Understanding the molecular details could lead to the development of new materials and new applications.

1.5 Dissertation Outline

The remaining body of this dissertation is organized as follows: Chapter 2 will discuss the characterization of metal nanoclusters in detail. A general overview of the various current characterization techniques will be presented. Additionally, gold and

silver systems discussed throughout this thesis will be introduced.. Chapter 3 will discuss the relevant techniques utilized in our investigation. Detailed explanations will be presented for the techniques used, including steady-state spectroscopy, two-photon excited fluorescence, time-resolved fluorescence up-conversion spectroscopy and ultrafast transient absorption. Chapter 4 will discuss the work published in the Journal of Physical Chemistry and Accounts of Chemical Research regarding our work on gold nanoclusters. The main discussion will be centered around the effect of size on the optical properties of metal clusters. This chapter will also discuss quantum confinement effects on clusters. This work is presented based on various optical approaches. A strong emphasis is placed on the emission of gold nanoclusters through time resolved fluorescence up-conversion. A detailed emission mechanism for gold nanoclusters is proposed. A overview of non-linear optical properties of gold nanoclusters will be presented along with optical acoustic vibrations. Chapter 5 will discuss the work related to two silver nanocluster systems: $Ag_{32}(SG)_{19}$ and DNA templated Ag nanoclusters. The work on DNA Ag nanoclusters was published in Nanoscale and the manuscript on Ag_{32} is to be submitted to the Journal of Physical Chemistry. The DNA templated Ag nanocluster is prepared by the Martinez group at the Los Alamos National Laboratory. The work on $Ag_{32}(SG)_{19}$ is based on samples synthesized by the Bigioni lab at the University of Toledo. Detailed analysis of the optical properties will be presented. The question regarding the commonalities of different metal nanoclusters is addressed in Chapter 6. A direct comparison of the silver and gold nanoclusters based on the optical results is the major focus of this chapter. Also, a discussion about the super atomy theory for different metals and its implications will be presented. A new model on the polarization of nanoclusters will be introduced and discussed. This chapter is based largely on the data presented in chapter 4 and 5 with a more in-depth analysis of the data.A summary of this work and its impact on the field of nanoclusters will be presented in Chapter 7 with an outlook of three future directions.

The field of metal nanosystems, including nanoparticles and nanoclusters, is currently experiencing a rapid expansion. The idea of these nanosystems has been around for over 100 years since the first predication by Mie, but it is not until the 20^{th} centry,

when advanced characterization techniques were developed, that scientists started to investigate there systems with confidence. The purity, stability and availability of mono-layered protected clusters allow for unprecedented investigation into the fine details of the electronic properties of these new systems, and provide insights into the transition from bulk to molecular systems. Metal nanosystems were always thought of as nanoparticles and colloids, and it is not until recently that our work demonstrated the differences between nanoparticles and nanoclusters. Nanocluster is a type of new material that is truly different than bulk, nanoparticles and molecular systems, and presents a new frontier that should be explored.

1.6 Reference

Jin, R. Quantum sized, thiolate-protected gold nanoclusters. *Nanoscale* **2010**, *2*, 343–62.

(2) Murray, R. W. Nanoelectrochemistry: metal nanoparticles, nanoelectrodes, and nanopores. *Chemical reviews* **2008**, *108*, 2688–720.

(3) Whetten, R. L.; Price, R. C. Nano-golden order. *Science* **2007**, *318*, 407–408.

(4) Yau, S. H.; Varnavski, O.; Goodson, T. An Ultrafast Look at Au Nanoclusters. *Accounts of chemical research* **2013**.

(5) Pyykkö, P. Theoretical chemistry of gold. III. *Chemical Society reviews* **2008**, *37*, 1967–97.

(6) Schmid, G. The relevance of shape and size of Au55 clusters. *Chemical Society reviews* **2008**, *37*, 1909–30.

(7) Daniel, M.-C.; Astruc, D. Gold nanoparticles: assembly, supramolecular chemistry, quantum-size-related properties, and applications toward biology, catalysis, and nanotechnology. *Chemical Reviews* **2004**, *104*, 293–346.

(8) Pasquato, L.; Pengo, P.; Scrimin, P. Functional gold nanoparticles for recognition and catalysis. *Journal of Materials Chemistry* **2004**, *14*, 3481–3487.

(9) Rosi, N. L.; Mirkin, C. A. Nanostructures in biodiagnostics. *Chemical reviews* **2005**, *105*, 1547–62.

(10) J Lin, C.-A.; Lee, C.-H.; Hsieh, J.-T.; Wang, H.-H.; K Li, J.; Shen, J.-L.; Chan, W.-H.; Yeh, H.-I.; H Chang, W. Synthesis of Fluorescent Metallic Nanoclusters

toward Biomedical Application: Recent Progress and Present Challenges. *Journal of Medical and Biological Engineering* **2009**, *29*, 276–283.

(11) Hicks, J. F.; Miles, D. T.; Murray, R. W. Quantized Double-Layer Charging of Highly Monodisperse Metal Nanoparticles. *Journal of the American Chemical Society* **2002**, *124*, 13322–13328.

(12) Walter, M.; Akola, J.; Lopez-Acevedo, O.; Jadzinsky, P. D.; Calero, G.; Ackerson, C. J.; Whetten, R. L.; Groenbeck, H.; Hakkinen, H.; Grönbeck, H.; Häkkinen, H. A unified view of ligand-protected gold clusters as superatom complexes. *Proceedings of the National Academy of Sciences of the United States of America* **2008**, *105*, 9157–9162.

(13) Varnavski, O.; Ispasoiu, R. G.; Balogh, L.; Tomalia, D.; Goodson, T. Ultrafast time-resolved photoluminescence from novel metal–dendrimer nanocomposites. *The Journal of Chemical Physics* **2001**, *114*, 1962.

(14) Aikens, C. M. Effects of core distances, solvent, ligand, and level of theory on the TDDFT optical absorption spectrum of the thiolate-protected Au(25) nanoparticle. *The journal of physical chemistry. A* **2009**, *113*, 10811–7.

(15) Ispasoiu, R. G.; Balogh, L.; Varnavski, O. P.; Tomalia, D. A.; Goodson, T. Large optical limiting from novel metal-dendrimer nanocomposite materials. *Journal of the American Chemical Society* **2000**, *122*, 11005–11006.

(16) Yau, S. H.; Abeyasinghe, N.; Orr, M.; Upton, L.; Varnavski, O.; Werner, J. H.; Yeh, H.-C.; Sharma, J.; Shreve, A. P.; Martinez, J. S.; Goodson, T. Bright two-photon emission and ultra-fast relaxation dynamics in a DNA-templated nanocluster investigated by ultra-fast spectroscopy. *Nanoscale* **2012**, *4*, 4247–54.

(17) Ramakrishna, G.; Bhaskar, A.; Goodson III, T. Ultrafast excited state relaxation dynamics of branched donor-pi-acceptor chromophore: Evidence of a charge-delocalized state. *Journal of Physical Chemistry B* **2006**, *110*, 20872–20878.

(18) Ramakrishna, G.; Varnavski, O.; Kim, J.; Lee, D.; Goodson, T. Quantum-sized gold clusters as efficient two-photon absorbers. *Journal of the American Chemical Society* **2008**, *130*, 5032–3.

(19) Goodson, T.; Varnavski, O.; Wang, Y. Optical properties and applications of dendrimer-metal nanocomposites. *International Reviews in Physical Chemistry* **2004**, *23*, 109–150.

(20) Ramakrishna, G.; Dai, Q.; Zou, J.; Huo, Q.; Goodson III, T. Interparticle electromagnetic coupling in assembled gold-necklace nanoparticles. *Journal of the American Chemical Society* **2007**, *129*, 1848–+.

(21) Varnavski, O.; Ramakrishna, G.; Kim, J.; Lee, D.; Goodson, T. Critical size for the observation of quantum confinement in optically excited gold clusters. *Journal of the American Chemical Society* **2010**, *132*, 16–7.

(22) Devadas, M. S.; Kim, J.; Sinn, E.; Lee, D.; Goodson, T.; Ramakrishna, G. Unique Ultrafast Visible Luminescence in Monolayer-Protected Au 25 Clusters. *The Journal of Physical Chemistry C* **2010**, *114*, 22417–22423.

(23) Mie, G. Beiträge zur Optik trüber Medien, speziell kolloidaler Metallösungen. *Annalen der Physik* **1908**, *330*, 377–445.

(24) Varnavski, O.; Ramakrishna, G.; Kim, J.; Lee, D.; Goodson, T. Optically excited acoustic vibrations in quantum-sized monolayer-protected gold clusters. *ACS nano* **2010**, *4*, 3406–12.

(25) Chen, S. Gold Nanoelectrodes of Varied Size: Transition to Molecule-Like Charging. *Science* **1998**, *280*, 2098–2101.

(26) Ingram, R. S.; Hostetler, M. J.; Murray, R. W.; Schaaff, T. G.; Khoury, J. T.; Whetten, R. L.; Bigioni, T. P.; Guthrie, D. K.; First, P. N. 28 kDa Alkanethiolate-Protected Au Clusters Give Analogous Solution Electrochemistry and STM Coulomb Staircases. *Journal of the American Chemical Society* **1997**, *119*, 9279–9280.

(27) Schaaff, T. G.; Shafigullin, M. N.; Khoury, J. T.; Vezmar, I.; Whetten, R. L.; Cullen, W. G.; First, P. N.; Gutiérrez-Wing, C.; Ascensio, J.; Jose-Yacamán, M. J. Isolation of Smaller Nanocrystal Au Molecules: Robust Quantum Effects in Optical Spectra. *The Journal of Physical Chemistry B* **1997**, *101*, 7885–7891.

(28) Yau, S. H.; Varnavski, O.; Gilbertson, J. D.; Chandler, B.; Ramakrishna, G.; Goodson, T. Ultrafast Optical Study of Small Gold Monolayer Protected Clusters: A Closer Look at Emission †. *The Journal of Physical Chemistry C* **2010**, *114*, 15979–15985.

(29) Wang, G.; Huang, T.; Murray, R. W.; Menard, L.; Nuzzo, R. G. Near-IR luminescence of monolayer-protected metal clusters. *Journal of the American Chemical Society* **2005**, *127*, 812–3.

(30) Zhu, M.; Aikens, C. M.; Hollander, F. J.; Schatz, G. C.; Jin, R. Correlating the crystal structure of a thiol-protected Au25 cluster and optical properties. *Journal of the American Chemical Society* **2008**, *130*, 5883–5.

(31) Devadas, M. S.; Bairu, S.; Qian, H.; Sinn, E.; Jin, R.; Ramakrishna, G. Temperature-Dependent Optical Absorption Properties of Monolayer-Protected Au 25 and Au 38 Clusters. *The Journal of Physical Chemistry Letters* **2011**, *2*, 2752–2758.

(32) Zsigmondy, R. *Colloids and the Ultramicroscope: A Manual of Colloid Chemistry and Ultramicroscopy*; Wiley: New York, 1909.

(33) Turkevich, J.; Stevenson, P. C.; Hillier, J. A STUDY OF THE NUCLEATION AND GROWTH PROCESSES IN THE SYNTHESIS OF COLLOIDAL GOLD. *Discussions of the Faraday Society* **1951**, 55–&.

(34) Frens, G. CONTROLLED NUCLEATION FOR REGULATION OF PARTICLE-SIZE IN MONODISPERSE GOLD SUSPENSIONS. *Nature-Physical Science* **1973**, *241*, 20–22.

(35) Kerker, M. *The Scattering of Light and Other Electromagnetics Radiation*; Academic: New York, 1969.

(36) U. Kreibig, M. V. *Optical Properties of Metal Clusters*; Springer-Verlag: New Work, 1995.

(37) Lang, H. F.; May, R. A.; Iversen, B. L.; Chandler, B. D. Dendrimer-encapsulated nanoparticle precursors to supported platinum catalysts. *Journal of the American Chemical Society* **2003**, *125*, 14832–14836.

(38) Lee, D.; Donkers, R. L.; Wang, G.; Harper, A. S.; Murray, R. W. Electrochemistry and optical absorbance and luminescence of molecule-like Au38 nanoparticles. *Journal of the American Chemical Society* **2004**, *126*, 6193–9.

(39) Burda, C.; Chen, X.; Narayanan, R.; El-Sayed, M. A. Chemistry and properties of nanocrystals of different shapes. *Chemical reviews* **2005**, *105*, 1025–102.

(40) Murphy, C. J.; Gole, A. M.; Hunyadi, S. E.; Orendorff, C. J. One-dimensional colloidal gold and silver nanostructures. *Inorganic Chemistry* **2006**, *45*, 7544–7554.

(41) Xia, Y. N.; Yang, P. D.; Sun, Y. G.; Wu, Y. Y.; Mayers, B.; Gates, B.; Yin, Y. D.; Kim, F.; Yan, Y. Q. One-dimensional nanostructures: Synthesis, characterization, and applications. *Advanced Materials* **2003**, *15*, 353–389.

(42) Parker, J. F.; Fields-Zinna, C. A.; Murray, R. W. The story of a monodisperse gold nanoparticle: Au25L18. *Accounts of chemical research* **2010**, *43*, 1289–96.

(43) Negishi, Y.; Chaki, N. K.; Shichibu, Y.; Whetten, R. L.; Tsukuda, T. Origin of magic stability of thiolated gold clusters: a case study on Au25(SC6H13)18. *Journal of the American Chemical Society* **2007**, *129*, 11322–3.

(44) Akola, J.; Walter, M.; Whetten, R. L.; Häkkinen, H.; Grönbeck, H. On the structure of thiolate-protected Au25. *Journal of the American Chemical Society* **2008**, *130*, 3756–7.

(45) Zheng, J.; Zhang, C. W.; Dickson, R. M. Highly fluorescent, water-soluble, size-tunable gold quantum dots. *Physical Review Letters* **2004**, *93*.

(46) Hodak, J. H.; Henglein, A.; Hartland, G. V. Size dependent properties of Au particles: Coherent excitation and dephasing of acoustic vibrational modes. *The Journal of Chemical Physics* **1999**, *111*, 8613.

(47) Alvarez, M. M.; Khoury, J. T.; Schaaff, T. G.; Shafigullin, M.; Vezmar, I.; Whetten, R. L. Critical sizes in the growth of Au clusters. *Chemical Physics Letters* **1997**, *266*, 91–98.

(48) Peng, S.; McMahon, J. M.; Schatz, G. C.; Gray, S. K.; Sun, Y. Reversing the size-dependence of surface plasmon resonances. *Proceedings of the National Academy of Sciences of the United States of America* **2010**, *107*, 14530–14534.

(49) Mohamed, M. B.; Volkov, V.; Link, S.; El-Sayed, M. A. The "lightning" gold nanorods: fluorescence enhancement of over a million compared to the gold metal. *Chemical Physics Letters* **2000**, *317*, 517–523.

(50) Dreaden, E. C.; El-Sayed, M. A. Detecting and destroying cancer cells in more than one way with noble metals and different confinement properties on the nanoscale. *Accounts of chemical research* **2012**, *45*, 1854–65.

(51) Bigioni, T. P.; Whetten, R. L.; Dag, O. Near-infrared luminescence from small gold nanocrystals. *Journal of Physical Chemistry B* **2000**, *104*, 6983–6986.

(52) J Lin, C.-A.; Lee, C.-H.; Hsieh, J.-T.; Wang, H.-H.; K Li, J.; Shen, J.-L.; Chan, W.-H.; Yeh, H.-I.; H Chang, W.; Lin, C.-A. J.; Li, J. K.; Chang, W. H. Synthesis of Fluorescent Metallic Nanoclusters toward Biomedical Application: Recent Progress and Present Challenges. *Journal of Medical and Biological Engineering* **2009**, *29*, 276–283.

(53) Knight, W.; Clemenger, K.; De Heer, W.; Saunders, W.; Chou, M.; Cohen, M. Electronic Shell Structure and Abundances of Sodium Clusters. *Physical Review Letters* **1984**, *52*, 2141–2143.

(54) Negishi, Y.; Nobusada, K.; Tsukuda, T. Glutathione-protected gold clusters revisited: bridging the gap between gold(I)-thiolate complexes and thiolate-protected gold nanocrystals. *Journal of the American Chemical Society* **2005**, *127*, 5261–70.

(55) Valden, M.; Lai, X.; Goodman, D. W. Onset of catalytic activity of gold clusters on titania with the appearance of nonmetallic properties. *Science* **1998**, *281*, 1647–1650.

(56) Long, C. G.; Gilbertson, J. D.; Vijayaraghavan, G.; Stevenson, K. J.; Pursell, C. J.; Chandler, B. D. Kinetic evaluation of highly active supported gold catalysts prepared from monolayer-protected clusters: An experimental Michaelis-Menten approach for determining the oxygen binding constant during CO oxidation catalysis. *Journal of the American Chemical Society* **2008**, *130*, 10103–10115.

(57) Bergeron, D. E.; Roach, P. J.; Castleman, A. W.; Jones, N. O.; Khanna, S. N. Al cluster superatoms as halogens in polyhalides and as alkaline earths in iodide salts. *Science (New York, N.Y.)* **2005**, *307*, 231–5.

(58) Khanna, S.; Jena, P. Assembling crystals from clusters. *Physical Review Letters* **1992**, *69*, 1664–1667.

(59) Hartig, J.; Stösser, A.; Hauser, P.; Schnöckel, H. A metalloid [Ga23{N(SiMe3)2}11] cluster: the Jellium model put to test. *Angewandte Chemie (International ed. in English)* **2007**, *46*, 1658–62.

(60) Kubo, R.; Kawabata, A.; Kobayashi, S. Electronic properties of small particles. *Annual Review of Materials …* **1984**, 49–66.

(61) De Heer, W. The physics of simple metal clusters: experimental aspects and simple models. *Reviews of Modern Physics* **1993**, *65*, 611–676.

(62) De Heer, W.; Selby, K.; Kresin, V.; Masui, J.; Vollmer, M.; Chatelain, A.; Knight, W. Collective dipole oscillations in small sodium clusters. *Physical Review Letters* **1987**, *59*, 1805–1808.

(63) De Heer, W. A.; Milani, P. Large ion volume time-of-flight mass spectrometer with position- and velocity-sensitive detection capabilities for cluster beams. *Review of Scientific Instruments* **1991**, *62*, 670.

(64) De Heer, W.; Milani, P.; Chtelain, A. Nonjellium-to-jellium transition in aluminum cluster polarizabilities. *Physical Review Letters* **1989**, *63*, 2834–2836.

(65) Kreibig, U.; Zacharias, P. Surface plasma resonances in small spherical silver and gold particles. *Zeitschrift f*  *r Physik* **1970**, *231*, 128–143.

(66) Ekardt, W. Work function of small metal particles: Self-consistent spherical jellium-background model. *Physical Review B* **1984**, *29*, 1558–1564.

(67) Payami, M.; Nafari, N. Stabilized spin-polarized jellium model and odd-even alternations in jellium metal clusters. *The Journal of Chemical Physics* **1998**, *109*, 5730.

(68) Jahn, H. A.; Teller, E. Stability of Polyatomic Molecules in Degenerate Electronic States. I. Orbital Degeneracy. *Proceedings of the Royal Society of London. Series A - Mathematical and Physical Sciences* **1937**, *161* , 220–235.

(69) Varnavski, O.; Goodson, T.; Mohamed, M.; El-Sayed, M. Femtosecond excitation dynamics in gold nanospheres and nanorods. *Physical Review B* **2005**, *72*, 235405–.

(70) Rao, C. N. R.; Kulkarni, G. U.; Thomas, P. J.; Edwards, P. P. Metal nanoparticles and their assemblies. *Chemical Society Reviews* **2000**, *29*, 27–35.

(71) Martin, T. P. Shells of atoms. *Physics Reports* **1996**, *273*, 199–241.

(72) Lin, C.-A. J.; Lee, C.-H.; Hsieh, J.-T.; Wang, H.-H.; Li, J. K.; Shen, J.-L.; Chan, W.-H.; Yeh, H.-I.; Chang, W. H. Synthesis of Fluorescent Metallic Nanoclusters toward Biomedical Application: Recent Progress and Present Challenges. *Journal of Medical and Biological Engineering* **2009**, *29*, 276–283.

(73) Iwasa, T.; Nobusada, K. Theoretical Investigation of Optimized Structures of Thiolated Gold Cluster [Au25(SCH3)18]+. *Journal of Physical Chemistry C* **2007**, *111*, 45–49.

(74) Tomalia, D. A. In quest of a systematic framework for unifying and defining nanoscience. *Journal of nanoparticle research : an interdisciplinary forum for nanoscale science and technology* **2009**, *11*, 1251–1310.

(75) Chen, W.; Tomalia, D. A.; Thomas, J. L. Unusual pH-Dependent Polarity Changes in PAMAM Dendrimers: Evidence for pH-Responsive Conformational Changes. *Macromolecules* **2000**, *33*, 9169–9172.

(76) Korkosz, R. J.; Gilbertson, J. D.; Prasifka, K. S.; Chandler, B. D. Dendrimer templates for supported Au catalysts. *Catalysis Today* **2007**, *122*, 370–377.

(77) Kim, Y. G.; Oh, S. K.; Crooks, R. M. Preparation and characterization of 1-2 nm dendrimer-encapsulated gold nanoparticles having very narrow size distributions. *Chemistry of Materials* **2004**, *16*, 167–172.

(78) Knecht, M. R.; Garcia-Martinez, J. C.; Crooks, R. M. Hydrophobic dendrimers as templates for Au nanoparticles. *Langmuir* **2005**, *21*, 11981–11986.

(79) Grohn, F.; Bauer, B. J.; Akpalu, Y. A.; Jackson, C. L.; Amis, E. J. Dendrimer templates for the formation of gold nanoclusters. *Macromolecules* **2000**, *33*, 6042–6050.

(80) Ramakrishna, G.; Bhaskar, A.; Bauerle, P.; Goodson III, T. Oligothiophene dendrimers as new building blocks for optical applications. *Journal of Physical Chemistry A* **2008**, *112*, 2018–2026.

(81) Schmid, G.; Pfeil, R.; Boese, R.; Bandermann, F.; Meyer, S.; Calis, G. H. M.; Vandervelden, W. A. AU55 P(C6H5)3 12CL6 - A GOLD CLUSTER OF AN EXCEPTIONAL SIZE. *Chemische Berichte-Recueil* **1981**, *114*, 3634–3642.

(82) Brust, M.; Fink, J.; Bethell, D.; Schiffrin, D. J.; Kiely, C. Synthesis and reactions of functionalised gold nanoparticles. *Journal of the Chemical Society, Chemical Communications* **1995**, 1655.

(83) Brust, M.; Fink, J.; Bethell, D.; Schiffrin, D. J.; Kiely, C. Synthesis and Reactiosn of Functionalized Gold Nanoparticles. *Journal of the Chemical Society-Chemical Communications* **1995**, 1655–1656.

(84) Brust, M.; Walker, M.; Bethell, D.; Schiffrin, D. J.; Whyman, R. Synthesis of Thiol-derivatized Gold Nanoparticles in a 2-Phase Liquid-liquid System. *Journal of the Chemical Society-Chemical Communications* **1994**, 801–802.

(85) Negishi, Y.; Takasugi, Y.; Sato, S.; Yao, H.; Kimura, K.; Tsukuda, T. Magic-numbered Au(n) clusters protected by glutathione monolayers (n = 18, 21, 25, 28, 32, 39): isolation and spectroscopic characterization. *Journal of the American Chemical Society* **2004**, *126*, 6518–9.

(86) Kumar, S.; Bolan, M. D.; Bigioni, T. P. Glutathione-stabilized magic-number silver cluster compounds. *Journal of the American Chemical Society* **2010**, *132*, 13141–3.

(87) Lopez-Acevedo, O.; Tsunoyama, H.; Tsukuda, T.; Häkkinen, H.; Aikens, C. M. Chirality and electronic structure of the thiolate-protected Au38 nanocluster. *Journal of the American Chemical Society* **2010**, *132*, 8210–8.

(88) Shichibu, Y.; Negishi, Y.; Tsukuda, T.; Teranishi, T. Large-scale synthesis of thiolated Au25 clusters via ligand exchange reactions of phosphine-stabilized Au11 clusters. *Journal of the American Chemical Society* **2005**, *127*, 13464–5.

(89) Wu, Z.; Suhan, J.; Jin, R. One-pot synthesis of atomically monodisperse, thiol-functionalized Au25 nanoclusters. *Journal of Materials Chemistry* **2009**, *19*, 622.

(90) Mrudula, K. V.; Bhaskara Rao, T. U.; Pradeep, T. Interfacial synthesis of luminescent 7 kDa silver clusters. *Journal of Materials Chemistry* **2009**, *19*, 4335.

(91) Ackerson, C. J.; Jadzinsky, P. D.; Kornberg, R. D. Thiolate ligands for synthesis of water-soluble gold clusters. *Journal of the American Chemical Society* **2005**, *127*, 6550–1.

(92) Schaaff, T. G.; Knight, G.; Shafigullin, M. N.; Borkman, R. F.; Whetten, R. L. Isolation and selected properties of a 10.4 kDa Gold□: Glutathione cluster compound. *Journal of Physical Chemistry B* **1998**, *102*, 10643–10646.

(93) Jadzinsky, P. D.; Calero, G.; Ackerson, C. J.; Bushnell, D. A.; Kornberg, R. D. Structure of a thiol monolayer-protected gold nanoparticle at 1.1 angstrom resolution. *Science* **2007**, *318*, 430–433.

(94) Lopez-Acevedo, O.; Akola, J.; Whetten, R. L.; Gronbeck, H.; Hakkinen, H. Structure and Bonding in the Ubiquitous Icosahedral Metallic Gold Cluster Au-144(SR)(60). *Journal of Physical Chemistry C* **2009**, *113*, 5035–5038.

(95) Shibu, E. S.; Muhammed, M. A. H.; Tsukuda, T.; Pradeep, T. Ligand Exchange of Au25SG18 Leading to Functionalized Gold Clusters: Spectroscopy, Kinetics, and Luminescence. *Journal of Physical Chemistry C* **2008**, *112*, 12168–12176.

(96) Templeton, A. C.; Wuelfing, W. P.; Murray, R. W. Monolayer-Protected Cluster Molecules. *Accounts of Chemical Research* **2000**, *33*, 27–36.

(97) Dass, A.; Dubay, G. R.; Fields-Zinna, C. A.; Murray, R. W. FAB mass spectrometry of Au-25(SR)(18) nanoparticles. *Analytical Chemistry* **2008**, *80*, 6845–6849.

(98) Huang, T.; Murray, R. W. Luminescence of tiopronin monolayer-protected silver clusters changes to that of gold clusters upon galvanic core metal exchange. *Journal of Physical Chemistry B* **2003**, *107*, 7434–7440.

(99) Hostetler, M. J.; Wingate, J. E.; Zhong, C. J.; Harris, J. E.; Vachet, R. W.; Clark, M. R.; Londono, J. D.; Green, S. J.; Stokes, J. J.; Wignall, G. D.; Glish, G. L.; Porter, M. D.; Evans, N. D.; Murray, R. W. Alkanethiolate gold cluster molecules with core diameters from 1.5 to 5.2 nm: Core and monolayer properties as a function of core size. *Langmuir* **1998**, *14*, 17–30.

(100) Donkers, R. L.; Lee, D.; Murray, R. W. Synthesis and Isolation of the Molecule-like Cluster Au 38 (PhCH 2 CH 2 S) 24. *Langmuir* **2004**, *20*, 1945–1952.

(101) Echt, O.; Sattler, K.; Recknagel, E. MAGIC NUMBERS FOR SPHERE PACKINGS - EXPERIMENTAL-VERIFICATION IN FREE XENON CLUSTERS. *Physical Review Letters* **1981**, *47*, 1121–1124.

(102) Hakkinen, H.; Walter, M.; Gronbeck, H. Divide and protect: Capping gold nanoclusters with molecular gold-thiolate rings. *Journal of Physical Chemistry B* **2006**, *110*, 9927–9931.

(103) Varnavski, O.; Goodson, T.; Sukhomlinova, L.; Twieg, R. Ultrafast Exciton Dynamics in a Branched Molecule Investigated by Time-Resolved Fluorescence,

Transient Absorption, and Three-Pulse Photon Echo Peak Shift Measurements †. *The Journal of Physical Chemistry B* **2004**, *108*, 10484–10492.

(104) Jin, R. Super robust nanoparticles for biology and biomedicine. *Angewandte Chemie-International Edition* **2008**, *47*, 6750–6753.

(105) Zipfel, W. R. W. Nonlinear magic: multiphoton microscopy in the biosciences. *Nature Biotechnology* **2003**, *21*, 1369–1257.

Chapter 2

Characterization of Metal Nanoclusters

Overview

Characterization of the nanoclusters is one of the most debated aspects of metal nanosystem research. This chapter presents a brief review of the characterization of nanoclusters. The characterization of nanoclusters is an indispensible part of nanoclusters research, but it is not the focus of this dissertation, and as such is separated from other chapters. In addition to the discussion about different characterization methods, the characterization of gold and silver nanoclusters presented in this dissertation is discussed in detail.

2.1 Characterization of Metal Nanoclusters

In the study of nanoclusters and nanoparticles, one of the biggest challenges is the characterization of the exact metal core composition and the fine details in the ligand coordination binding.[1–4] Without careful characterization work, the research on the optical or physical properties can be diverged by impurities. Metal clusters in the gas phase was produced by heating bulk metal to near its melting point, which produces atomic vapor of dimmer, trimer and larger clusters in low yields.[5–8] Gas phase clusters can easily be characterized by mass spectrometry. The discovery of metal clusters in the condensed phase (solution) requires a different approach compare to has phase, because the ionization methods for nanoclusters was not initially available.[9–13] In the early days of nanocluster research, researchers relied heavily on the use of transmission electron microscopy (TEM) to directly image the nanoclusters on a substrate (sample figure

2.1).[2,9,14–17] The TEM images can resolve the metal core sizes and their distribution on the surface. TEM was the first piece of evidence that there are certain sizes of nanoclusters, like "magic clusters" in the gas phase.[6] The purity of the nanoclusters were based on the size distribution. Pure materials are mono-dispersed in size. However, the information provided by TEM is very limited. In particular, the accuracy and the resolution of TEM are not always adequate to resolve nanoclusters. The recorded TEM sizes of the major species do not provide information of the structure of the nanocluster. The core metal number is calculated based on the size, which is fitted to a basic packing model, like the full shell model or the face-centered cubic (like bulk gold).[9] This initial approach using TEM achieved certain levels of success, but this approach was more appropriate for larger nanoparticles.

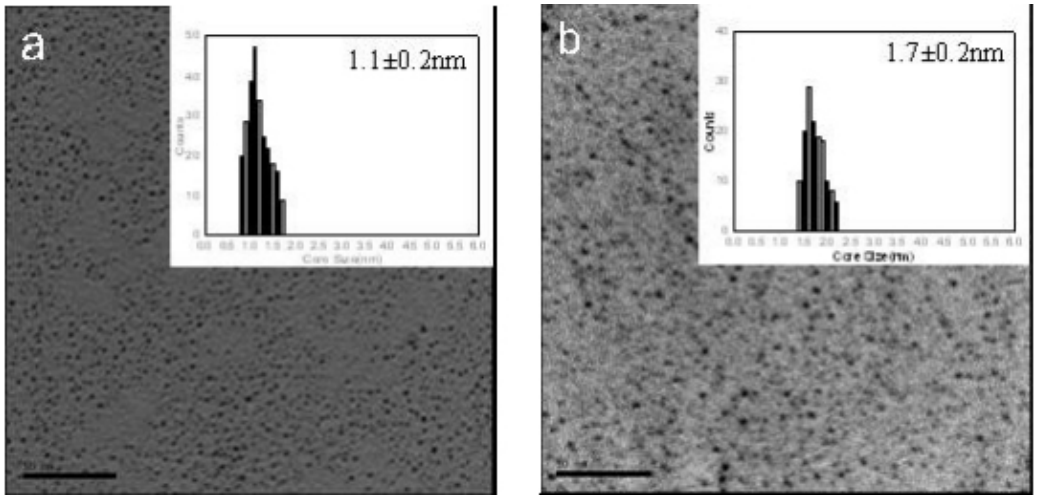

Figure 2.1 TEM images for gold nanoclusters Au_{25} and Au_{140}.[18]

To better understand the exact structure of nanoclusters, two different requirements must first be met. First, samples of higher purity are required. Second, a new technique that gives structural detail must be developed. The work of Brust, Whetten, Murray and others outlined in chapter 1 explored the use of a variety of thiol ligands to improve the size distribution or the purity of nanoclusters.[19–23] Post synthetic separation was also explored using size-selective precipitation by phase separation, chromatography or thermal treatments.[21,24–30] The exploratory synthetic work lead to a few adjustment to the Brust protocol, namely the thiol to gold ratio was increased ten

times to 3:1 (thiol to gold), and excess reducing agent ($NaBH_4$) was used. Using electrospray ionization mass spectrometry (ESI-MS) to identify nanoclusters was developed by Royce Murray at UNC Chapel Hill and Rob Whetten at Georgia Tech.[2,3,16,20,31–33] Using the softer ionization technique, researchers were able to ionize gold nanoclusters without degrading the major species. Using ESI-MS, the Murray group was able to the assign the metal to ligand ratio by monitoring the time resolved ligand exchange process of gold nanoclusters.[34,35] The ligand-metal ratio assignment lead to the name Mono-layered protected clusters (MPC).[2,3,22,34,36–38] The use of polyacrylamide gel electrophoresis (PAGE) separation further improve the purity of the MPCs and lead to precise mass determinations.[3,39] The work of R. Jin et. al. and Tsuskuda et. al. improved the purity of MPCs further through kinetic control.[3,30,34,40] In their investigations, close monitoring of the reaction mixture showed that unstable sizes are "etched" or self-cleaved to from stable species over time.[30,41] The size focusing mechanism provided proof to the self assembly nature of metal nanoclusters. The highly pure (mono-dispersion) gold nanoclusters paved way to the breakthrough of a total structural determination.[12,37,42,43]

The use of ESI-MS improved on the characterization of nanoclusters, but in the early stage of mass spectrometry research, mislabeling of nanoclusters are common. The most noted example is the assignment of Au_{38} to the 5 kDa species , which was later discovered to be Au_{25}.[34,44,45] However, a new minor 8 kDa species has been characterized as Au_{38} recently.[46,47] Mass spectrometry can provide some metal core characterization, but it cannot provide other structural details such as ligand binding. X-ray cryptography uses the diffraction pattern of x-ray off crystals at different angle and can be used to explain the exact structure with the aid of computers. The use of X-ray crystallography is challenging, because the crystallization of samples require extremely high purity. Fortunately, the synthesis of some nanoclusters has achieve such high purity that crystallization is possible.[30,48,49] To this day, only two MPCs ($Au_{25}(SG)_{18}$ and $Au_{102}(SR)_{44}$) have been characterized using X-ray crystallogrpahy.[42,43] Au_{25} and Au_{102} has become the bases of the major models used in gold nanoclusters.[43,50] While X-ray crystallography can offer more detail, ESI-MS has proven to be much more user-friendly

and has become one of the standard methods of characterization. [1–4,35,39,48,51,52] The result from the mass spectrometry of metal nanoclusters correlates very well to the crystal structure, which also has high sensitivity to impurities.

2.2 Gold Nanoclusters

The gold nanoclusters used in our experiments were synthesized using the Burst method, performed by our collaborators.[16,53–57] In chapter 4, the nanocluster Au_{55} was capped by troponin after phase transfer from dendrimer capture. The other nanoclusters were capped with glutathione (water soluble) or hexanethiolate (in toluene).[34,57,58]. The TEM images of clusters of various sizes clusters are available (figure 2.2). TEM images were obtained with JEOL JEM-1230. The TEM images in figure 2.2 show nanoclusters Au_{25}, Au_{140}, Au_{309} and nanoparticles Au_{976} and Au_{2406} in order. The inserts to the figures represent the size distribution, with the reported major species.

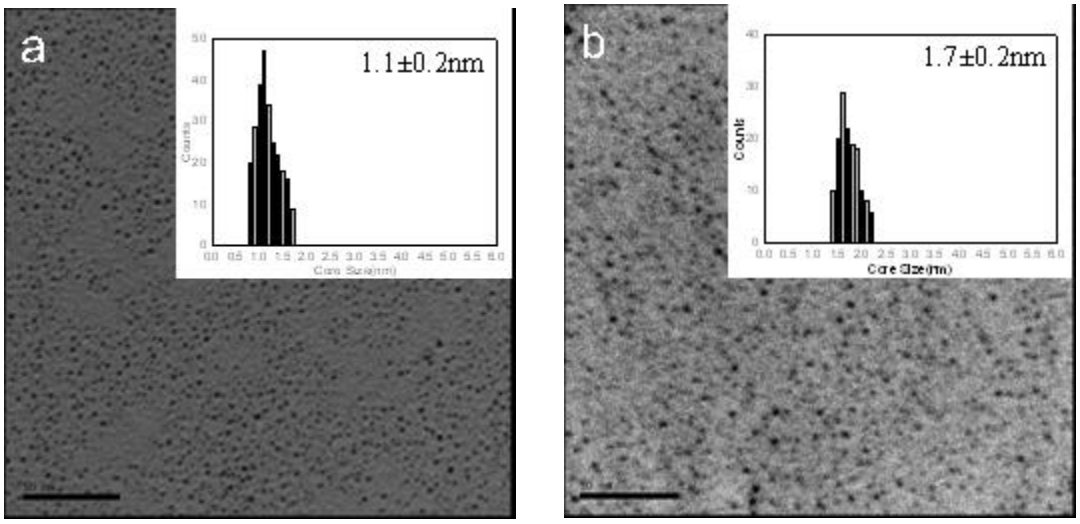

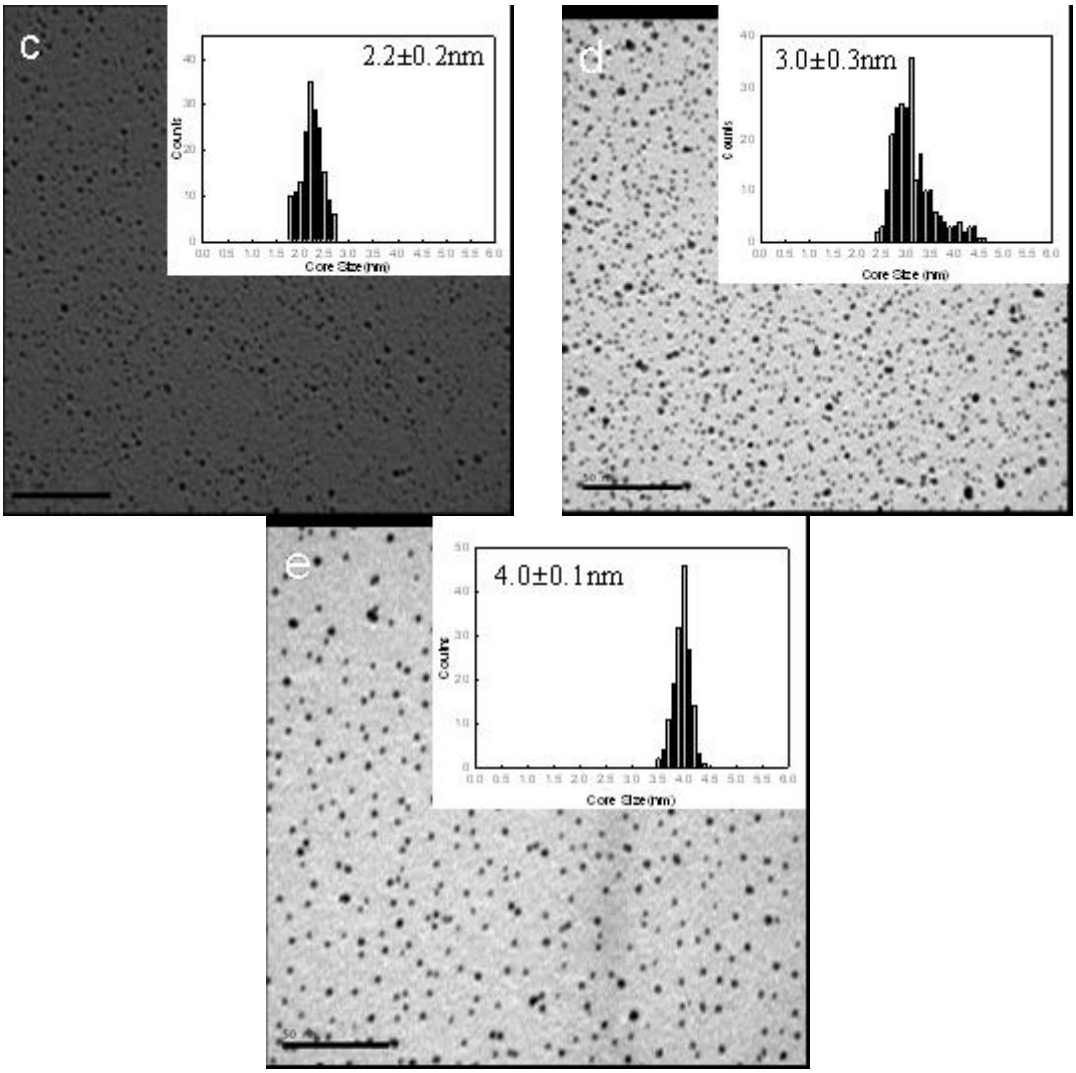

Figure 2.2 TEM images and corresponding histograms of the core diameters of hexanethiolate-coated (a) Au_{25}, (b) Au_{140}, (c) Au_{309}, (d) Au_{976}, and (e) Au_{2406} MPCs. TEM images were obtained with JEOL JEM-1230. Scale bar = 50 nm.

In addition to TEM images, the absorption spectra were collected on site to check for sample purity. For Au_{25}, the absorption spectrum has distinct features (chapter 4), which can be easily obscured by impurities such as larger nanoparticles. The absorption spectra of other gold nanoclusters were used as a control. Gold nanoclusters can degrade into atoms, and the absorption spectra will lose its characteristic peaks. Nanoclusters can also aggregate when degraded. If the sample has aggregated, the surface plasmon resonance in absorption spectrum around 550 nm will be observed. It is important to note

that Au_{309} and Au_{2406} are nanoparticles of 3 nm and 4 nm, respectively, and the SPR at 500 nm is expected.

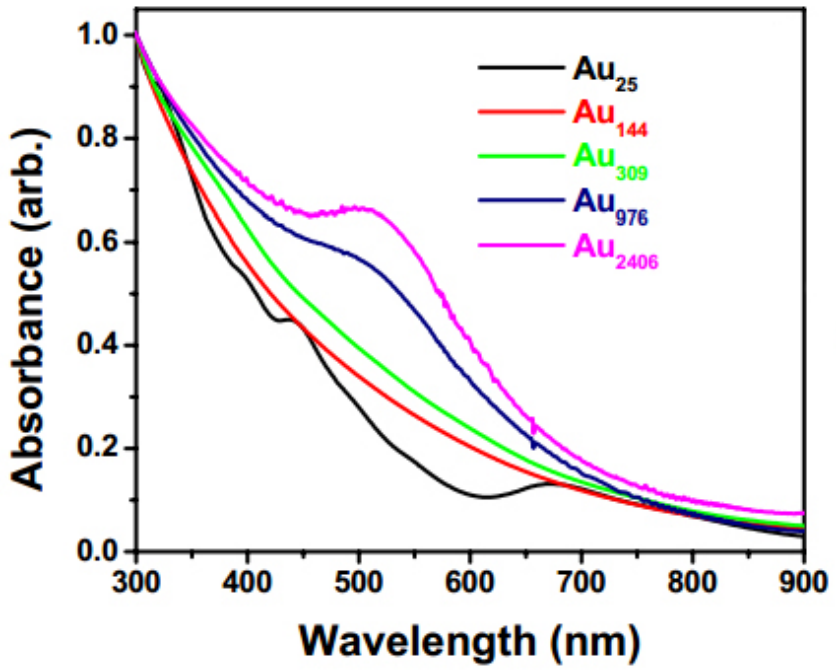

Figure 2.3 *Normalized a*bsorption spectrum of various gold nanosystems in hexane.[59]

2.3 Silver Nanoclusters

Mono-layered protected silver nanoclusters were first synthesized by the Bigioni Group at the University of Toledo.[60] Their synthetic approach is based on the Brust synthesis and uses glutathione as the ligand. $AgNO_3$ in water was mix with glutathione in a 1:4 ratio, and a cloudy white suspension of silver thiolate is formed. The mixture was cooled for 30 minutes before excess NaBH4 is added drop wise while stirring at ~1100 rpm. The solution turned to brownish black color after 25 minutes and concentrated to about 10 times less in volume. The silver nanoclusters were precipitated with methanol, and washed with methanol through ultrasonic dispersion-centrifugation. The precipitated was dried under vacuum. The powder silver nanoclusters were purified using a customized polyacrylamide gel electrophoresis procedure.[60] The reaction produces nanoclusters of various sizes (figure 2.4).[60] The product was separated using

Polyacrylamide Gel Electrophoresis (PAGE) with some modification. The gel was made by the Bigioni group without denaturating agents like sodium dodecyl sulphate and the gel density was also increased to improve resolution. The gel was run at constant voltage using a Thermo Scientific vertical electrophoresis system (P10DS) at a constant voltage of 200 V, the gel is also cooled during the experiment. A sample image of the produced gel is shown in figure 2.4

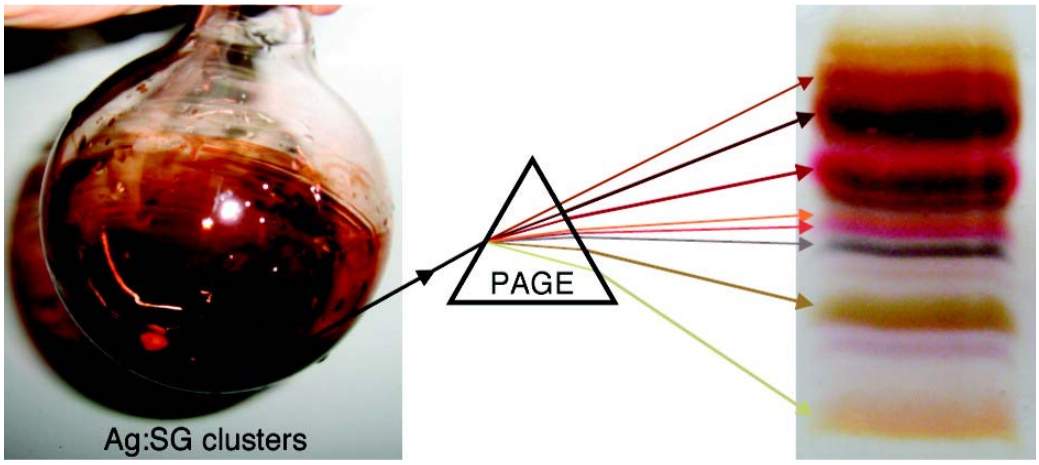

Figure 2.4 Silver nanocluster produced based on the Burst synthesis, separated by gel electrophoresis.[60]

The resulting gel forms bands which contains silver nanoclusters of specific sizes (figure 2.4).

The initial series of silver nanoclusters were compared to gold nanoclusters separated under the same PAGE condition. Size similarities between the silver and gold nanoclusters were observed (figure 2.5).[60] It is important to point out that Band 2 and Band 6 are the most stable species, thus became our study target. Band 2 is similar in size to Au_{15} while Band 6 is similar in size to Au_{29}. The size comparison in the gel is only an estimate, however the Bigoni group is currently developing size marker that can improve the accuracy of this method. The use of PAGE separation may one day achieve the resolution of TEM.

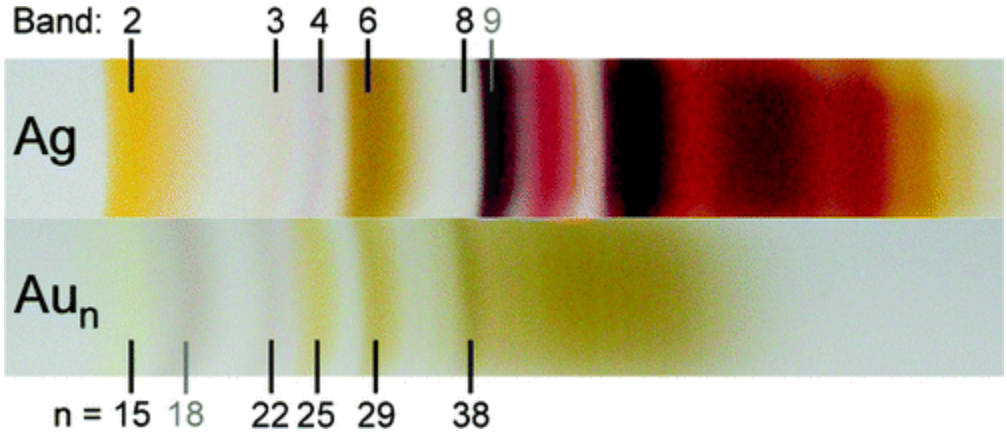

Figure 2.5 Comparison of Au and Ag nanosystems under the same condition of PAGE separation.

Specific bands are physically removed from the gel by cutting and are crushed. The crushed gel is submerged in water so that the nanoclusters are diffused out of the gel. For the small nanoclusters, the final supernatant was filtered through a 0.22 μm syringe filter, concentrated with a 3 kDa cutoff filter and dried by an Ependorf Vacufuge Concentrator Speed-vac. The silver nanoclusters Band 2 and 6 were received in various forms, including dry power, gel and solution. Silver nanoclusters captured in the gel after PAGE should contain the highest purity and stability. However the gel medium cannot withstand laser excitation. The gel samples (figure 2.6) were damaged by the laser excitation beam within seconds of exposure. Nanoclusters in solution were also tested, but it was found that shelf-life of nanoclusters is poor in solution, which can degrade in a few hours. The transport of nanoclusters in solution not ideal. The Improved yields of the silver nanocluster synthesis allow for silver nanoclusters to be dried into powder, which proves to be very stable.[48] The silver nanoclusters are solvated *in situ*, and the absorption, emission and excitation spectra are tested to ensure purity (figure 2.7).

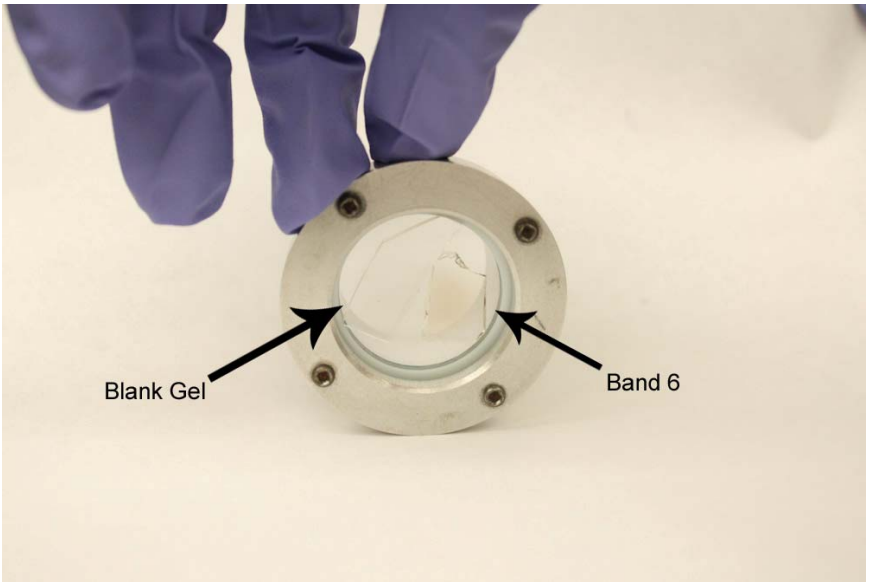

Figure 2.6 Rotating cell contains Band 6 cut from the PAGE gel.

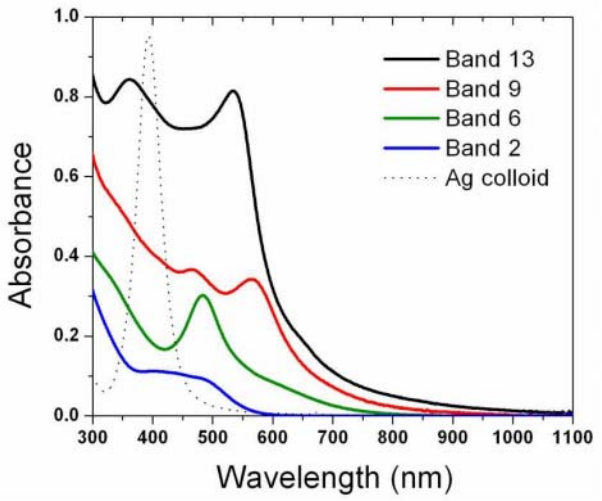

Figure 2.7 Absorption spectrum of various Bands of silver nanoclusters[60]

Both Band 2 and Band 6 silver nanoclusters were initially studied, but only Band 6 was characterized by mass spectrometry, and was identified as $Ag_{32}(SG)_{19}$ (figure 2.8).[48] The successful characterization was based on the optimized condition for Au_{25}, with adjustment to the ionization condition to minimize the fragmentation of the sample. Optical studies of Band 2 were halted due to the lack of structural information. Initially the absorption spectrum of silver nanoclusters was used to ensure sample purity, but the Bigioni group found that Band 6 can degrade into Band 2. The absorption spectrum of

band 2 cannot be separated from band 6, instead excitation spectrum was used to ensure the purity of the Band 6 clusters with excellent sensitivity (figure 2.9). It is worth mentioning that the maximum excitation wavelength for band 2 and band 6 are 50 nm apart, and they have distinct features, almost like the "finger prints" for these clusters.

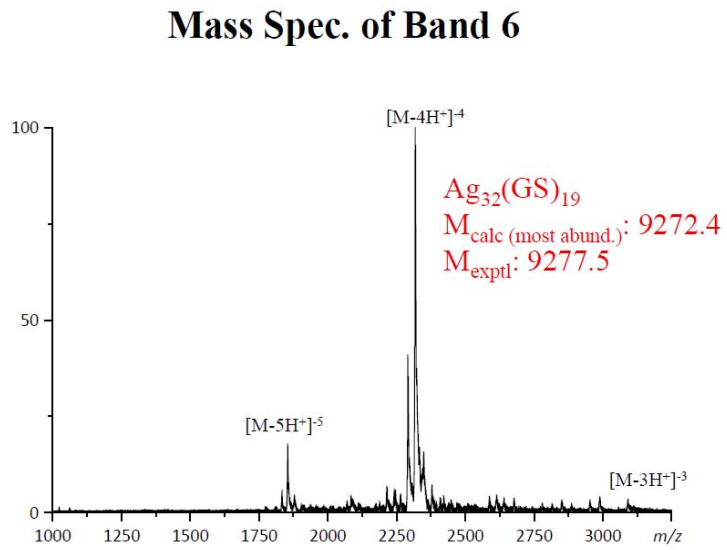

Figure 2.8 The mass spectrum of Band 6 that leads to the assignment of $Ag_{32}(SG)_{19}$.[48]

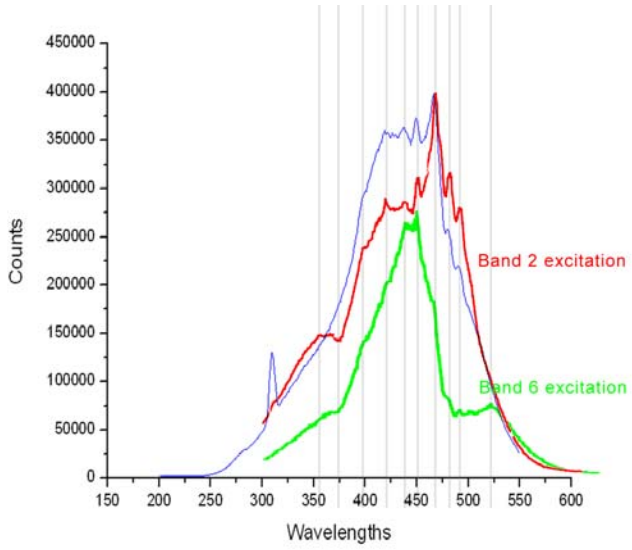

Figure 2.9 *A sample e*xcitation spectrum for Band 6 and Band 2, the excitation spectrum fine detail is used to identify the purity of the sample. A sample containing both band 2 and band 6 is shown in blue.

The DNA-templated Ag nanoclusters in Chapter 6 are synthesized by the Martinez Group at the Los Alamos National Laboratory.[61–63] Their synthetic approach was based on the earlier work by Dickson et. al.[64–67] It is important to note that the samples provided by the Martinez Group show spectroscopic differences compared to what was reported by the Dickson group for the same system.[68,69] We strongly believe in the quality of the samples provided by the Martinez group due to their detailed characterization. DNA-templated Ag nanoclusters were characterized by K-edge Extended X-ray Absorption Fine Structure (EXAFS).[62] Metal-metal and metal-ligand binding were detected and a metal core size of 8-20 atoms was calculated based on the molecular distances. The EXAFS data published provided a sound argument for the assignment of silver nanoclusters within the DNA scaffold. Like other nanoclusters, the absorption spectra were used in the characterization of the samples *in situ*.

2.4 Reference

(1) Shibu, E. S.; Muhammed, M. A. H.; Tsukuda, T.; Pradeep, T. Ligand Exchange of Au25SG18 Leading to Functionalized Gold Clusters: Spectroscopy, Kinetics, and Luminescence. *Journal of Physical Chemistry C* **2008**, *112*, 12168–12176.

(2) Templeton, A. C.; Wuelfing, W. P.; Murray, R. W. Monolayer-Protected Cluster Molecules. *Accounts of Chemical Research* **2000**, *33*, 27–36.

(3) Parker, J. F.; Fields-Zinna, C. A.; Murray, R. W. The story of a monodisperse gold nanoparticle: Au25L18. *Accounts of chemical research* **2010**, *43*, 1289–96.

(4) Dass, A.; Dubay, G. R.; Fields-Zinna, C. A.; Murray, R. W. FAB mass spectrometry of Au-25(SR)(18) nanoparticles. *Analytical Chemistry* **2008**, *80*, 6845–6849.

(5) Taylor, K. J.; Pettiettehall, C. L.; Cheshnovsky, O.; Smalley, R. E. Ultraviolet Photoelecton-Spectra of Coinage Metal-Clusters. *Journal of Chemical Physics* **1992**, *96*, 3319–3329.

(6) De Heer, W. The physics of simple metal clusters: experimental aspects and simple models. *Reviews of Modern Physics* **1993**, *65*, 611–676.

(7) Knight, W.; Clemenger, K.; De Heer, W.; Saunders, W.; Chou, M.; Cohen, M. Electronic Shell Structure and Abundances of Sodium Clusters. *Physical Review Letters* **1984**, *52*, 2141–2143.

(8) Bergeron, D. E.; Roach, P. J.; Castleman, A. W.; Jones, N. O.; Khanna, S. N. Al cluster superatoms as halogens in polyhalides and as alkaline earths in iodide salts. *Science (New York, N.Y.)* **2005**, *307*, 231–5.

(9) Schmid, G. The relevance of shape and size of Au_{55} clusters. *Chemical Society reviews* **2008**, *37*, 1909–30.

(10) Brust, M.; Fink, J.; Bethell, D.; Schiffrin, D. J.; Kiely, C. Synthesis and reactions of functionalised gold nanoparticles. *Journal of the Chemical Society, Chemical Communications* **1995**, 1655.

(11) Brust, M.; Walker, M.; Bethell, D.; Schiffrin, D. J.; Whyman, R. Synthesis of Thiol-Derivated Gold Nanopartilces in a 2-Phase Liquid-Liquid System. *Journal of the Chemical Society-Chemical Communications* **1994**, 801–802.

(12) Jin, R. Quantum sized, thiolate-protected gold nanoclusters. *Nanoscale* **2010**, *2*, 343–62.

(13) Ispasoiu, R. G.; Balogh, L.; Varnavski, O. P.; Tomalia, D. A.; Goodson, T. Large optical limiting from novel metal-dendrimer nanocomposite materials. *Journal of the American Chemical Society* **2000**, *122*, 11005–11006.

(14) Briant, C. E.; Theobald, B. R. C.; White, J. W.; Bell, L. K.; Mingos, D. M. P.; Welch, A. J. Synthesis and X-ray structural characterization of the centred icosahedral gold cluster compound $[Au_{l3}(PMe_2Ph)10C_{l2}](PF_6)_3$; the realization of a theoretical prediction. *Journal of the Chemical Society, Chemical Communications* **1981**, 201.

(15) Long, C. G.; Gilbertson, J. D.; Vijayaraghavan, G.; Stevenson, K. J.; Pursell, C. J.; Chandler, B. D. Kinetic evaluation of highly active supported gold catalysts prepared from monolayer-protected clusters: An experimental Michaelis-Menten approach for determining the oxygen binding constant during CO oxidation catalysis. *Journal of the American Chemical Society* **2008**, *130*, 10103–10115.

(16) Lee, D.; Donkers, R. L.; Wang, G.; Harper, A. S.; Murray, R. W. Electrochemistry and optical absorbance and luminescence of molecule-like Au_{38} nanoparticles. *Journal of the American Chemical Society* **2004**, *126*, 6193–9.

(17) Schmid, G.; Pfeil, R.; Boese, R.; Bandermann, F.; Meyer, S.; Calis, G. H. M.; Vandervelden, W. A. $AU_{55}P(C_6H_5)_312CL_6$ - A Gold Cluster of an Exceptional Size. *Chemische Berichte-Recueil* **1981**, *114*, 3634–3642.

(18) Ramakrishna, G.; Varnavski, O.; Kim, J.; Lee, D.; Goodson, T. Quantum-sized gold clusters as efficient two-photon absorbers. *Journal of the American Chemical Society* **2008**, *130*, 5032–3.

(19) Hostetler, M. J.; Green, S. J.; Stokes, J. J.; Murray, R. W. Monolayers in three dimensions: Synthesis and electrochemistry of omega-functionalized alkanethiolate-stabilized gold cluster compounds. *Journal of the American Chemical Society* **1996**, *118*, 4212–4213.

(20) Ingram, R. S.; Hostetler, M. J.; Murray, R. W.; Schaaff, T. G.; Khoury, J. T.; Whetten, R. L.; Bigioni, T. P.; Guthrie, D. K.; First, P. N. 28 kDa Alkanethiolate-Protected Au Clusters Give Analogous Solution Electrochemistry and STM Coulomb Staircases. *Journal of the American Chemical Society* **1997**, *119*, 9279–9280.

(21) Alvarez, M. M.; Khoury, J. T.; Schaaff, T. G.; Shafigullin, M.; Vezmar, I.; Whetten, R. L. Critical sizes in the growth of Au clusters. *Chemical Physics Letters* **1997**, *266*, 91–98.

(22) Hostetler, M. J.; Wingate, J. E.; Zhong, C. J.; Harris, J. E.; Vachet, R. W.; Clark, M. R.; Londono, J. D.; Green, S. J.; Stokes, J. J.; Wignall, G. D.; Glish, G. L.; Porter, M. D.; Evans, N. D.; Murray, R. W. Alkanethiolate gold cluster molecules with core diameters from 1.5 to 5.2 nm: Core and monolayer properties as a function of core size. *Langmuir* **1998**, *14*, 17–30.

(23) Chen, S. W.; Murray, R. W. Arenethiolate monolayer-protected gold clusters. *Langmuir* **1999**, *15*, 682–689.

(24) Wilcoxon, J. P.; Provencio, P. Etching and aging effects in nanosize Au clusters investigated using high-resolution size-exclusion chromatography. *Journal of Physical Chemistry B* **2003**, *107*, 12949–12957.

(25) Song, Y.; Jimenez, V.; McKinney, C.; Donkers, R.; Murray, R. W. Estimation of size for 1-2 nm nanoparticles using an HPLC electrochemical detector of double layer charging. *Analytical Chemistry* **2003**, *75*, 5088–5096.

(26) Zhong, C. J.; Zhang, W. X.; Leibowitz, F. L.; Eichelberger, H. H. Size and shape evolution of core-shell nanocrystals. *Chemical Communications* **1999**, 1211–1212.

(27) Lin, X. M.; Wang, G. M.; Sorensen, C. M.; Klabunde, K. J. Formation and dissolution of gold nanocrystal superlattices in a colloidal solution. *Journal of Physical Chemistry B* **1999**, *103*, 5488–5492.

(28) Stoeva, S.; Klabunde, K. J.; Sorensen, C. M.; Dragieva, I. Gram-scale synthesis of monodisperse gold colloids by the solvated metal atom dispersion method and

digestive ripening and their organization into two- and three-dimensional structures. *Journal of the American Chemical Society* **2002**, *124*, 2305–2311.

(29) Prasad, B. L. V; Stoeva, S. I.; Sorensen, C. M.; Klabunde, K. J. Digestive ripening of thiolated gold nanoparticles: The effect of alkyl chain length. *Langmuir* **2002**, *18*, 7515–7520.

(30) Wu, Z.; Suhan, J.; Jin, R. One-pot synthesis of atomically monodisperse, thiol-functionalized Au25 nanoclusters. *Journal of Materials Chemistry* **2009**, *19*, 622.

(31) Balasubramanian, R.; Guo, R.; Mills, A. J.; Murray, R. W. Reaction of Au(55)(PPh(3))(12)Cl(6) with thiols yields thiolate monolayer protected Au(75) clusters. *Journal of the American Chemical Society* **2005**, *127*, 8126–32.

(32) Schaaff, T. G.; Shafigullin, M. N.; Khoury, J. T.; Vezmar, I.; Whetten, R. L.; Cullen, W. G.; First, P. N.; Gutiérrez-Wing, C.; Ascensio, J.; Jose-Yacamán, M. J. Isolation of Smaller Nanocrystal Au Molecules: Robust Quantum Effects in Optical Spectra. *The Journal of Physical Chemistry B* **1997**, *101*, 7885–7891.

(33) Schaaff, T. G.; Shafigullin, M. N.; Khoury, J. T.; Vezmar, I.; Whetten, R. L. Properties of a ubiquitous 29 kDa Au: SR cluster compound. *Journal of Physical Chemistry B* **2001**, *105*, 8785–8796.

(34) Donkers, R. L.; Lee, D.; Murray, R. W. Synthesis and Isolation of the Molecule-like Cluster Au 38 (PhCH 2 CH 2 S) 24. *Langmuir* **2004**, *20*, 1945–1952.

(35) Tracy, J. B.; Crowe, M. C.; Parker, J. F.; Hampe, O.; Fields-Zinna, C. A.; Dass, A.; Murray, R. W. Electrospray ionization mass spectrometry of uniform and mixed monolayer nanoparticles: Au25[S(CH2)2Ph]18 and Au25[S(CH2)2Ph]18-x(SR)x. *Journal of the American Chemical Society* **2007**, *129*, 16209–15.

(36) Huang, T.; Murray, R. W. Luminescence of tiopronin monolayer-protected silver clusters changes to that of gold clusters upon galvanic core metal exchange. *Journal of Physical Chemistry B* **2003**, *107*, 7434–7440.

(37) Schaaff, T. G.; Knight, G.; Shafigullin, M. N.; Borkman, R. F.; Whetten, R. L. Isolation and selected properties of a 10.4 kDa Gold: Glutathione cluster compound. *Journal of Physical Chemistry B* **1998**, *102*, 10643–10646.

(38) Jimenez, V. L.; Georganopoulou, D. G.; White, R. J.; Harper, A. S.; Mills, A. J.; Lee, D. I.; Murray, R. W. Hexanethiolate monolayer protected 38 gold atom cluster. *Langmuir* **2004**, *20*, 6864–6870.

(39) Negishi, Y.; Takasugi, Y.; Sato, S.; Yao, H.; Kimura, K.; Tsukuda, T. Magic-numbered Au(n) clusters protected by glutathione monolayers (n = 18, 21, 25, 28,

32, 39): isolation and spectroscopic characterization. *Journal of the American Chemical Society* **2004**, *126*, 6518–9.

(40) Qian, H.; Zhu, M.; Lanni, E.; Zhu, Y.; Bier, M. E.; Jin, R. Conversion of Polydisperse Au Nanoparticles into Monodisperse Au-25 Nanorods and Nanospheres. *Journal of Physical Chemistry C* **2009**, *113*, 17599–17603.

(41) Schaaff, T. G.; Whetten, R. L. Controlled Etching of Au:SR Cluster Compounds. *The Journal of Physical Chemistry B* **1999**, *103*, 9394–9396.

(42) Zhu, M.; Aikens, C. M.; Hollander, F. J.; Schatz, G. C.; Jin, R. Correlating the crystal structure of a thiol-protected Au25 cluster and optical properties. *Journal of the American Chemical Society* **2008**, *130*, 5883–5.

(43) Jadzinsky, P. D.; Calero, G.; Ackerson, C. J.; Bushnell, D. A.; Kornberg, R. D. Structure of a thiol monolayer-protected gold nanoparticle at 1.1 angstrom resolution. *Science* **2007**, *318*, 430–433.

(44) Dass, A.; Holt, K.; Parker, J. F.; Feldberg, S. W.; Murray, R. W. Mass Spectrometrically Detected Statistical Aspects of Ligand Populations in Mixed Monolayer Au25L18 Nanoparticles. *Journal of Physical Chemistry C* **2008**, *112*, 20276–20283.

(45) Shichibu, Y.; Negishi, Y.; Tsukuda, T.; Teranishi, T. Large-scale synthesis of thiolated Au25 clusters via ligand exchange reactions of phosphine-stabilized Au11 clusters. *Journal of the American Chemical Society* **2005**, *127*, 13464–5.

(46) Lopez-Acevedo, O.; Tsunoyama, H.; Tsukuda, T.; Häkkinen, H.; Aikens, C. M. Chirality and electronic structure of the thiolate-protected Au38 nanocluster. *Journal of the American Chemical Society* **2010**, *132*, 8210–8.

(47) Devadas, M. S.; Bairu, S.; Qian, H.; Sinn, E.; Jin, R.; Ramakrishna, G. Temperature-Dependent Optical Absorption Properties of Monolayer-Protected Au 25 and Au 38 Clusters. *The Journal of Physical Chemistry Letters* **2011**, *2*, 2752–2758.

(48) Guo, J.; Kumar, S.; Bolan, M.; Desireddy, A.; Bigioni, T. P.; Griffith, W. P. Mass spectrometric identification of silver nanoparticles: the case of Ag32(SG)19. *Analytical chemistry* **2012**, *84*, 5304–8.

(49) Zhu, M.; Lanni, E.; Garg, N.; Bier, M. E.; Jin, R. Kinetically controlled, high-yield synthesis of Au-25 clusters. *Journal of the American Chemical Society* **2008**, *130*, 1138–+.

(50) Walter, M.; Akola, J.; Lopez-Acevedo, O.; Jadzinsky, P. D.; Calero, G.; Ackerson, C. J.; Whetten, R. L.; Groenbeck, H.; Hakkinen, H.; Grönbeck, H.; Häkkinen, H. A

unified view of ligand-protected gold clusters as superatom complexes. *Proceedings of the National Academy of Sciences of the United States of America* **2008**, *105*, 9157–9162.

(51) Chaki, N. K.; Negishi, Y.; Tsunoyama, H.; Shichibu, Y.; Tsukuda, T. Ubiquitous 8 and 29 kDa gold: Alkanethiolate cluster compounds: Mass-spectrometric determination of molecular formulas and structural implications. *Journal of the American Chemical Society* **2008**, *130*, 8608–+.

(52) Negishi, Y.; Nobusada, K.; Tsukuda, T. Glutathione-protected gold clusters revisited: bridging the gap between gold(I)-thiolate complexes and thiolate-protected gold nanocrystals. *Journal of the American Chemical Society* **2005**, *127*, 5261–70.

(53) Gilbertson, J. D.; Vijayaraghavan, G.; Stevenson, K. J.; Chandler, B. D. Air and water free solid-phase synthesis of thiol stabilized au nanoparticles with anchored, recyclable dendrimer templates. *Langmuir□: the ACS journal of surfaces and colloids* **2007**, *23*, 11239–45.

(54) Yau, S. H.; Varnavski, O.; Gilbertson, J. D.; Chandler, B.; Ramakrishna, G.; Goodson, T. Ultrafast Optical Study of Small Gold Monolayer Protected Clusters: A Closer Look at Emission †. *The Journal of Physical Chemistry C* **2010**, *114*, 15979–15985.

(55) Lang, H. F.; May, R. A.; Iversen, B. L.; Chandler, B. D. Dendrimer-encapsulated nanoparticle precursors to supported platinum catalysts. *Journal of the American Chemical Society* **2003**, *125*, 14832–14836.

(56) Lee, C.; Yang, W.; Parr, R. G. Development of the Colle-Salvetti correlation-energy formula into a functional of the electron density. *Physical Review B* **1988**, *37*, 785–789.

(57) Kim, J.; Lee, D. Size-controlled interparticle charge transfer between TiO2 and quantized capacitors. *Journal of the American Chemical Society* **2007**, *129*, 7706–+.

(58) Kim, J.; Lee, D. Electron hopping dynamics in Au-38 nanoparticle Langmuir monolayers at the air/water interface. *Journal of the American Chemical Society* **2006**, *128*, 4518–4519.

(59) Varnavski, O.; Ramakrishna, G.; Kim, J.; Lee, D.; Goodson, T. Critical size for the observation of quantum confinement in optically excited gold clusters. *Journal of the American Chemical Society* **2010**, *132*, 16–7.

(60) Kumar, S.; Bolan, M. D.; Bigioni, T. P. Glutathione-stabilized magic-number silver cluster compounds. *Journal of the American Chemical Society* **2010**, *132*, 13141–3.

(61) Yeh, H.-C.; Sharma, J.; Han, J. J.; Martinez, J. S.; Werner, J. H. A DNA-Silver Nanocluster Probe That Fluoresces upon Hybridization. *Nano Letters* **2010**, *10*, 3106–3110.

(62) Neidig, M. L.; Sharma, J.; Yeh, H.-C.; Martinez, J. S.; Conradson, S. D.; Shreve, A. P. Ag K-Edge EXAFS Analysis of DNA-Templated Fluorescent Silver Nanoclusters: Insight into the Structural Origins of Emission Tuning by DNA Sequence Variations. *Journal of the American Chemical Society* **2011**, *133*, 11837–11839.

(63) Sharma, J.; Yeh, H.-C.; Yoo, H.; Werner, J. H.; Martinez, J. S. A complementary palette of fluorescent silver nanoclusters. *Chemical Communications* **2010**, *46*, 3280–3282.

(64) Richards, C. I.; Choi, S.; Hsiang, J.-C.; Antoku, Y.; Vosch, T.; Bongiorno, A.; Tzeng, Y.-L.; Dickson, R. M. Oligonucleotide-stabilized Ag nanocluster fluorophores. *Journal of the American Chemical Society* **2008**, *130*, 5038–+.

(65) O'Neill, P. R.; Velazquez, L. R.; Dunn, D. G.; Gwinn, E. G.; Fygenson, D. K. Hairpins with Poly-C Loops Stabilize Four Types of Fluorescent Ag-n:DNA. *Journal of Physical Chemistry C* **2009**, *113*, 4229–4233.

(66) Petty, J. T.; Fan, C.; Story, S. P.; Sengupta, B.; Iyer, A. S. J.; Prudowsky, Z.; Dickson, R. M. DNA Encapsulation of 10 Silver Atoms Producing a Bright, Modulatable, Near-Infrared-Emitting Cluster. *Journal of Physical Chemistry Letters* **2010**, *1*, 2524–2529.

(67) Petty, J. T.; Zheng, J.; Hud, N. V; Dickson, R. M. DNA-templated Ag nanocluster formation. *Journal of the American Chemical Society* **2004**, *126*, 5207–5212.

(68) Zheng, J.; Zhang, C. W.; Dickson, R. M. Highly fluorescent, water-soluble, size-tunable gold quantum dots. *Physical Review Letters* **2004**, *93*.

(69) Yau, S. H.; Abeyasinghe, N.; Orr, M.; Upton, L.; Varnavski, O.; Werner, J. H.; Yeh, H.-C.; Sharma, J.; Shreve, A. P.; Martinez, J. S.; Goodson, T. Bright two-photon emission and ultra-fast relaxation dynamics in a DNA-templated nanocluster investigated by ultra-fast spectroscopy. *Nanoscale* **2012**, *4*, 4247–54.

Chapter 3

Experimental Techniques

Overview

The various optical experimental techniques in this dissertation are utilized over several publications. This section presents a general introduction and some relevant operational details for specific instruments. Outlining the experimental techniques this chapter will allow the reader to focus on the materials studied in the later chapters.

3.1 Steady State Absorption and Emission

Steady state spectroscopy conducted in our group focus on two major processes: absorption and fluorescence. In the spectroscopic study of metal nanosystems, steady state spectroscopy provides a significant amount of details as a starting point for characterization. The information obtained by the steady state spectroscopy help guide the ultra-fast and non-liner studies.

Ultra Violet and Visible (UV/Vis) absorption spectroscopy is based on the the principle of the Beer-Lambert law (equation 3.1).[1] The intensity of the light (I) absorbed is related to the concentration ([c], mol/L), path length (l, cm) and the molar extinction coefficient (ε, $M^{-1}cm^{-1}$) (equation 3.1). The absorption of light corresponds to the excitation of specific transitions.[1] The experiment is usually performed in the solution phase in a quartz cuvette. The absorption of light is measured by the ratio of the power of the incident light and the power of the light after passing through the sample. Absorption at specific wavelength (optical density, O.D.) can be used to determine the concentration

of a specific sample using the molar extinction coefficient (ε, $M^{-1}cm^{-1}$). In practice, the use of the molar extinction coefficient is the only way to determine the concentration of metal nanocluster systems. Additionally, the control of O.D serves as a quick way to maximize the signal to noise ratio for ultrafast experiments. The O.D. for the samples is adjusted by the concentration. For time correlated fluorescence up-conversion the O.D is adjusted to 1 at the excitation wavelength and 0.5 for ultrafast transient absorption at the excitation wavelength.

Equation 3.1 $$A = \log\frac{I_o}{I} = \varepsilon \times [c] \times l$$

Absorption experiments are carried out with an Agilent Model 8341 spectrophotometer. The spectrometer utilizes two set of lamps for UV/Vis generation. The lamps are deuterium and tungsten and provide a spectra ranging from 200-1100 nm. The samples were contained in a quartz cuvette manufactured by Starna. The cuvette (or cell) has a path length of 0.5 cm. To ensure that absorption data is free from contaminations from the environment, a blank spectrum is taken with the same cell containing either solvent or air. The collected blank spectrum was subtracted from the final spectrums. The cell is capped to ensure sample stability and is stored in a dark environment to protect against possible photo degradation.

Steady state emission (fluorescence) measures the light emitted by the sample under specific excitation. The emission process is the reverse process of the absorption, and is typically lower in energy than absorption.[1] There are two major parameters for the emission process, the wavelength of the emission and the emission strength. The wavelength of the emission can be directly measured by the instrument. The emission strength is represented by the quantum yield (Q.Y. or Φ), which is the efficiency of the system to convert absorbed photons into emitted photons.[2] The determination of the quantum yield for the unknown solution is based on the quantitative comparison between a standard and the unknown across a series of concentrations. The unknown sample and

the standard should have similar absorption and emission wavelengths to maximize accuracy.[3] Equation 3.2 is used to calculate the Q.Y.

$$\textbf{Equation 3.2}\quad \Phi_{sample} = \Phi_{STD}\left(\frac{Grad_{sample}}{Grad_{STD}}\right)\left(\frac{\eta^2_{sample}}{\eta^2_{STD}}\right)$$

The Q.Y of the sample (Φ_{sample}) is calculated by the product of the Q.Y of the standard (Φ_{STD}) multiplied by the gradient of sample ($Grad_{sample}$) divided by the gradient of the standard ($Grad_{STD}$). The Q.Y. is also corrected by the respective reflective index of the solvents (η). The gradient of the sample and standard is the slop of the concentration vs integrated fluorescence counts.

The steady state emission spectra were measured using a SPEX Fluoromax-2 fluorimeter. A Xenon lamp is the main excitation light source and a diffraction grating is used for wavelength selection. The SPEX fluorimeter has a resolution of ~1 nm for both excitation and emission. The emission spectrum is collected with a photomultiplier tube and has excellent sensitivity from 300 nm to about 750 nm. The sample cell used in absorption is used for emission measurement to ensure consistency. The emission spectrum is collected 90° to the excitation beam. In addition to fluorescence detection, the SPEX Fluoromax-2 allows for excitation measurement. The excitation spectrum measures emission strength over a range of excitation wavelengths. The measurement is usually carried out by monitoring the maximum emission wavelength. The observed maximum wavelength corresponds to the maximum absorption wavelength that couples strongly to the emission, but it is not necessarily the strongest absorption wavelength.

3.2 Time resolved fluorescence up-conversion

Steady state emission measurements can give useful information about the emission process of nanosystems, however these measurements do not give any detail about the chemical dynamics of the system. The chemical dynamics are important for understanding the electronic processes that occur in the excited state. Fluorescence up-

conversion has a time resolution of ~100 femtoseconds (fs, 1×10^{-15} second) and can measure the relaxation of the excited state.

Fluorescence up-conversion is based on the principle that emission signal from the sample can be mixed with a laser signal using the up-conversion process inside a β-barium borate (BBO) crystal. The up-conversion of the emission and laser signal (gate pulse) only occurs when the time and phase of both signals are the same. Time delays between the gate pulse and the excitation pulse is introduced by a delay line, which allows the emission process to be observed with respect to time. The fluorescence up-conversion setup uses a Millennia-pumped, Tsunami Mode-Locked Ti:Sapphire laser (Spectra Physics) (figure 3.1). The laser has a pulse duration of 120 fs at 780-820 nm with a repetition rate of 82 MHz and an average output power of ~700 mW. The main up-conversion process is provided by a FOG-100 system (CDP Inc.). The main excitation uses the 800 nm pulse (figure 3.1, red) converted to a 400 nm pulse (figure 3.1, blue) using a BBO crystal (Nonliear Crystal 1, NC1). The 400 nm beam is the main excitation source of this system. It is important to note that 800 nm excitation is possible by removing the BBO (NC1), which will provide a two-photon excitation process.[4] The 800 nm photons not converted to 400 nm are used as the gate pulse (figure 3.1, red). The gate pulse is guided into an optical delay line (figure 3.1). The delay line is a computer controlled mirror that changes the beam path. Lengthening and shortening of the beam path allows for respective increase or decrease in beam travel time. The gate pulse is different in time compared to the excitation beam. The 400 nm excitation beam is focused on the sample (S) after a Berek compensator (B) to control for the polarization of excitation. Fluorescence up conversion has the advantage of investigating the relative polarization of the excitation and emission beam, but it is not required in this work due to the high symmetry of the nanoclusters.

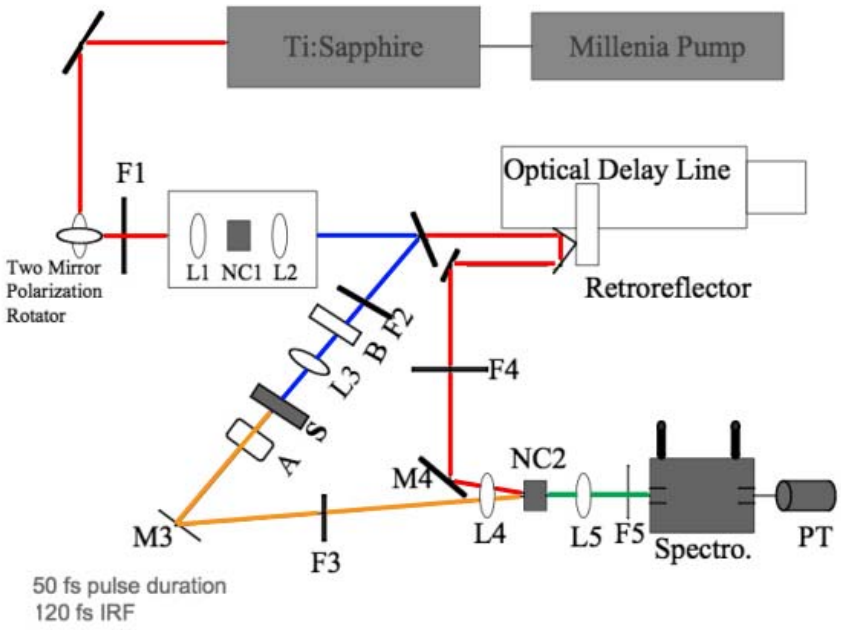

Figure 3.1 Optical diagram for time resolve fluorescence up-conversion.

The fluorescence from the sample (figure 3.1, orange) and the gate pulse are is focused onto a second BBO crystal (NC2). The emission and the 800 nm (gate) beams are spatially and temporally overlapped. The resulting sum frequency radiation (figure 3.1, green) has a wavelength typically around 300-400 nm, this is the up-converted signal. The exact wavelength is calculated by the program used during the data collection. The up-converted signal is focused onto a monochromator. The monochromater uses a grating to select for a specific wavelength. The selected wavelength is detected by a photomultiplier tube (PMT), whose signal is collected by the computer. The computer software Lumex controls the delay line for the gate pulse and gives time-correlate emission signals. The resulting kinetics date represents the fluorescence dynamics at a specific wavelength, with a step resolution of 6.25 fs, limited by the delay line step size. The experiment can collect emission information up to ~1 ns. To ensure sample stability, steady state measurements were performed prior and post-excitation as a method of sample verification.

Unlike steady state emission and absorption, samples were prepared in a rotating cell. Using two quartz glass plates and a teflon spacer, the cell is housed inside a metal

casing. The optical density (absorption at specific wavelength) of 1 is desired to give the best signal to noise ratio. The cell is mounted on a ball bearing and attached to a motor through a plastic bell. The cell is rotated at a controlled speed to minimize photo-damage from prolonged exposure to the high-energy beam.

The florescence up-conversion data collected by the software is analyzed in Origin and math-lab. Because the laser has a pulse duration of ~100 fs, the laser excitation is measured as the instrument response function (IRF). The IRF is part of the detected signal and has a Gaussian shape. The IRF also establish the zero (time) position for the measurement. Chemical dynamics near the timescale of the instrument function is obscured by the IRF, but the signal can be deconvoluted using a program wrote by our lab using the MatLab environment. Briefly, the program calculates the signal by taking the dot product of four different exponential functions, with the IRF being the first exponential. Manual variation of the different parameters such as amplitude and lifetime allows us to fit the experimental data to the calculated signal. The fitted life-times (up to four) provide detailed dynamics to the emission process.

3.3 Ultrafast Transient Absorption

Beside fluorescence up-conversion, our group also employs other ultrafast instrument to measure chemical dynamics. Transient Absorption (TA) is a pump probe technique for investigating the excited state dynamics.[5] TA using an ultrafast excitation beam (~120fs) by a single photon excitation and a probe beam from 450-750 nm. The probe beam is a white light continuum (WLC) probe and it is time-delayed with respect to the excitation bea,. The absorbance measured by the probe is subtracted from the steady state absorption spectrum. The recorded difference in absorption is the measure TA spectrum. The TA spectrum contains three dimensions of data: changes in absorbance, wavelength and time. Figure 3.4 illustrate the principle of TA spectroscopy. The pump excites the sample from the S_0 state to the S_1 state, after a certain amount of time the probe beams measures the absorption from the S_1 state to the S_n state (figure

3.2). The time delay between the pump and the probe pulse is controlled by a optical delay line.

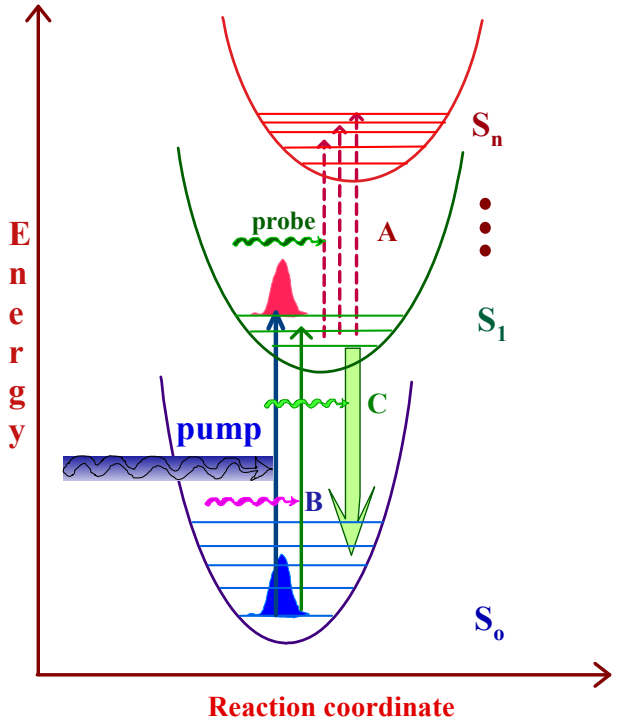

Figure 3.2 Basic principles behind transient absorption spectroscopy. The system is excited by the pump beam and is probe by the probe beam at a later time.

Base on the wavelength and the life-times of TA features, it is possible to monitor singlet→triplet transitions, bleach recovery of the ground state, vibrational cooling, thermalization and several other important transitions. There are three types of transient absorption signals. A positive change in absorbance (ΔA) is recorded when the sample have transitions that can absorption photons in the excited state, known as excited state absorption (ESA). When the ground state of the sample has already absorbed some photons prior to the excitation pulse, the probe beam will not be absorbed and a negative change in absorption ΔA is recorded, this is known as bleaching. It is also possible for the excited state to be emissive, which also result in a negative ΔA signal, and this is the case of stimulated emission.

The transient absorption setup used in the Goodson lab is based on a Helios system produced by Ultrafast Systems Inc (figure 3.3). In order to use the Helios with multi-wavelength excitation, a much higher power source is needed. The light source used in this set up is a 532 m, continuous wave laser (Millennia, Spectra-Physics) at 4.61 Amps output. The output beam is guided into a Tsunami (Spectra Physics) Ti:Sapphire system. The Tsunami is an active acoustic driver pulsed system, capable of generating seed pulses at 800 nm and ~20 fs resolution at ~100 MHz. The seed pulse has energy on the order of nanoJoules. The seed pulse is measured by an ocean optics unit for pulse width and wavelength (figure 3.5). The typical seed pulse is center around 800 nm with a width of 50 nm at half max. The seed pulse is used in regenerative amplification to produce the high energy pulse usesd in the Helios. The regenerative amplification process first stretches the wavelength of the seed pulse, and combines it with a high power beam (Empower at 7.5W output) in the Ti:Sapphire crystal. The resulting beam is gated by Pockel Cells. The final beam is recompressed to produce an amplified pulse with a time resolution of ~100f s, at 800 nm and 1KHz. The average power for the system is 900 mw – 1 W.

The amplified beam is split by a beam splitter into 20/80 pulses. 20% of the pulse is directed into the Helios unit for probe beam white light generation, while 80% of the beam is guided into the Optical Parametric Amplifier (OPA, Spectra Physics). The OPA allows for a large range of wavelength tuning, and is used as the excitation beam. The OPA uses a variety of nonlinear frequency conversion process, which could be either an up-conversion or down-conversion process to achieve a wide spectra range from 350 nm to 2000 nm. Inside the OPA, the output beam from the amplifier (80%) is further split into two separate beams. One of beams is used for white light generation and the other for optical parametric generation (or know as the pre-amp). The white light is generated by a Ti:Sapphire plate and is focused onto the main BBO Crystal (here by refer to as BBO1). Optical parametric generation (OPG) is the amplification of a specific part of the white light inside BBO1. The pre-amp beam passes through a delay stage before arrive at BBO1. The pre-amp beam arrives at the same spot as the white light on BBO1, under

spatial and temporal overlap at BBO1, a OPG signal should be visible with a strong intensity (know as the "green flash"). The successful generation of OPG signal depends largely on the stability of the white light. An excellent white light should not flicker and should be circular. Stable white light generation is also a sign that the amplified beam has the correct duration. The spatial and temporal overlap of the pre-amp and the white light is essential in detecting the OPG. During my work with the OPA, the best method for white light and pre-amp alignment is the lengthening of the BBO1 cavity as the usual distance of the alignment is not sufficient. Since part of the pre-amp beam is in the infrared, the use of a CCD camera also aids the alignment process. The timing selection of the overlap should also be handled with care and patient. A stable OPG will affect all optics down stream and should be treated with utmost care. The generated OPG after BBO1 should be focused 6 cm after BBO1, any other focus distance, (epsically closer to the crystal) can damage the BBO and should be avoided. The resulting output (OPG) from the crystal consists of a signal and an idler beam. The signal is removed using dichroic mirrors and is redirected into the other side of BBO1.

Power amplification increases the power output of the final beam. The power amplification process also requires temporal and spatial over lap of the OPG beam and the power amplification beam. The resulting beam centers around 500 nm and has a average power of 100 mw. The beam consists of a signal and idler component and can be separated based on their polarization. Residual 800 nm beam is removed using a dichroic mirror. Additional BBO crystals (BBO2 and BBO3) allow for second or fourth harmonic generation and proved wavelengths from 300 nm – 2 μm.

The Helios unit uses the output beam from the amplifier and guided into the optical delay line. The time controlled pulse is focused onto a Ti:Sapphire plate after the delay line. The generated while light ranges from 450 to 750 nm. The probe beam is time delayed from the excitation beam with a computer controlled optical delay line. The white light is then overlapped with the pump beam in a 2 mm quartz cuvette containing the sample, the change in absorbance of the probe light is collected by a CCD detector (Ocean optics® 2000). Data acquisition is controlled by the software from Ultrafast

Systems Inc. Typical power of the probe beam is ~ 10 □J/cm^2 while the pump beam is ~1000 □J/cm^2. Magic angle polarization is maintained between the pump and probe using a wave plate in order to avoid any contributions from anisotropy due to polarization. Pulse duration is obtained from the non-resonant fitting of the solvent response, and it is found to be ~120 fs. The sample is stirred with a rotating magnetic stirrer to prevent degradation.

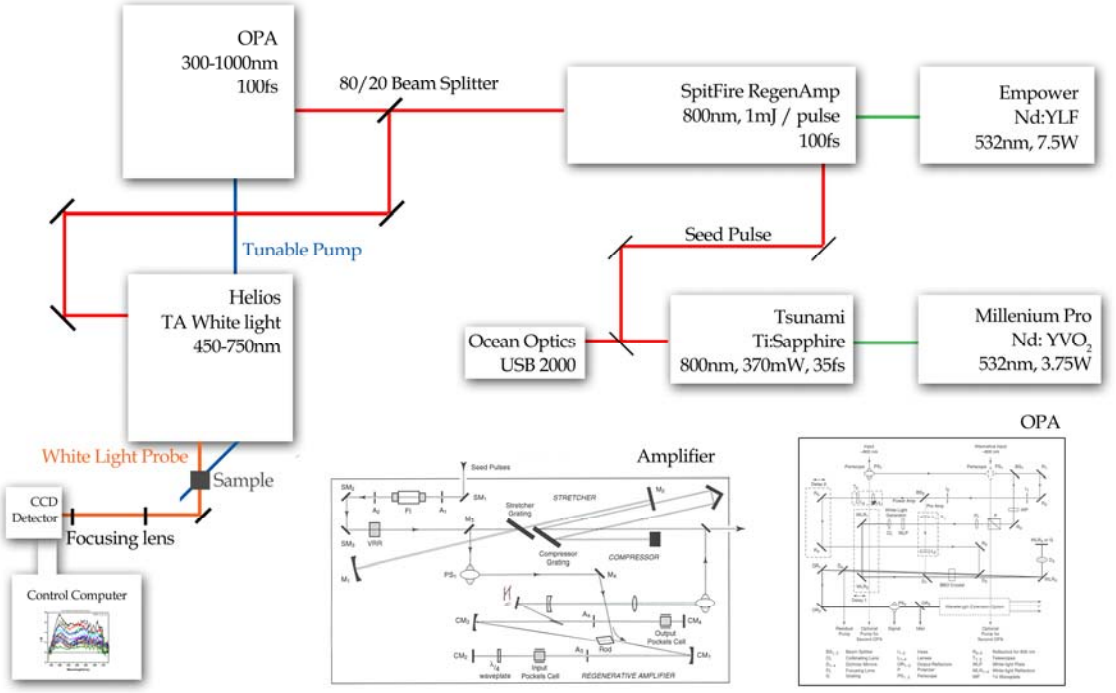

Figure 3.3 Transient absorption spectrometer in the Goodson Lab, an amplified system is used to drive a Helios and a OPA unit.

3.4 Two-photon excited Fluorescence

Two-photon absorption is a non linear optical process that requires two-photon of lower energy to excite a system.[6] This process requires the simultaneous absorption of two photons, and can only be achieved by pulsed laser systems. Due to the fact that two different excitation photons are required for this process, it is an intensity-squared dependent process. An example of this process is the absorption of two 800 nm photons to excited an system to a state that requires a 400 nm photon. (Figure 3.4) The relaxation

of the excited state should be similar to the one photon process, which can emissive or non-emissive.

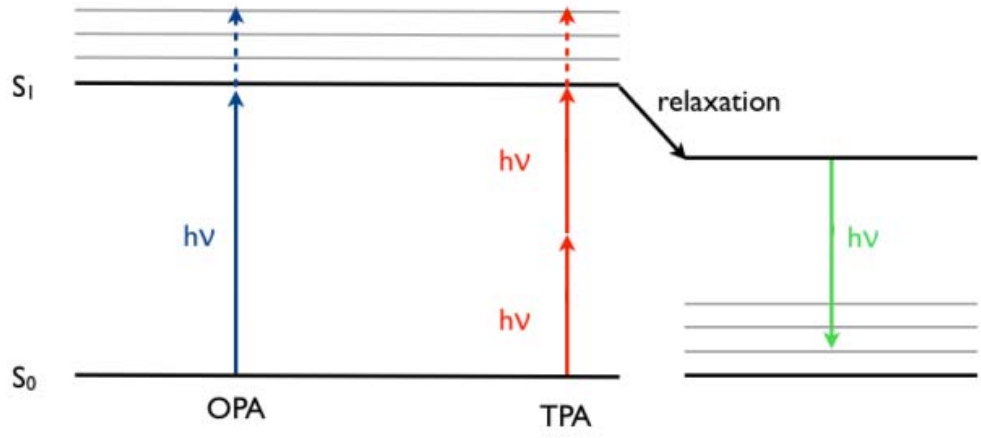

Figure 3.4 Jabolonski diagram for two-photon absorption process

Two-photon absorption spectroscopy was first predicted by Maria Göppert-Mayer, and was experimentally proven when laser systems were developed decades later.[6] The low average power of pulsed systems makes observation of two-photon excited fluorescence possible. Experiments performed by the Goodson group focused on two-photon excited fluorescence, which can be used to calculate the two-photon absorption cross section. Two-photon excited fluorescence is essentially the same process as one-photon excited fluorescence. However, the accessible excited state by two-photon excitation is restricted by different selection rules.

There are two different two-photon excited fluorescence (TPEF) setup used in our group. The results presented in this work originated from one single system. The TPEF setup in the basement lab utilizes a Kapteyn Murnane Laboratories diode-pumped mode-locked Ti:sapphire laser with an excitation range from ~770-830 nm, with peak output powers of ~250-320 mW and ~40 nm pulse widths. The laser output is divided by a piece of optical glass into monitor beam and excitation beam. The monitor beam is guided into a fiber optic cable attached to an OceanOptics spectrometer that provides the wavelength and pulse duration information (figure 3.5). Beam quality and mode-locking (pulsing) of

the laser is adjusted by changing the laser cavity characteristics, specifically the internal prism and slit positions. The excitation beam is directed into a periscope which redirects the laser to the required height and direction. The excitation beam is further guided into a circular variable neutral-density (N.D) filter wheel, which control the excitation power. To monitor the power output of the experiment using a computer interface, the excitation beam is further divided and focuses onto a high-speed silicon photodiode. The photodiode is connected to a computer interfaced multimeter that allows for direct power level recording during fluorescence acquisition. The readout from the multimeter is calibrated per experiment against the average power of the excitation beam (figure 3.5) measured by a power meter.

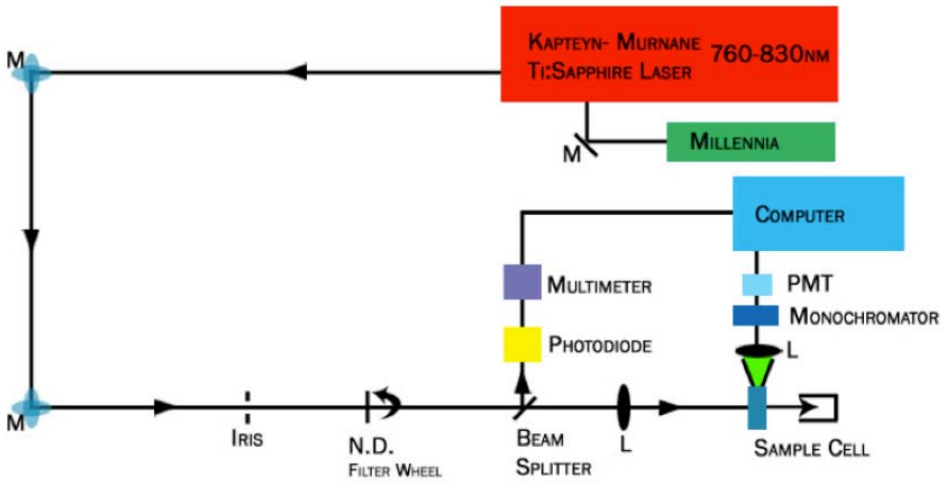

Figure 3.5 Two-photon excited emission set up

The excitation beam is focused onto the sample which is housed inside the protective box for the photomultiplier tube (PMT) and the monochromator. The protective box prevents background light sources from entering the PMT. Emission from the sample is collected perpendicular to the sample, and is focused into the monochromator before being collected by the PMT. The photomultiplier tube is connected to the computer via a photo-counting unit (Hamamatsu) that interfaces and attenuates the detected signal. The set up is control by a set of LabView programs that are developed by our lab, and provide a graphical user interface for data collection. The

programs contain a few parts, the master control program for the PMT, a wave scanning routine and a power dependence routine.

Two-photon absorption cross-sections for samples were calculated base on comparison to a known reference. Typically Coumarin 307 dissolved in methanol is used for studies near 800 nm.[7] The two-photon excited emission is presented in equation 3.3.[7]

$$\textbf{Equation 3.3}\quad F(t) = \frac{1}{2}\eta\delta[c]n * \frac{g_p}{\pi\lambda f\tau}\phi < P(t) >^2$$

F(t) is the fluorescence photons collected per second; η is the fluorescence quantum yield; δ is the two-photon absorption cross-section of the sample in GM; [c] is the sample concentration in molarity; n is the refractive index of the solvent. This first part of the equation is similar to typical quantum yield calculated. It is important to note that since the two-photon excitation process requires high intensity, it is localized in the focus region, so the path length of the sample is not considered. The next term of the equation describes the laser, where g_p is the shape factor for the laser pulse (generally 0.664 for a Gaussian shape); f is the frequency of the pulses from the laser source; τ is the pulse duration. The system collection efficiency is represented by φ. Finally the input intensity is represented by $<P(t)>^2$. Two-photon absorption cross section can be calculated using equation 3.3, but the process can be simplified by comparing the concentration and quantum yield of samples to a known standard, because the laser parameters do not change during the same experiment. The calculation of the cross-section can be done following the outlined procedure below. A simple logarithm of Equation 3.3 has a simple linear form for y = mx+b (equation 3.4).

$$\textbf{Equation 3.4}\quad \log[F(t)] = 2\log[< P(t) >] + \log\left[\frac{1}{2}\eta\delta[c]n * \frac{g_p}{\pi\lambda f\tau}\phi\right]$$

Data from the experiment can be graphed as the log of the fluorescence vs the log of the input power. The data can be fitted with a linear line with a slope of 2. The log-log

plot of the power dependence of a sample and a standard should have the same slope. The product of the slope and the input power should be the same for both the sample and the standard. This equivalent relationship than makes the log of the fluorescence intensity minus the b term $b = \log\left[\frac{1}{2}\eta\delta[c]n * \frac{g_p}{\pi\lambda f\tau}\phi\right]$ of the sample and the stand equals to each other which can be further simplified as equation 3.5

$$\textbf{Equation 3.5} \quad \frac{F(t)_{sample}}{F(t)_{std}} = 10^{b_{sample}-b_{std}}$$

At the y intercept, where the log of power (P(t)) is equation to 0, F(t) = b and equation 3.5 can be rearranged into equation 3.6.

$$\textbf{Equation 3.6} \quad \delta_{sample} = \frac{10^{b_{sample}-b_{std}} \times \eta_{std}\delta_{std}[c]_{std}n_{std}}{\eta_{sample}[c]_{sample}n_{sample}}$$

Using equation 3.6, the two-photon absorption of a sample can be calculated using the intercepts from the intensity-power log-log plots, given that the slope is two for the plots. Quantum yields of the samples can be determined using procedures descried in section 3.2. Two-photon absorption crosssections are reported in Göppert-Mayer (GM) with 1 GM = 10^{-50} cm^4 □s□$photon^{-1}$

3.5 Reference

(1) Lakowicz, J. R. *Principles of Fluorescence Spectroscopy*; Springer: New York, 2006.

(2) Rurack, K.; Spieles, M. Fluorescence quantum yields of a series of red and near-infrared dyes emitting at 600-1000 nm. *Analytical chemistry* **2011**, *83*, 1232–42.

(3) Williams, A. T. R.; Winfield, S. A.; Miller, J. N. Relative fluorescence quantum yields using a computer-controlled luminescence spectrometer. *Analyst* **1983**, *108*, 1067–1071.

(4) Ramakrishna, G.; Varnavski, O.; Kim, J.; Lee, D.; Goodson, T. Quantum-sized gold clusters as efficient two-photon absorbers. *Journal of the American Chemical Society* **2008**, *130*, 5032–3.

(5) Ohsako, Y.; Thorne, J. R. G.; Phillips, C. M.; Hochstrasser, R. M.; Zeigler, J. M. Picosecond transient absorption spectroscopy of polysilanes. *The Journal of Physical Chemistry* **1989**, *93*, 4408–4411.

(6) Göppert-Mayer, M. Über Elementarakte mit zwei Quantensprüngen. *Annalen der Physik* **1931**, *401*, 273–294.

(7) Xu, C.; Webb, W. W. Measurement of two-photon excitation cross sections of molecular fluorophores with data from 690 to 1050 nm. *Journal of the Optical Society of America B-Optical Physics* **1996**, *13*, 481–491.

Chapter 4

Gold Nanoclusters

4.1 Original Publication Information

The work in this chapter was published in two separate publications:

"Ultrafast Optical Study ofSmall Gold Monolayer Protected Clusters: A Closer Look at Emission" Sung Hei Yau, Oleg Varnavski, John D. Gilbertson, Bert Chandler, Guda Ramakrishna, and Theadore Goodson III. *Journal of Physical Chemistry C,* **2010**, *114*, 15979-15985

"An Ultrafast Look at Au Nanoclusters" Sung Hei Yau, Oleg Varnavski, and Theadore Goodson III. *Accounts of Chemical Research*, ***2013*** Article ASAP DOI: 10.1021/ar300280w

Modifications to the original document were made solely for adapting the content to present the two papers in a coherent manner. This chapter is base largely on the second publication, as to provide a larger scope of the work of the Goodson group in the field of nanoclusters. The impact of the first paper on Au_{55} is inserted through out the chapter.

4.2 Abstract

Research involving nano-materials in the past 20 years is credited with the discovery of many new and interesting properties not found in bulk materials. Extensive research has focused on metal nanoparticles (> 2 nm) because of their useful applications and unusual optical properties. The discovery of metal nanoclusters (< 2 nm) has greatly

expanded the horizon of nano-material research. Metal nanoclusters exhibit molecular-like characteristics as their size approaches the Fermi-wavelength of an electron. The relationships between size and physical properties for nanomaterials are very interesting. Particularly, the changes in the optical properties have provided tremendous insight into the electronic structure of nanoclusters. The success of synthesizing monolayer protected clusters (MPCs) in the condensed phase has allowed scientists to probe the metal core directly. Gold MPCs have become the "gold" standard in nanocluster science, thanks to the rigorous structural characterization already accomplished. The use of ultrafast laser spectroscopy on MPCs in solution provides the benefit of directly studying the chemical dynamics of metal nanoclusters (core), and their non-linear optical properties.

Various nanoclusters and nanoparticles were studied using steady state and ultrafast spectroscopy in the visible region. Quantum size effects are easily observed in the absorption spectrum. An emission mechanism for nanoclusters is proposed based on the fluorescence up-conversion kinetics and steady state emission results. Nanoclusters and nanoparticles have different emission life-times and two-photon cross-sections. These differences highlight the finer details between the nanoparticles and the nanoclusters, known as quantum size effect. Investigation of the transient (excited state) absorption revealed the excited state dynamics for these nanomaterials. The excited state dynamics of nanoclusters also have unique vibrational breathing modes.

4.3 Introduction

In the past 10 years, nanoscopic materials have elucidated new frontiers in science, medicine and engineering. The development of new types of nanomaterials has lead to the discovery of metal nanoclusters, which have gathered tremendous attention. Bulk metals are well-defined by classical dielectrics,[1,2] and are very well-understood. Recent studies on metal nanomaterials focus on systems comprised of a small group of metal atoms in the nanometer scale. Metal nanosystems have interesting physical properties, such as quantum confinement,[3–6] emission,[7,8] two-photon absorption[9] and other optical phenomena.[10,11] Extensive research in the past decade [6,12–14] initially focused

on the synthesis of size-controlled metal systems; particularly those that approach the Fermi-wavelength of an electron. These metal nanosystems were classified as nanoparticles and nanoclusters. [6,14–17] It is interesting to note that for metal nanosystems in this size regime, the electronic properties are dictated by their sizes and shapes. The tunable size of metal nanosystems offers the possibility of a wide range of applications, including molecular electronics,[3–5,18,19] image markers[8,20] and catalysts[21].

Metal nanoparticles and nanoclusters are defined by their size. Nanoparticles have a metal core larger than about 2 nm, and nanoclusters smaller than about 2 nm.[6,7] However with the exact divide between nanoparticles and nanoclusters are not clear until recently. The division of nanoclusters and nanoparticles arises from their drastically different optical properties.[7,9,16,17] Nanoparticles are already used in many fields, most notably in the field of imaging. In an effort to extend the nano-tool box to an even smaller scale, the community search for even smaller systems, which was later characterized as nanoclusters. Nanoclusters could provide an opportunity for an even wider array of applications. Metal topologies with a small number of atoms such as nanoparticles were first studied in the gas phase[22] (detailed in chapter 1). However, it was not until the condensed phase synthesis of metal nanomaterials that leads to tremendous interest experienced recently. The advancement of the synthesis processes also lead to an expansion of applications, and the study of fundamental physics of these nanosystems. [6,10,14,15,18,23–28] Of the many different synthetic routes developed, Brust's synthesis[29,30] became the foundation for synthesis development, and is the most commonly used.[6,18] In brief, Brust's synthesis use an organic shell (Glutathione) to stabilize and regulate cluster formation from metal salt, creating highly stable metal systems. These systems were later labeled as monolayered protected clusters (MPCs). Using a straightforward "single-pot" synthesis strategy[31], Au(MPCs) can be synthesized with high stability[6,15,18,29,32], and receive much interest in the field. MPCs are considered to have two parts: a metal core and a single layer ligand shell.[15] The simple outer shell allows direct investigation of the metal core in the condense phase and it can be functionalized and adjusted to both polar and non-polar solvents.[13,33] The self-assembly nature of MPCs facilitates the synthesis of highly mono-dispersed products, and the metal core size can be adjusted by the reaction

conditions.[6,15,29,31] The high purity (mono-disperse) and yield of MPCs synthesis allows for the accelerated characterization efforts.[7,18,34,35]

Detailed characterization work on Au nanoclusters leads to the identification of $Au_{25}(SG)_{18}$ [6,18,36–38] and various other species. One of the most definitive characterizations of Au MPCs is the x-ray crystal structure of $Au_{102}(SR)_{44}$[35] and $Au_{25}(SR)_{18}$.[6,10,38,39] The identification of $Au_{25}(SG)_{18}$ also coincides with theoretical work done on Au_{25}[39], giving further evidence to the structural details of the system. Theoretical works on Au_{25} gave insight into the binding motif and the electronic structure of the metal core.[10,15,27,28,39–42]

In this dissertation, nanoclusters Au_{25}, Au_{55}, Au_{102} and Au_{144} are compared to larger Au_{976} and Au_{2406} nanoparticles. I started my work with nanoclusters by studying the optical properties of Au_{55} (the first publication) using steady state and ultrafast spectroscopy in the visible region. The work on Au_{55} highlights the potential of using MPCs as imaging markers and was the first publication on the emission properties of Au_{55} using time-resolved fluorescence technique. The large range of nanoclusters and nanoparticles allows for ultrafast investigation into the fine details between nanocluster and nanoparticles. Some of the works presented on the quantum size effect were investigated with Dr. Oleg Varnavski and Dr. Ramakrishna. This chapter summarizes the work on the optical properties nanoclusters and their impact on the understanding of nanoclusters. The overarching goal of this dissertation is to investigate the fundamental scientific properties of nanoclusters, and further the understanding of nanomaterials in general.

4.4 Sample Preparation

Au_{55} was prepared by previously reported methods[23,43]. Dodecane functionalized generation 5 PAMAM Dendrimers were used to capture gold from an $AuCl_4^-$ solution. The complexed Au cations were subsequently reduced with $NaBH_4$ in pH 9.0 base. Control of the PAMAM generation and metal:dendrimer ratio allows for size control of

the templated particles. The dendrimer-encapsulated Au nanoparticles were extracted into an aqueous solution with tiopronin. The extraction results in Au_{55} nanoclusters with tiopronin as the ligand shell. The sample was initially characterized by UV-visible spectroscopy, specifically looking for the lack the SPR and the presence of small features in the spectrum.

The Au_{25}, Au_{140}, Au_{976} and Au_{2406} samples were prepared using a previously reported procedure, which is a variation of the Brust reaction and capping procedures.[29,44] A metal salt in solution, in this case gold, is reduced with a solution of organic thiols in a reducing environment ($NaBH_4$). For water soluble MPCs, a ligand exchange phase transfer is performed to place polar ligand on the MPCs.

The calculated absorption spectrum utilized the calculation method based on our previous paper following the Gans extension of the Mie Theory (chapter 1).[1,45] The dielectric constant of the surrounding medium was taken to be 2, the simulated metal system is considered to be spherical with a diameter of particle is 1.1 nm (Au_{25}). The spectrum is calculated from 390 to 800 nm, at 10 nm intervals.

4.5 Electronic Absorption and Structure of Gold Clusters

The structure of metal nanoparticles and their electronic and optical properties are directly related, so it is important to understand the structure of MPCs for our discussion. The characterization of gas phase metal clusters various MPCs leads to the discovery of "magic numbers", similar to metal nanoparticles in the gas phase. [22] Only metal cores with certain sizes are found for MPCs, these magic number nanoclusters exhibit high stability with similar optical and physical properties. [32,46] These small metal clusters can be modeled based on their physical packing.[24] The stability of the larger nanoparticles can be explained by the physical packing of the metal core. However, physical packing alone cannot account for the various sizes observed and leads to the development of the "super atom" theory.[15] The super atom theory adopts ideas from semi-conductors and gas phase metals, and it treats the metal core as a single atom within the system. The highly

stable cluster core numbers are the result of the systematic closing of outer electronic shells, similar to the Jellium and Kubo models.[2,22] The simplest unit of Au MPCs was identified to be a 13 atom icosahedral core[34,37,38] and some of the magic clusters are found to be based on the same motif (physical packing or electron shell closing). It should be noted that Au_{102} does not follow the icosahedral packing, but it does follow the electronic shell closing regime.[35] Most of the MPCs share a fundamental unit (Au_{13}), and should exhibit very similar physical properties. The treatment of the metal core as a super atom also gives rise to the idea of discrete (molecular like) energy levels for metal nanoclusters. Beside the super atom theory, the free electron modelcan also be used to describe nanoclusters (chapter 1). [6]

The direct effect of core size on the electronic structure for nanoclusters is known as the Quantum Size Effect. Our detailed investigations used various optical techniques to investigate the quantum size effect for Au MPCs and found that the major optical difference between nanoparticles and nanoclusters can be observed around 2.2-3 nm, in agreement with the free electron model. Moreover, nanoparticles were found to be more similar to bulk metals and could be described by Mie theory.[1,7,45] Mie Theory utilizes Maxwell's equation to describe light interaction with metal nanoparticles and accounts for the Surface Plasmon Resonance (SPR). SPR is the collective excitation mode of the conduction electrons in the metal core, and it has been shown that enhanced emission from metal nanoparticles is caused by the SPR.[16,20,21] Control of the size and shape can directly affect the SPR, making nanoparticles a tunable image marker.[20] A comparison of the various steady state absorption spectra in figure 4.1 indicates the difference between nanoclusters and nanoparticles. The SPR at 500 nm is only observed for the nanoparticle, Au_{2406}. Based on Mie theory, [1,7,45] a simple model is used to simulate the absorption spectrum for a gold nanoparticle similar in size to Au_{25}. The calculated absorption spectrum used the dielectric constant of the surrounding medium to be 2, and the system is spherical with a diameter of 1.1 nm. The calculation predicts the appearance of a surface plasmon band at 520 nm, which is not observed in the experiment. This demonstrates that Mie theory (and its extensions), does not apply to nanoclusters. [1,2,45,47,48] Fine comparison between the various nanoclusters indicates the difference in

core size and their electronic structure. It is reported that absorption peaks for Au_{25} are correlated to the icosahedral structure of the core.[15,25,27,34] In particular, the three distinct features in the absorption in the absorption feature at 688 nm, 450 nm and 400 nm can be correlated to sp-d, sp-sp and a mix of sp-sp sp-d transitions respectively. As the size of the nanoclusters increases, these features are weakened, and suggest that molecular characteristic of the system is decreasing. The change in absorption spectrum in respect to size is a direct evidence of quantum size effect.

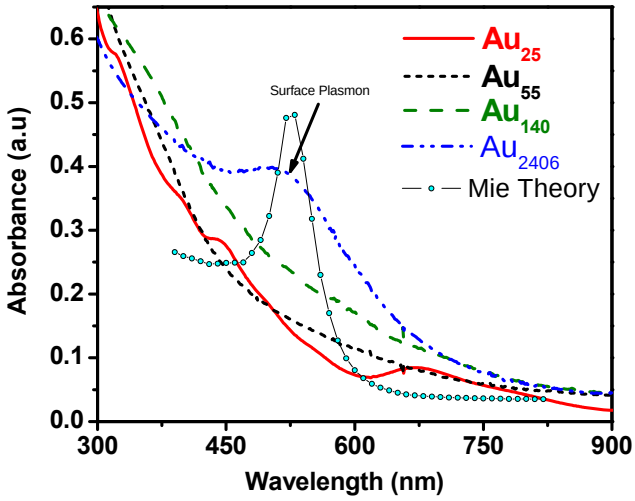

Figure 4.1 Steady state absorption for Au_{25} Au_{55}, $Au_{140,}$ Au_{2406} and Mie theory calculation using parameter similar to $Au_{25.}$[7]

The absorption features for Au_{25} can also be correlated to the transient absorption spectrum.[15,25,27,34] In our transient absorption spectra, we observed an additional absorption feature that we proposed to be related to the ground state.[7] The details will be discussed in the transient absorption section. In an attempt to resolve more details from the absorption spectrum, the Ramakrishna group[11] looked at the absorption spectra for Au_{25} and Au_{38} systems at low temperatures and observed changes to the absorption maximum, along peak sharpening and an increase in the oscillator strength.[11] Their model attributes the effect of the electron-phonon interaction with phonons in the metal-ligand interface.[11] Overall the absorption spectra of various Au nanoclusters and particles are clear evidence for quantum size effects.

4.6 Emission Mechanism of Gold Clusters

Quantum confinement effects clearly predict discrete energy levels within the nanoclusters systems, and it is theoretically possible to observe emission.[2,7,15] Emission from MPCs was initially affronted with skepticism, due to the uncertainty in the purity of the materials and the less-than-satisfactory characterization. Studies were carried out to look at the contribution from the ligand shell and the metal core separately, and it was found that neither component contributes to the emission.[49,50] In our contribution, one–photon excitation was used to observe two different emission wavelengths in the steady state, confirmed by time-resolved kinetics.[7] In particular, a complete study was done on Au_{55}. The emission of nanoclusters is commonly found to be in the visible and the near-infrared region.[7,8,47,50] For Au_{55} fluorescence centered at 500 nm was detected under 390 nm excitation (figure 4.2). Using Coumarin 307 as a standard, the quantum yield of Au_{55} is calculated to be 1.25 $x10^{-5}$. The sample was also excited with different wavelengths in the range of 360-390 nm, No shift in the emission spectra was detected (figure 4.2), which rule our contributions from solvent or scattering. The emission of Au_{55} has been an area of interest since its discovery as a dendrimer-captured nanocluster. The synthetic materials used in the synthesis of gold nanoclusters are found be non-fluorescent. This emission from the native metal core have many applications in imaging.[50,51] The emission from Au_{55} was also investigated by the Murray group in an Ag exchange reaction.[38] Their experiment started with Ag MPCs, and the silver is exchanged for gold while the emission from the system is monitored. However, their investigation was using the emission as a method to trace the metal exchange process, and did not provide detail into the emission process itself. It is exciting to note that fluorescence from Au_{25} and Au_{140} has been reported previously (table 4.1).[50,52] The quantum yield for visible emission of Au_{55} is 5 orders of magnitude stronger than the 10^{-10} reported for bulk gold.[7,53]Compared to the estimated Q.Y for Au_{25} and the experimental result from Au_{140}, the Q.Y for Au_{55} is comparable in the visible reign. For $Au_{25,}$ the Q.Y for the NIR it is much stronger than the visible emission.[50]

	Au25	Au 55	Au 140-145
Q. Y. (%)	$2.5x10^{-4}$* (3.5 x 10^-3)	2.5x10^-5	Not reported ($4.4x10^{\wedge-5}$)
Excitation (λ)	300-900nm(800nm)	390nm	400nm (1064nm)
Emission (λ)	500 nm (1100nm)	500nm	525nm (1100nm-1600nm)

Table 4-1 Comparison of quantum yield, excitation wavelength and emission wavelength of various gold nanoclusters, values in parentheses are for fluorescence in the near infared.[7,49,50,52,54]

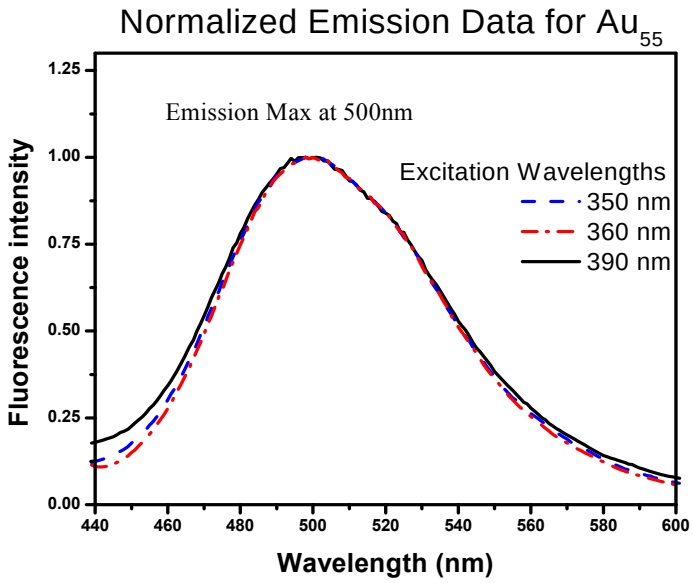

Figure 4.2 Normalized Emission spectra for Au $_{55}$, excited at 350, 360 and 390nm.

To better understand the emission mechanism, time-resolved fluorescence up-conversion was used to resolve the fluorescence life-time of various gold nanoparticles and nanoclusters (Figure 4.3).[7,9] Fluorescence up-conversion data for Au_{55} is shown in figure 4.4 to demonstrate the experimental data and fitting. The comparison between the fluorescence life-time of nanoclusters and nanoparticles from 1.1 nm to 4 nm yields interesting results (Figure 4.3). There is a clear distinction between the emission life-times of nanoparticles and nanoclusters. In our previous investigation,[16] emission from nanoparticles is associated with the recombination of the *d*-hole by an Auger type process, which has a short life-time of 50 fs (Figure 4.4), on the order of the instrument response function (see Chapter 2 for detail explanation of the instrument respond function). The emission life-time for nanoclusters, however, is much longer than that of

nanoparticles and can be fitted with a single exponential, which is characteristic of molecular-like singlet decay relaxation process.[7] (Figure 4.3, 4.4) The longer life-times are caused by the energy transition of discrete energy levels, similar to molecular emissions. The rise of molecular emission life-time can also be associated with the quantum size effect, a clear distinction between nanoparticles and nanoclusters at 2.2 nm can be made.

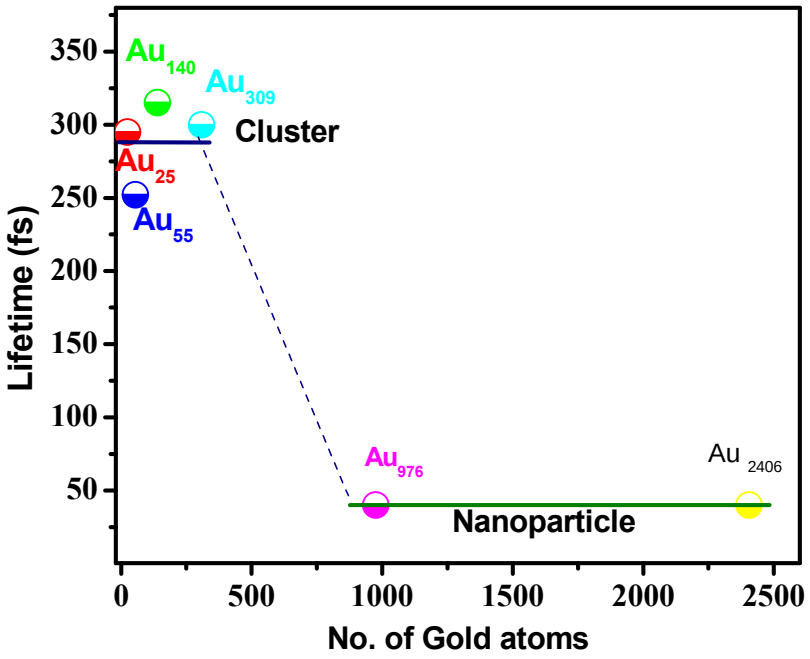

Figure 4.3 Fluorescence life time comparisons for MPCs of various sizes. The most notable difference is between the nanoparticle and nanoclusters.[7]

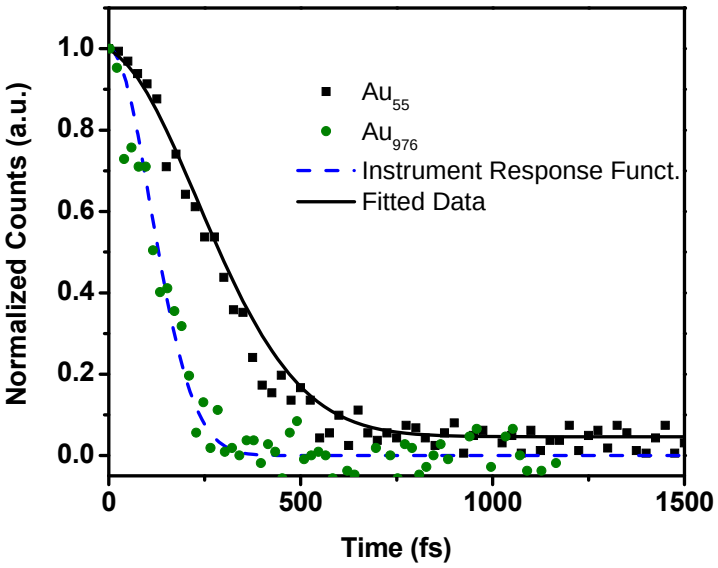

Figure 4.4 Time resolved visible emission for Au_{55} and Au_{976}. The life time of Au55 is about ~250fs. The emission from Au_{976} is faster than the instrument response function (blue line).[7]

Based on our steady state and fluorescence life-time studies, we proposed an energy diagram for nanoclusters (Figure 4.5) using Au_{55} as a base model. The steady state emission studies suggest that the dual-wavelength emission from Au MPCs follows two very different mechanisms.[7] The emission in the visible region is fast and very short-lived (hundreds of fs), and it is most likely to be associated with the metal core (State B).[7,17] The near-infrared emission is related to the surface states that arise from the interaction with the ligands.[8,15,50] It has been reported that the polarity of the ligand has a direct effect on the emission efficiency.[6,50] In MPCs, the metal core and the metal-ligands bonds do not contribute directly to the metal core, based on the super atom theory. However, when we treat the metal core as one single "super atom", the ligands field can split the energy levels of the metal core, which can give rise to emissive states, also know as surface states.[8,27,54]

The time-resolved fluorescence studies suggest that the short-lived visible emission originates from the filling of the ground state hole by an electron from the

excited state (Figure 4.4, B band).[7] This mechanism, however, is very different from the Auger recombination process for nanoparticles, which has a much faster life-time.[16,45] Compared to theoretical studies of Au_{25} clusters, this transition is similar to the HOMO-LUMO+1 process.[10,15] It is possible that the small quantum efficiency observed is cause by non-radiative transition of the HOMO-LUMO gap (A band). The near-infrared emission is the result of energy transitions from the surface states, the energy originates from the A band, but the exact couple strength between the two states are not known. Additionally, the absence of dynamic Stokes shift in our results suggests that the energy transfer between the A state and the surface state is quick, leading to the strong near infrared (NIR) emission.[7,8,15,47,50]

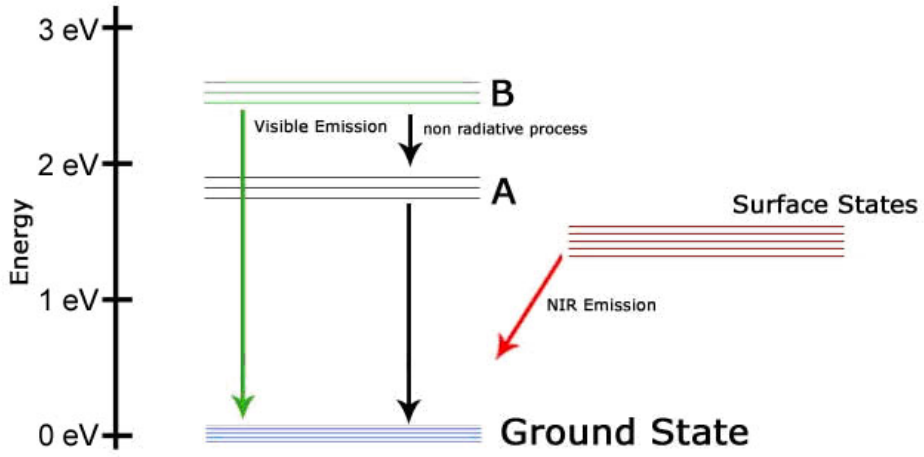

Figure 4.5 Transition energy diagram for the emissions for MPCs, using data from steady state emission, fluorescence up conversion and transient absorption.[7]

4.7 Two Photon Excited Emission in Gold Clusters

The relatively strong emission under single-photon excitation for Au MPCs leads to the possibility of two-photon excited emission. Two-photon/multi photon excited emissions are beneficial for low power medical imaging. Au MPCs also have the potential to be an optical limiting material with its large two-photon cross-section.[9] We expected to observe a scaling law for the two-photon absorption (TPA) coefficient as a function of the core size.[7,9] Two-photon excited emission was first reported with Au_{25}

under 1290 nm excitation, and the emission peak was found at 830 nm (Figure 4.6a). The quadratic intensity dependence of the fluorescence indicates that it is a two-photon excited emission (Figure 4.6b) or a non-linear process. The TPA cross-section was measured to be 2700 GM using H_2TPP (Tetraphenylporphyrin) in toluene as a standard, about 1-2 orders of magnitude higher than many organic chromophores.[9]

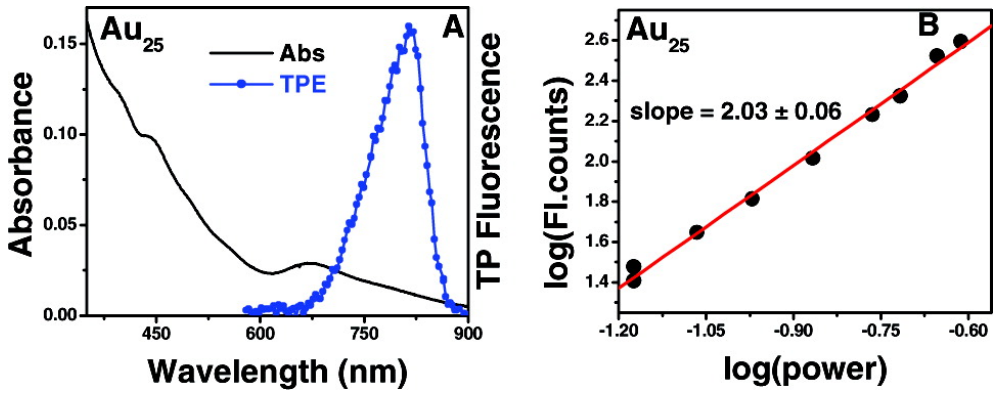

Figure 4.6 A) Two-photon excited fluorescence from Au_{25}. B) Pump power dependence for the two-photon excited emission.[9]

In addition to the two-photon emission in the near-infrared region, the emission in the visible region is also observed (Figure 4.7). A large scale study done by Dr. Ramakrishna investigated a range of sizes from gold nanoparticle (4 nm) down to Au_{25} clusters (1.1 nm), under 800 nm excitation. The emission wavelength maxims were found to have a dependence on size for both nanoparticles and nanoclusters. For nanoclusters, the emission is in the 500-535 nm range, while nanoparticles emit around 550 nm. The difference in the emission wavelengths for the nanoclusters and nanoparticles is the result of the difference in energy gaps between HOMO and LUMO, which is affected by the variation in size.[9] The tunable emission wavelengths for nanoclusters is one of the most attractive features for imaging. The fluorescence quantum yield under two-photon excitation is on the order of 10^{-7} to 10^{-8}. Fig. 4.7b, d, f, h, j presents the power dependce for the observed emission, clearly indicating the emission is two-photon excited.[9]

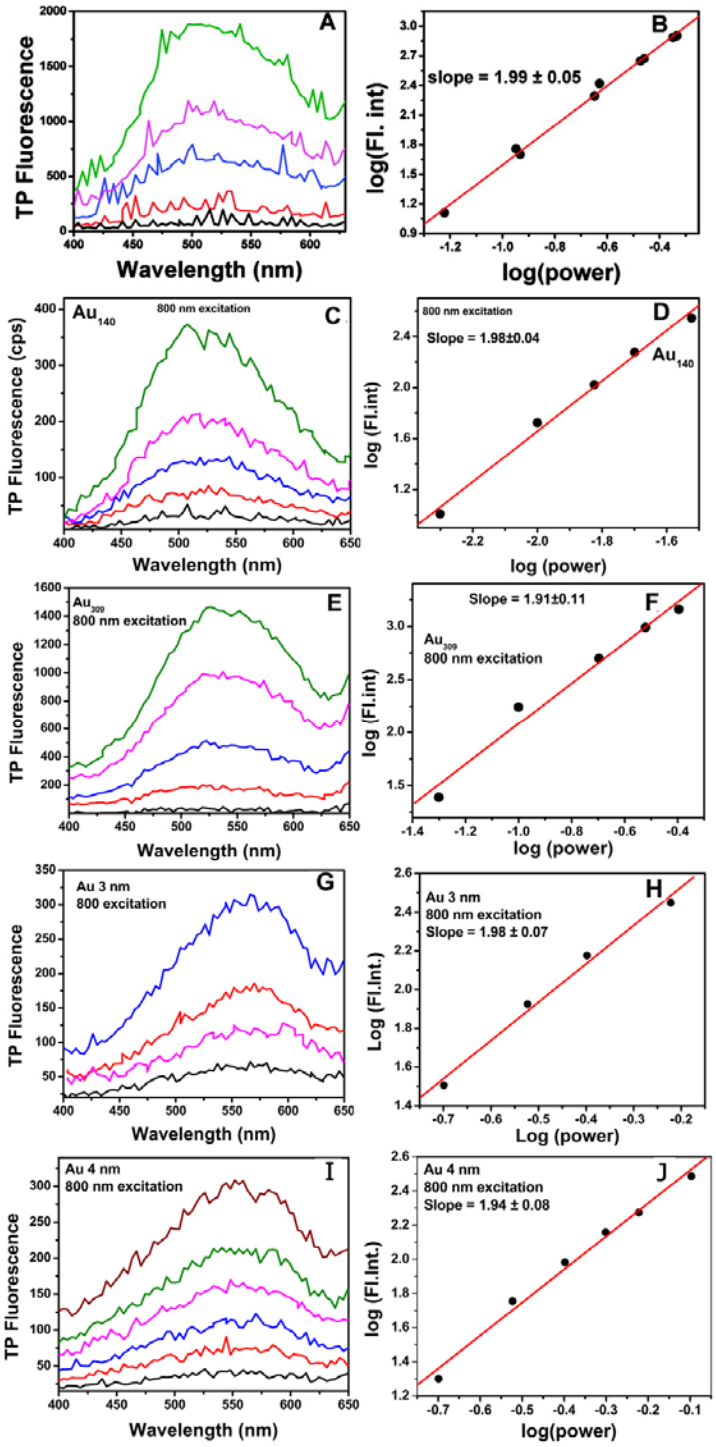

Figure 4.7 Two-photon excited emission and corresponding power dependence for MPCs of various sizes. A,C,E,G,I are the emission spectrum for Au_{25}, Au_{140}, Au_{309}, Au 3nm and Au 4nm respectively. B,D,F,H,J are corresponding power dependence.[9]

Due to the low quantum efficiency of these systems, measurement with a Spex-Fluorolog fluorimeter is difficult; two-photon excited femtosecond time-resolved fluorescence up-conversion[9] was used to ensure accurate measurement of the TPA cross-section. The fluorescence kinetic traces for all gold clusters are measured with both one- and two-photon excitation. Using the ratio of the relative counts per second at 100 fs time delay, the TPA cross-sections for the gold clusters are determined. Absolute TPA cross-sections observed for the gold clusters are much larger than any of the experimentally investigated organic macromolecules or semiconductor nanocrystals.[9] The TPA cross-section for Au_{25} is 427,000 GM and Au_{309} is 1,476,000 GM, much larger compared to a typical value of approximately 1000 GM at 800 nm for organic macromolecules. The large TPA cross-sections prophet the application of MPCs in optical power limiting, nanolithography, and multiphoton biological imaging. Comparisons of the two-photon cross sections of various MPCs also reveal scaling laws regarding core size and two-photon absorption cross-section (Figure 4.8a). There are two different trends, one for nanoclusters and the other nanoparticles. For nanoclusters, an increase in size is accompanied by an increase of the total two-photon cross-section. Nanoparticles Au_{976} and Au_{2406} follow a separate but similar trend. Analysis of the cross-section per atom (Figure 4.8b) reveals that the cross-section decreases with increasing cluster size. However, the correlation of size vs. cross-section is much smaller for nanoparticles. The increase in cross-section per atom between nanoparticles and nanoclusters could be due to quantum confinement effect. The increase in cross-section within nanoclusters could possible be due to the confinement of the d-electrons of the metal core, which is the result of the interband and intraband mix transition under 800 nm excitation.

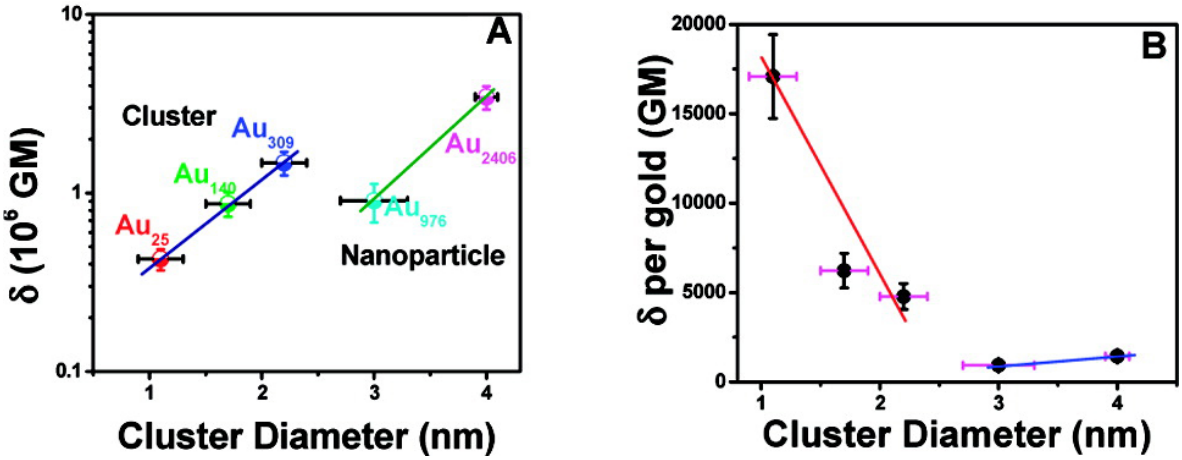

Figure 4.8 A) TPA cross sections for Au_{25} to Au_{2406} using two-photon excited fluorescence up-conversion. B) The TPA cross section calculated per atom. Red is for nanoclusters and blue is for nanoparticles.[9]

Results from our fluorescence life-time measurements and two-photon cross-sections clearly demonstrate that there are differences between nanoclusters and nanoparticles. The distinction between nanoclusters and nanoparticles occurs at 2.2 nm, very close to the estimation made with the free electron model.[6] The very large cross section for Au nanoclusters in the infrared IR spectral regions hold tremendous potential as an imaging tool, due to the fact that two-photon excitation in the IR region would allow for much deeper penetration into tissues with lower overall energy, which is a very desirable trait for medical imaging. [9,20,55–58]

4.8 Transient Electronic Effects in Gold Nanoclusters

Transient absorption spectroscopy in the femtosecond scale allows for the study of excited state dynamics. The transient absorption of nanoparticles and nanoclusters has been studied previously.[7,17,26,59,60] Our group focuses on the degenerate transient absorption (same wavelength pump and probe) as well as multi-color transient absorptions (450 nm – 750nm) of Au_{25}, Au_{55} and Au_{140} .[7,26] Transient absorption spectra of Au_{25}, Au_{55} and Au_{140} are compared at a time delay of 550 fs in figure 4.9.[7] The characteristic SPR at 530 nm is not observed for the three nanoclusters. Excited state absorption (ESA) can be observed at 500 nm and 675 nm. The analysis of transient

dynamics of Au_{25} nanoclusters with different charges (0,-1)[59] shows that the ESA signal near 670 nm can be bleached after 1 ns. This signal corresponds to the HOMO-LUMO transition in the Au core[7,26,27]. Comparison of the various Au nanoclusters emphasizes a positive correlation between the absorption and the core size, which we believe to be related to the quantum size effect.[7] The kinetic trace at 640 nm for Au_{55} (Figure 4.9) exhibits a quick initial relaxation to the intermediate state and then a slow decay back to the ground state. This decay profile is analogous to molecular-like systems with single electron relaxation processes.[7,16,607,16,55] Based on the work of Miller et al[26] and Qian et al[59], the observed dynamics of the nanoclusters suggest a core-core HOMO-LUMO charge transfer (~1 ps) followed by a core-shell charge transfer (>1 ns).[59]

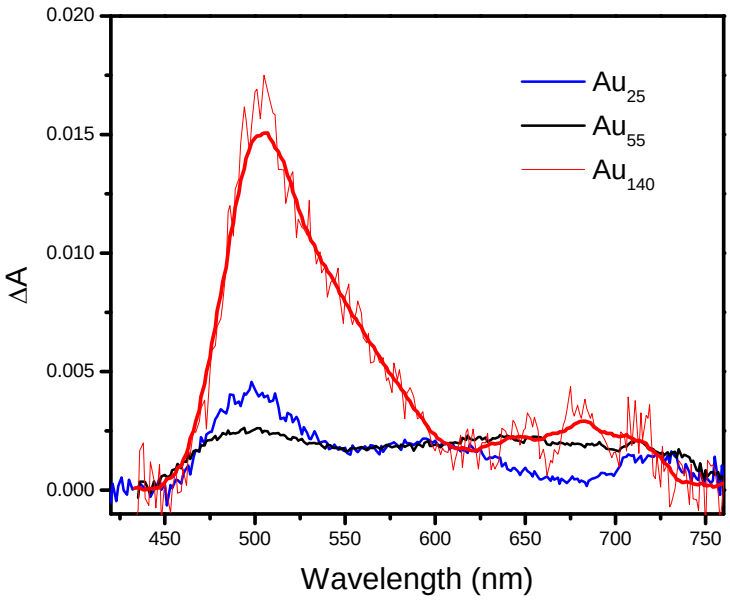

Figure 4.9 Transient absorption for Au_{25}, Au_{55} and Au_{140}, at 550 fs.[7]

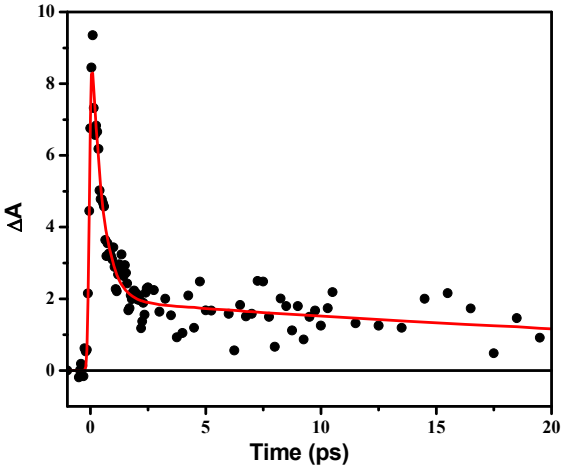

Figure 4.10 The kinetic trace from transient absorption for Au_{55} at 640nm.[7]

For nanopartilces, transient absorption can often resolve energy transfer in the system and other processes such as the electron-electron scattering and electron-phonon coupling.[54,58,61–63] The change in transmission of light of metals can be describe as the interaction of light with the dielectrics of the systems (equation 4.1).

Equation 4.1 $$\frac{\Delta T}{T}(\omega_s) = \frac{\partial \ln T}{\partial \varepsilon_1}(\omega_s)\Delta\varepsilon_1(\omega_s) + \frac{\partial \ln T}{\partial \varepsilon_2}(\omega_s)\Delta\varepsilon_2(\omega_s)$$

Equation 4.1 can be rewritten as the change in the density of states under laser excitation, which two different energy pathways are possible (equation 4.2). After excitation of an electron *L(k,t)*, the excited electron can redistribute its energy by electron-electron (e-e) scattering, which occurs in the hundreds of femtoseconds time scale. After the energy is redistributed within the electron gas (thermalization of internal temperature), energy of the electron gas can be transfer to the lattice via electron-phonon (e-ph) coupling which occurs in the picoseconds time scales.[61–63]

Equation 4.2 $$\frac{df(k)}{dt} = \left.\frac{df(k)}{dt}\right|_{e-e} + \left.\frac{df(k)}{dt}\right|_{e-ph} + L(k,t)$$

Interpreting the excitated state kinetics, equcation 4.2 can be written as equation 4.3. The e-e scatting and e-ph coupling can be measured directly in the excited state dynamics as a rise time and decay time respectively (equation 4.3).

Equation 4.3 $u(t) = H(t)[1 - \exp(-t/\tau_{e-e})]\exp(-t/\tau_{ph})$

For the e-e scatting process, the energy redistribution is a very fast process under weak excitation, and is power independent, but depends strongly on the system size.[61] For e-ph coupling, the laser excitation energy can affect the specific heat of the electrons gas which affects the decay life-time.[63] Using power dependence for $Au_{55,}$ the electron-electron and electron-phonon relaxation processes (figure 4.13) can be investigated. The life-time of the dynamics of Au_{55} is not power dependent, which is consistent with the reported very weak e-ph coupling strength based on temperature dependent fluorescence study. [64] The weak e-ph coupling of nanoclusters also strongly suggest that nanoclusters are molecular like, and lacks the electron gas which is required for electron-phonon coupling. It is important to point out that because e-ph coupling is a type of non-radiative decay, the lack of e-ph coupling can be used to explain the increase Q.Y for Au nanoclusters. Even though the e-ph coupling is weak, phonons affects can be observed as coherent oscillations (see below).

Detailed analysis of the transient data also uncovers additional information about Au nanoclusters, the bleach near 550 nm (Figure 4.11, 4.12) can be correlated the absorption spectrum.[7] Using the same analysis as the work by Moran et al, the bleach at 550 nm could be assigned to another ground state for the Au_{25} system.[7,26] This new major ground state has not been reported in other publications, and could potentially be used in refining existing models.

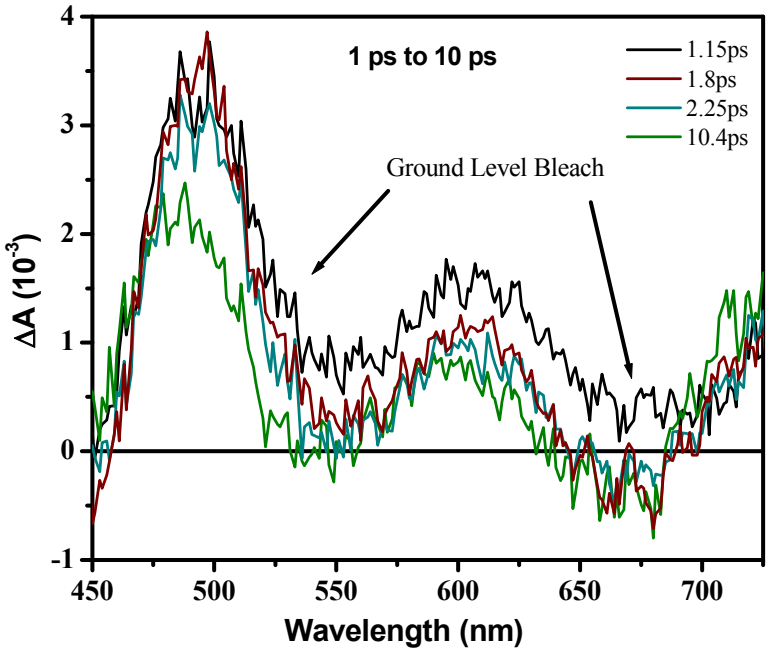

Figure 4.11 Transient absorption of Au_{25} in hexane, probed from 450nm to 750nm. Ground level bleach can be observed at 550 nm and 675 nm.

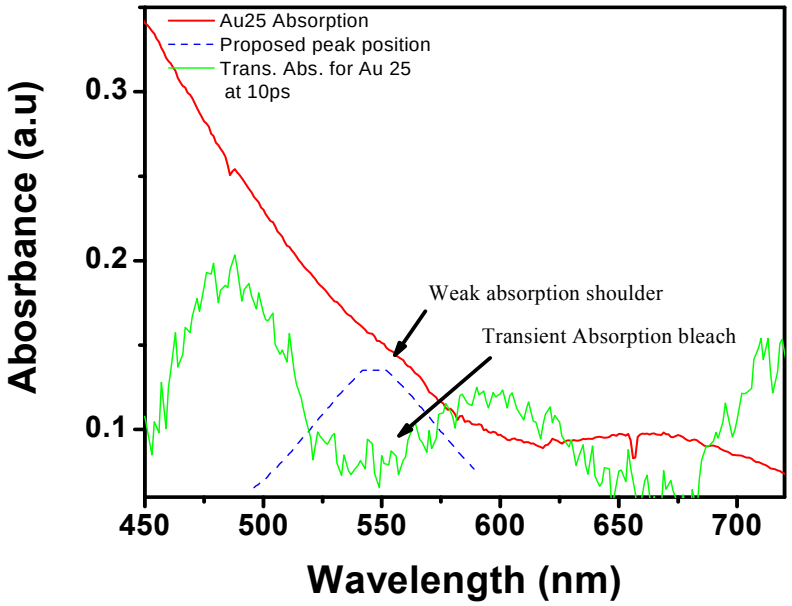

Figure 4.12 Steady state absorption compared to transient absorption for Au_{25}, with ground level bleach at 550 nm.[7]

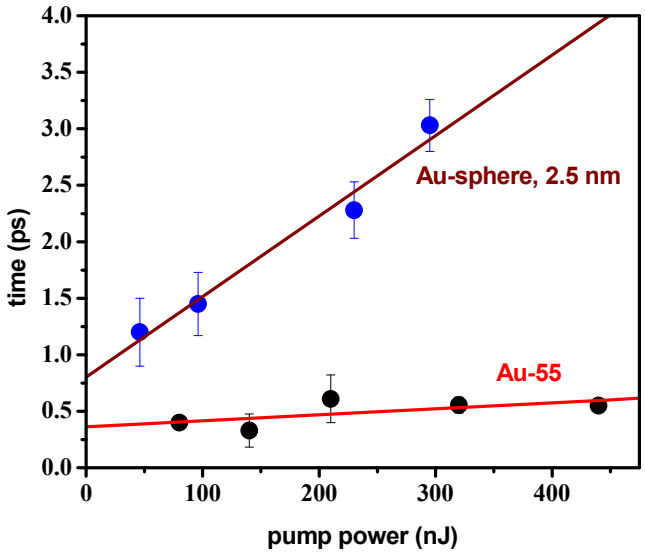

Figure 4.13 Pump power dependence against average life time for 2.5nm nanoparticle and Au_{55} (1.4nm).[7]

Using degenerate pump-probe experiments, the excited state dynamics of the MPCs can be measured in a high time resolution.[7,60] The work by Dr. Varnavski on the acoustic modes and their excitation characteristics in nanomaterials contain important information about the structure, geometry, and their interactions with the environment. The structural assignment of both Au_7 and Au_{20} in the gas phase is accomplished using vibrational spectroscopy, and it is also theoretically predicted that the nature of internal vibrational energy redistribution is a key factor in promoting reactivity of small gold clusters.[65] For gold nanoclusters with polypeptide chains, vibration transfer in the THz range has been predicted using molecular dynamics simulations.[66] Coherently excited "breathing" vibrational modes for gold nanoparticles are proposed with a response time spanning from a few picoseconds to tens of picoseconds.[62,67–69] The breathing mode frequency is also inversely proportional to the particle size. This vibration can be considered the oscillatory motion of the positive charges, or the coherent phonon oscillations. The mechanism for such breathing mode in nanoparticles can be explained using the Jellium model, under the impulsive heating of the particle lattice after short pulse laser excitation, the fast dynamics of the electron gas causes the relative displacement of the positive core. [62,67,68]

Our degenerate transient pump-probe experiment detected oscillations with a period of ~450 fs (2.2 THz, figure 4.15), which compares well to the low-frequency vibrational density of states theoretically calculated for gold clusters. [45,70,71,72] The fast oscillation period is similar to oscillatory features reported for Au_{25}.[71] Based on the oscillatory period, the mechanism is different than nanoparticles and is more closely related to semiconductors and/or molecular systems.[73] Compare to the lack of oscillatory features for nanoparticles, the appearance of the oscillations for small MPCs can be correlated to the emergence of an optical energy gap near the Fermi level.[60] Au nanoclusters of various sizes were tested (Figure 4.14b) and showed frequency independent breathing modes. The lack of size correlation may be an indication that the oscillatory feature is a shared core phenomenon. This oscillatory feature is unique to nanoclusters and could potentially be used in the future as a characterization method.

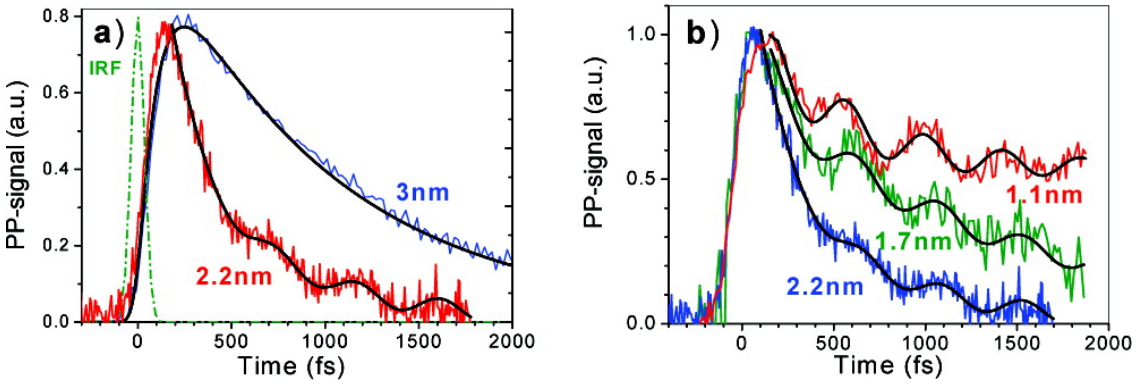

Figure 4.14 A) Degenerate pump-probe experiment on Au MPCs shows clear oscillatory features for nanoclusters. B) Comparison of oscillatory features of nanoclusters of various sizes.[60]

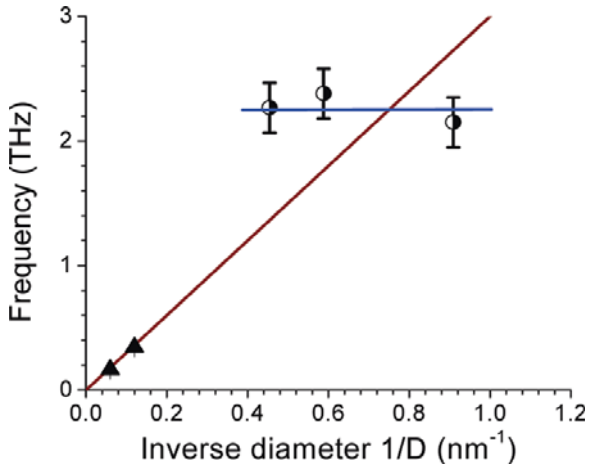

Figure 4.15 Acoustic vibration frequency size dependence. Solid triangles are frequencies of the "breathing" vibrational modes previously observed for larger gold particles. Solid brown line is the classical mechanic calculations for the elastic gold sphere. Horizontal blue solid line is a guide to the eye.[60]

4.8 Transient Electronic Effects in Gold Nanoclusters

Monolayered protected clusters have unique physical and optical properties. The steady state absorption and emission illustrated the quantum size effect of MPCs. The dual emission nature for MPCs confirmed the super atom nature of these materials. Based on various ultrafast spectroscopy techniques, different mechanisms were proposed to explain the visible and infrared emissions of MPCs. Time resolved florescence spectroscopy serves as proof for the weak emission in the visible region for Au_{55}. The quantum yields in the visible region for Au_{55} are five orders of magnitude larger than that of bulk gold. The emission enhancement is due to the discrete energy levels of metal core. The emission can also be assign to the core or the surface state based on their life times. Very large two photon cross-sections were observed for Au MPCs, which suggests future applications of MPCs as an optical limiting material. Based on the fluorescence life-time results, the size distinction between nanoparticles and nanoclusters is ~2.2 nm. Two-photon excited emissions were observed for both nanoclusters and nanoparticles. Nanoclusters have very large two-photon absorption cross-sections, and have tremendous potential as a optical limiting material. Additionally, a scaling law was observed for core size and cross section per atom, adding to quantum size effects. Transient absorptions can be used to resolve the core and surface state transitions. Based on the life-times of the

excited states, the excited state transitions of metal nanoclusters follow molecular like relaxations, very different than nanoparticles. An excited state absorption was identified as an additional ground state that has not been reported previously. The transient kinetic traces of nanoparticles and nanoclusters can directly investigate the e-e scattering and e-ph coupling processes, which are the effects of the electrons. While the vibrational breathing mode found in degenerate transient absorption is a effect of the nucleus and could used in the characterization of nanoclusters in the future. Overall, our optical studies yield many interesting results and also raised many more interesting questions. One of the biggest challenges ahead will be the refinement of unified laws (such as the super atom theory) that govern all nanoclusters, and investigate the relationship between the metal core and its environment, which will better describe the emission and two-photon absorption size effects.

4.9 Thermal Heating of Nanoparticle and Nanoclusters

One of the most promising applications of nanoparticles is the use of nanoparticles in cancer treatment.[74–78] Generally, the nanoparticles are conjugated to a specific bio-target (such as antibodies or antigens) and introduced into the system. The nanoparticles will bind to the specific sites, such as a cancer growth. Optical excitation of the nanoparticle at the plasmon wavelength will cause the absorption of the laser excitation light, and the energy will be dissipated to the surrounding as heat.[77,79,80] The rise in temperature of the nanoparticle leads to cell death of the cancer growth.[74,76,77,81] In the case of nanoclusters, the use of optical thermal heating has not been investigated, however, the small Q.Y and the lack of electron-phonon coupling of nanoclusters could potentially increase the heat transferred through non-radiative pathways. This section aims to provide a basic discussion on the optical heating of nanoclusters using simple assumptions. Using a fs-pulsed laser excitation, the laser energy can be characterized as an average irradiance $<I>$, pulsation rate f at a specific wavelength. Under laser excitation the absorbed energy (ε_0) is presented in equation 4.4.[80]

Equation 4.4 $$\varepsilon_0 = \sigma_{abs} < I > / f_0$$

For nanoclusters and nanoparticle, the transient kinetics proves that the electron-electron scattering occurs ~100 fs, which suggests that "electrons gas" or the core thermalizes instantaneously. So that equation 4.4 holds true for both systems. After the energy is absorbed, the energy can be transfer to the lattice by electron-phonon coupling for nanoparticles or coherent phonons for nanoclusters. After this energy transfer, the lattice should achieve a uniform temperature, but is not in equilibrium with the surrounding medium. The energy is eventually transferred to the medium by external heat diffusion.[80] Under the assumption that the external heat diffusion is the rate limiting step the energy transfers, the nanosystem would reach a maximum temperature (T_{NS}^{0}) above surrounding which is directly related to the input energy (ε_0), volume *(V)*, density *(ρ)* and heat capacity *(c)* (equation 4.5).

Equation 4.5 $$\varepsilon_0 = V\rho_{Au}c_{au}T_{NS}^{0}$$

The maximum temperate achieved for the nanosytems is the most important factor for the external heat transfer and can be rewritten as equation 4.6

Equation 4.6 $$T_{NS}^{0} = \frac{\sigma_{abs} < I >}{V\rho_{Au}c_{Au}f}$$

Consider that a Ti:sapphire laser system would have the a average energy of $1\times10^{2} W/m^{2}$ and a repetition rate of 1 KHz, the density of gold can be taken to be $19\times10^{3} kg/m^{3}$, with a heat capacity of 129 $J/Kg*K$, we can calculate the maximum temperate in the case of nanoparticles and nanoclusters under femtosecond excitation. For a 20 nm nanoparticle, the molar extinction has been reported to be $8\times10^{9} M^{-1}cm^{-1}$ which equals to an absorption cross-section of $3.06\times10^{-15} m^{2}$, and using the above parameter a spherical 20 nm nanoparticle will achieve a internal temperature of 29.3 K.[82] For the case of Au_{25}, the diameter is 1.2 nm and the molar extinction has been reported to be

$8\times10^{3}\,M^{-1}cm^{-1}$ at 670 nm and can be calculated based on the absorption spectrum to be $1.6\times10^{4}\,M^{-1}cm^{-1}$ and a cross-section of $6.11\times10^{-21}\,m^{2}$ at 500 nm.[54,83] (Closer to the SPR of nanoparticles for comparison), and Au_{25} would obtain a maximum temperature of 0.28 K. The dramatic different between nanoclusters and nanoparticles is mainly caused by the dramatic decrease in the absorption cross-section. For nanoparticles, there is a scaling law for the absorption cross-section and the radius where the cross-section increases linearly with increasing volume.[78] In respect to heat exchange, the heat absorbed by the nanoparticle is not strongly dependent on the size. However there is a 6 orders of magnitude decrease in the cross-section from the 20 nm nanoparticle to the 1.2 nm nanocluster while the volume is only changing by 3 orders of magnitude. This results in the low temperature in the case of Au_{25}, which is unexpected and should be investigated in the future. The simple explanation is that SPR greatly enhances the absorption cross-section which is the major factor in the thermal heating. However, this simple calculation does not internal energy lost, which is weaker in the case of nanoclusters due to the weaker electron-phonon coupling.

For the case of two-photon excitation, the calculation of the energy absorbed is based on the number of photons absorbed times the energy per photon, represented by equation 4.7.[9] The calculations are based on a laser system with averaged 260mW power, with a repetition rate of 82MHz.

Equation 4.7 $$\varepsilon_0 = \left(\frac{\sigma_{TPA} n l W_{TPE}^2}{4\pi^{3/2} r_\omega^2 \tau_p (\hbar\omega_{TPE})^2}\right)\hbar\omega_{TPE}$$

The σ_{TPA} is the two-photon absorption cross-section, W_{TPE} is the two-photon excitation power (3.2×10^{-9} J), r_ω is the spatial width of the laser (5.85×10^{-4} cm), τ_p is the pulse duration (100 fs), n is the concentration and l is the path length (assume to be 0.1nm) and $\hbar\omega_{TPE}$ is the energy per photon (at 800 nm, 2.48×10^{-19} J).

Assuming nanosystems with a concentration of 10 nM, Au_{25} with a cross section of 467000 GM, the maximum temperature can be calculated to be 39 K. For Au_{2409} with a diameter of 4 nm and a cross section of 3452000 GM, the maximum temperature is 7.9 K.[9] This result is a reversal of what was observed for the one-photon case, but it is consistent with the increase in cross-section per atom. Au_{25} has the highest two-photon absorption per atom among the gold nanosystems, which should lead to more energy absorbed.

The use of nanoclusters in medical thermal thearpy is not yet explored and deserves some basic investigations, especially the use of nanoclusters under two-photon excited in the NIR, which carries the added benefit of deeper tissue penetration by the longer wavelength excitation.

4.10 Summary

Monolayered protected clusters have unique physical and optical properties. The steady state absorption and emission illustrated the quantum size effect of MPCs. The dual emission nature for MPCs confirmed the super atom nature of these materials. Based on various ultrafast spectroscopy techniques, different mechanisms were proposed to explain the visible and infrared emissions of MPCs. Time resolved florescence spectroscopy serves as proof for the weak emission in the visible region for Au_{55}. The quantum yields in the visible region for Au_{55} are five orders of magnitude larger than that of bulk gold. The emission enhancement is due to the discrete energy levels of metal core. The emission can also be assign to the core or the surface state based on their life times. Very large two photon cross-sections were observed for Au MPCs, which suggests future applications of MPCs as an optical limiting material. Based on the fluorescence life-time results, the size distinction between nanoparticles and nanoclusters is ~2.2 nm. Two-photon excited emissions were observed for both nanoclusters and nanoparticles. Nanoclusters have very large two-photon absorption cross-sections, and have tremendous potential as a optical limiting material. Additionally, a scaling law was observed for core size and cross section per atom, adding to quantum size effects. Transient absorptions can

be used to resolve the core and surface state transitions. Based on the life-times of the excited states, the excited state transitions of metal nanoclusters follow molecular like relaxations, very different than nanoparticles. An excited state absorption was identified as an additional ground state that has not been reported previously. The vibrational breathing mode found in degenerate transient absorption shows no size dependence on the mode frequencies and could used in the characterization of nanoclusters. But the vibrational breathing modes are not detected for the larger nanoparticles. Overall, our optical studies yield many interesting results and also raised many more interesting questions. One of the biggest challenges ahead will be the refinement of unified laws (such as the super atom theory) that govern all nanoclusters, and investigate the relationship between the metal core and its environment, which will better describe the emission and two-photon absorption size effects. The field of MPCs is still at its infancy, with many application and fundamental science yet to be explored. We look forward to the new discoveries and opportunities ahead.

4.11 Reference

(1) Mie, G. *Annalen der Physik* **1908**, *330*, 377–445.

(2) Kubo, R.; Kawabata, A.; Kobayashi, S. *Annual Review of Materials ...* **1984**, 49–66.

(3) Chen, S. *Science* **1998**, *280*, 2098–2101.

(4) Ingram, R. S.; Hostetler, M. J.; Murray, R. W.; Schaaff, T. G.; Khoury, J. T.; Whetten, R. L.; Bigioni, T. P.; Guthrie, D. K.; First, P. N. *Journal of the American Chemical Society* **1997**, *119*, 9279–9280.

(5) Schaaff, T. G.; Shafigullin, M. N.; Khoury, J. T.; Vezmar, I.; Whetten, R. L.; Cullen, W. G.; First, P. N.; Gutiérrez-Wing, C.; Ascensio, J.; Jose-Yacamán, M. J. *The Journal of Physical Chemistry B* **1997**, *101*, 7885–7891.

(6) Jin, R. *Nanoscale* **2010**, *2*, 343–62.

(7) Yau, S. H.; Varnavski, O.; Gilbertson, J. D.; Chandler, B.; Ramakrishna, G.; Goodson, T. *The Journal of Physical Chemistry C* **2010**, *114*, 15979–15985.

(8) Wang, G.; Huang, T.; Murray, R. W.; Menard, L.; Nuzzo, R. G. *Journal of the American Chemical Society* **2005**, *127*, 812–3.

(9) Ramakrishna, G.; Varnavski, O.; Kim, J.; Lee, D.; Goodson, T. *Journal of the American Chemical Society* **2008**, *130*, 5032–3.

(10) Zhu, M.; Aikens, C. M.; Hollander, F. J.; Schatz, G. C.; Jin, R. *Journal of the American Chemical Society* **2008**, *130*, 5883–5.

(11) Devadas, M. S.; Bairu, S.; Qian, H.; Sinn, E.; Jin, R.; Ramakrishna, G. *The Journal of Physical Chemistry Letters* **2011**, *2*, 2752–2758.

(12) Alvarez, M. M.; Khoury, J. T.; Schaaff, T. G.; Shafigullin, M.; Vezmar, I.; Whetten, R. L. *Chemical Physics Letters* **1997**, *266*, 91–98.

(13) Ackerson, C. J.; Jadzinsky, P. D.; Kornberg, R. D. *Journal of the American Chemical Society* **2005**, *127*, 6550–1.

(14) Templeton, A. C.; Wuelfing, W. P.; Murray, R. W. *Accounts of Chemical Research* **2000**, *33*, 27–36.

(15) Walter, M.; Akola, J.; Lopez-Acevedo, O.; Jadzinsky, P. D.; Calero, G.; Ackerson, C. J.; Whetten, R. L.; Groenbeck, H.; Hakkinen, H.; Grönbeck, H.; Häkkinen, H. *Proceedings of the National Academy of Sciences of the United States of America* **2008**, *105*, 9157–9162.

(16) Varnavski, O.; Ispasoiu, R. G.; Balogh, L.; Tomalia, D.; Goodson, T. *The Journal of Chemical Physics* **2001**, *114*, 1962.

(17) Varnavski, O.; Ramakrishna, G.; Kim, J.; Lee, D.; Goodson, T. *Journal of the American Chemical Society* **2010**, *132*, 16–7.

(18) Murray, R. W. *Chemical reviews* **2008**, *108*, 2688–720.

(19) Hicks, J. F.; Miles, D. T.; Murray, R. W. *Journal of the American Chemical Society* **2002**, *124*, 13322–13328.

(20) Rosi, N. L.; Mirkin, C. A. *Chemical reviews* **2005**, *105*, 1547–62.

(21) Daniel, M.-C.; Astruc, D. *Chemical Reviews* **2004**, *104*, 293–346.

(22) Knight, W.; Clemenger, K.; De Heer, W.; Saunders, W.; Chou, M.; Cohen, M. *Physical Review Letters* **1984**, *52*, 2141–2143.

(23) Gilbertson, J. D.; Vijayaraghavan, G.; Stevenson, K. J.; Chandler, B. D. *Langmuir : the ACS journal of surfaces and colloids* **2007**, *23*, 11239–45.

(24) Schmid, G. *Chemical Society reviews* **2008**, *37*, 1909–30.

(25) Pyykkö, P. *Chemical Society reviews* **2008**, *37*, 1967–97.

(26) Miller, S. A.; Womick, J. M.; Parker, J. F.; Murray, R. W.; Moran, A. M. *Journal of Physical Chemistry C* **2009**, *113*, 9440–9444.

(27) Aikens, C. M. *The Journal of Physical Chemistry C* **2008**, *112*, 19797–19800.

(28) Aikens, C. M. *The journal of physical chemistry. A* **2009**, *113*, 10811–7.

(29) Brust, M.; Fink, J.; Bethell, D.; Schiffrin, D. J.; Kiely, C. *Journal of the Chemical Society, Chemical Communications* **1995**, 1655.

(30) Brust, M.; Schiffrin, D. J.; Bethell, D.; Kiely, C. J. *Advanced Materials* **1995**, *7*, 795–&.

(31) Wu, Z.; Suhan, J.; Jin, R. *Journal of Materials Chemistry* **2009**, *19*, 622.

(32) Negishi, Y.; Takasugi, Y.; Sato, S.; Yao, H.; Kimura, K.; Tsukuda, T. *Journal of the American Chemical Society* **2004**, *126*, 6518–9.

(33) Shibu, E. S.; Muhammed, M. A. H.; Tsukuda, T.; Pradeep, T. *Journal of Physical Chemistry C* **2008**, *112*, 12168–12176.

(34) Briant, C. E.; Theobald, B. R. C.; White, J. W.; Bell, L. K.; Mingos, D. M. P.; Welch, A. J. *Journal of the Chemical Society, Chemical Communications* **1981**, 201.

(35) Jadzinsky, P. D.; Calero, G.; Ackerson, C. J.; Bushnell, D. A.; Kornberg, R. D. *Science* **2007**, *318*, 430–3.

(36) Negishi, Y.; Nobusada, K.; Tsukuda, T. *Journal of the American Chemical Society* **2005**, *127*, 5261–70.

(37) Tracy, J. B.; Crowe, M. C.; Parker, J. F.; Hampe, O.; Fields-Zinna, C. A.; Dass, A.; Murray, R. W. *Journal of the American Chemical Society* **2007**, *129*, 16209–15.

(38) Heaven, M. W.; Dass, A.; White, P. S.; Holt, K. M.; Murray, R. W. *Journal of the American Chemical Society* **2008**, *130*, 3754–5.

(39) Akola, J.; Walter, M.; Whetten, R. L.; Häkkinen, H.; Grönbeck, H. *Journal of the American Chemical Society* **2008**, *130*, 3756–7.

(40) Iwasa, T.; Nobusada, K. *Journal of Physical Chemistry C* **2007**, *111*, 45–49.

(41) Jiang, D.; Luo, W.; Tiago, M. L.; Dai, S. *Journal of Physical Chemistry C* **2008**, *112*, 13905–13910.

(42) Lopez-Acevedo, O.; Tsunoyama, H.; Tsukuda, T.; Häkkinen, H.; Aikens, C. M. *Journal of the American Chemical Society* **2010**, *132*, 8210–8.

(43) Long, C. G.; Gilbertson, J. D.; Vijayaraghavan, G.; Stevenson, K. J.; Pursell, C. J.; Chandler, B. D. *Journal of the American Chemical Society* **2008**, *130*, 10103–10115.

(44) Balasubramanian, R.; Guo, R.; Mills, A. J.; Murray, R. W. *Journal of the American Chemical Society* **2005**, *127*, 8126–32.

(45) Varnavski, O.; Goodson, T.; Mohamed, M.; El-Sayed, M. *Physical Review B* **2005**, *72*, 235405–.

(46) Negishi, Y.; Chaki, N. K.; Shichibu, Y.; Whetten, R. L.; Tsukuda, T. *Journal of the American Chemical Society* **2007**, *129*, 11322–3.

(47) Lee, D.; Donkers, R. L.; Wang, G.; Harper, A. S.; Murray, R. W. *Journal of the American Chemical Society* **2004**, *126*, 6193–9.

(48) De Heer, W. *Reviews of Modern Physics* **1993**, *65*, 611–676.

(49) Parker, J. F.; Fields-Zinna, C. A.; Murray, R. W. *Accounts of chemical research* **2010**, *43*, 1289–96.

(50) Wang, G.; Guo, R.; Kalyuzhny, G.; Choi, J.-P.; Murray, R. W. *The journal of physical chemistry. B* **2006**, *110*, 20282–9.

(51) J Lin, C.-A.; Lee, C.-H.; Hsieh, J.-T.; Wang, H.-H.; K Li, J.; Shen, J.-L.; Chan, W.-H.; Yeh, H.-I.; H Chang, W.; Lin, C.-A. J.; Li, J. K.; Chang, W. H. *Journal of Medical and Biological Engineering* **2009**, *29*, 276–283.

(52) Devadas, M. S.; Kim, J.; Sinn, E.; Lee, D.; Goodson, T.; Ramakrishna, G. *The Journal of Physical Chemistry C* **2010**, *114*, 22417–22423.

(53) Mooradia.A; Mooradian, A. *Physical Review Letters* **1969**, *22*, 185–&.

(54) Yau, S. H.; Varnavski, O.; Goodson, T. *Accounts of chemical research* **2013**.

(55) Nam, J. M.; Thaxton, C. S.; Mirkin, C. A. *Science* **2003**, *301*, 1884–1886.

(56) Jin, R. *Angewandte Chemie-International Edition* **2008**, *47*, 6750–6753.

(57) Zipfel, W. R. W. *Nature Biotechnology* **2003**, *21*, 1369–1257.

(58) Goodson, T.; Varnavski, O.; Wang, Y. *International Reviews in Physical Chemistry* **2004**, *23*, 109–150.

(59) Qian, H.; Y. Sfeir, M.; Jin, R. *The Journal of Physical Chemistry C* **2010**, *114*, 19935–19940.

(60) Varnavski, O.; Ramakrishna, G.; Kim, J.; Lee, D.; Goodson, T. *ACS nano* **2010**, *4*, 3406–12.

(61) Voisin, C.; Christofilos, D.; Del Fatti, N.; Vallee, F.; Prevel, B.; Cottancin, E.; Lerme, J.; Pellarin, M.; Broyer, M. *Physical Review Letters* **2000**, *85*, 2200–2203.

(62) Voisin, C.; Del Fatti, N.; Christofilos, D.; Vallée, F. *The Journal of Physical Chemistry B* **2001**, *105*, 2264–2280.

(63) Arbouet, A.; Voisin, C.; Christofilos, D.; Langot, P.; Del Fatti, N.; Vallee, F.; Lerme, J.; Celep, G.; Cottancin, E.; Gaudry, M.; Pellarin, M.; Broyer, M.; Maillard, M.; Pileni, M. P.; Treguer, M. *Physical Review Letters* **2003**, *90*.

(64) Toh, Y.-R.; Yu, P.; Wen, X.; Tang, J. *Journal of colloid and interface science* **2013**, *402*, 86–9.

(65) Mitrić, R.; Bürgel, C.; Bonacić-Koutecký, V. *Proceedings of the National Academy of Sciences of the United States of America* **2007**, *104*, 10314–7.

(66) Miao, L.; Seminario, J. M. *Journal of Physical Chemistry C* **2007**, *111*, 8366–8371.

(67) Hartland, G. V *Annual review of physical chemistry* **2006**, *57*, 403–30.

(68) Hodak, J. H.; Henglein, A.; Hartland, G. V. *The Journal of Chemical Physics* **1999**, *111*, 8613.

(69) Plech, A.; Cerna, R.; Kotaidis, V.; Hudert, F.; Bartels, A.; Dekorsy, T. *Nano letters* **2007**, *7*, 1026–31.

(70) Varnavski, O.; Goodson, T.; Sukhomlinova, L.; Twieg, R. *The Journal of Physical Chemistry B* **2004**, *108*, 10484–10492.

(71) Stanzel, J.; Burmeister, F.; Neeb, M.; Eberhardt, W.; Mitrić, R.; Bürgel, C.; Bonacić-Koutecký, V. *The Journal of chemical physics* **2007**, *127*, 164312.

(72) Sun, D.; Gong, X.; Wang, X.-Q. *Physical Review B* **2001**, *63*, 193412.

(73) Zeiger, H.; Vidal, J.; Cheng, T.; Ippen, E.; Dresselhaus, G.; Dresselhaus, M. *Physical Review B* **1992**, *45*, 768–778.

(74) Koo, Y.-E. L.; Reddy, G. R.; Bhojani, M.; Schneider, R.; Philbert, M. A.; Rehemtulla, A.; Ross, B. D.; Kopelman, R. *Advanced drug delivery reviews* **2006**, *58*, 1556–77.

(75) Lee, Y.-E. K.; Kopelman, R. *Wiley interdisciplinary reviews. Nanomedicine and nanobiotechnology 1*, 98–110.

(76) Pissuwan, D.; Valenzuela, S. M.; Killingsworth, M. C.; Xu, X.; Cortie, M. B. *Journal of Nanoparticle Research* **2007**, *9*, 1109–1124.

(77) Dreaden, E. C.; El-Sayed, M. A. *Accounts of chemical research* **2012**, *45*, 1854–65.

(78) Link, S.; El-Sayed, M. A. *International Reviews in Physical Chemistry* **2000**, *19*, 409–453.

(79) Richardson, H. H.; Carlson, M. T.; Tandler, P. J.; Hernandez, P.; Govorov, A. O. *Nano Letters* **2009**, *9*, 1139–1146.

(80) Baffou, G.; Rigneault, H. *Physical Review B* **2011**, *84*, 035415.

(81) Govorov, A. O.; Richardson, H. H. *Nano Today* **2007**, *2*, 30–38.

(82) Jain, P. K.; Lee, K. S.; El-Sayed, I. H.; El-Sayed, M. A. *The Journal of Physical Chemistry B* **2006**, *110*, 7238–7248.

(83) Kogo, A.; Takahashi, Y.; Sakai, N.; Tatsuma, T. *Nanoscale* **2013**.

Chapter 5

Silver Nanoclusters

5.1 Original Publication Information

The work in this chapter was published in two separate publications:

> **"Bright two-photon emission and ultra-fast relaxation dynamics in a DNA-templated nanocluster investigated by ultra-fast spectroscopy"** Sung Hei Yau, Neranga Abeyasinghe, Meghan Orr, Leslie Upton, Oleg Varnavski, James H. Werner, Hsin-Chih Yeh, Jaswinder Sharma, Andrew P. Shreve, Jennider S. Martinez, Theodore Goodson III, *Nanoscale*, **2012,** 4, 4247-4254
>
> **"Ultrafast spectroscopy of $Ag_{32}(SG)_{19}$"** Sung Hei Yau, Oleg Varnavski, and Theadore Goodson III. *Submitted*

Modifications to the original document were made solely for adapting the content to present the two papers in a coherent manner. This chapter will be divided into two major sections, first on $Ag_{32}(SG)_{19}$ followed by DNA-Templated silver nanocluster. A general introduction will address the importance of studying silver nanoclusters. Separate introductions for each system will highlight the importance of each system. An overall comparison between gold and silver nanocluster can be found in Chapter 6.

5.2 Abstract

As introduced in previous chapters, metal nanoparticles under 2 nm are considered nanoclusters and they have many fascinating optical properties. Nanoclusters have tunable optical properties that directly related to their size and topology. Nanoclusters of gold have been studied extensively. Many promising applications in the field of catalysis and imaging have been found. To further our understanding of metal nanoclusters, we focused on investigating clusters with different metal cores. Silver nanoclusters provide an excellent opportunity due to its similarity with gold systems in terms of physical packing and electronic properties. Silver nanocluster with a 32 metal core and 19 thiolate ligand shell, $Ag_{32}(SG)_{19,}$ has been synthesized in high purity and has been characterized by mass spectrometry. The steady state absorption spectrum of $Ag_{32}(SG)_{19}$ shows a lack of Surface Plasmon Resonance, and a major absorption state at 500 nm. Ag_{32} has dual wavelength emissions. Using time-resolved fluorescence up-conversion, the kinetics of the emission peaks are resolved with very different lifetimes at 500 nm and 700 nm. The quantum efficiency for the emission is found to be around two orders of magnitude higher than gold systems. The emission can also be excited by a two-photon process at 800 nm with a absorption cross-section of ~1000 GM. The ultrafast visible transient absorption of $Ag_{32}(SG)_{19}$ at 450-750 nm showed a ground state bleach signal at 470 nm and a strong excited state absorption at 500 nm. The emission mechanism of $Ag_{32}(SG)_{19}$ shows a unique dual emission state in the visible region, which has not been reported for nanoclusters before.

In addition to silver MPCs, another subclass of fluorescent silver nanoclusters (Ag NC) known NanoCluster Beacons were studied. NanoCluster Beacons consist of a weakly emissive Ag NC templated on a single stranded DNA (“Ag NC on ssDNA”) that becomes highly fluorescent when a DNA enhancer sequence is brought in proximity to the Ag NC by DNA base pairing (“Ag NC on dsDNA”). Steady state fluorescence was observed at 540 nm for both Ag NC on ssDNA and dsDNA; emission at 650 nm is observed for Ag NC on dsDNA. The emission at 550 nm is eight times weaker than that at 650 nm. Fluorescence Up-conversion was used to study the dynamics of the emission.

Bi-exponential fluorescence decay was recorded at 550 nm with lifetimes of 1 ps and 17 ps. The emission at 650 nm was not observed at the time scale investigated but has been reported to have a lifetime of 3.48 ns. Two-photon excited fluorescence was detected for Ag NC on dsDNA at 630 nm when excited at 800 nm. The two-photon absorption cross section was calculated to be ~3000 GM. Femtosecond transient absorption experiments were performed to investigate the excited state dynamics of DNA/Ag NC. An excited state unique to AgNC on dsDNA was identified at ~580 nm as an excited state bleach that directly correlate to the emission at 650 nm. Based on the optical results, a simple four level system is used to describe the emission mechanism for Ag NC on dsDNA.

5.3 Introduction

Metal nanoclusters are metal nanoparticles smaller than 2.2 nm.[1–7] Nanoclusters exhibit interesting optical properties and have been an integral part of fundamental nanomaterials research.[1,2,8–11] Metal nanoclusters protected by a single outer organic layer lead to the name Mono-layer Protected Clusters (MPCs).[4,5,12–17] One of the major advantages of MPCs is the accessible metal core through photophysical methodologies.[2,9,18–22] Research on the fundamental properties of nanoclusters has been centered around gold, and many different models have been developed to address the core packing, electron configurations and to explain some of the observed optical properties (see Chapter 4) .[1–3,5,13,16,23] Gold and silver in their atomic state shares the same number of valence electrons and bulk packing distances. Moreover, gold and silver share similar HOMO-LUMO gap at 5.5 eV for the bulk metal. The similarities between silver to gold systems make silver an excellent candidate to extend the current work on MPCs. Additionally, silver nanoclusters show tremendous potential in fluorescence imaging. In this chapter, we turn our attention to two different silver based nanoclusters. First we will investigate a silver MPC system produced at the Univeristy of Toledo, and has been recently identified as $Ag_{32}(SG)_{19}$. The second system of interest is based on DNA-scaffolded systems, where silver atoms are captured inside a single strand of DNA to form nanoclusters, very similar to the early work on dendrimer captured systems. [20,24–27]

The main advantage of the DNA template silver nanocluster is their direct application toward bio-imaging and is highlighted in the corresponding section.

The two silver nanocluster systems were investigated using various optical techniques, including steady state emission and fluorescence, fluorescence up-conversion and transient absorption (detailed in chapter 3). Because of the potential of using the non-linear optical response of gold in imaging, the two-photon excited emission silver nanoclusters were also investigated. Finally the direct comparison of gold and silver nanoclusters can be found in chapter 6.

5.4 $Ag_{32}(SG)_{19}$

Recent work by Professor Bigioni at the University of Toledo produced stable silver nanoclusters in the condensed phase, purified by gel separation.[28–30] The basic synthetic approach is similar to that of gold nanoclusters. However, the silver nanoclusters have not been optimized like some other nanoclusters, where high purity can be achieved in a "single-pot" synthesis.[31,32] Moreover, the stability of silver nanoclusters is also a major concern. By utilizing gel separation methods in their synthesis, Professor Bigioni and coworkers have been able to purify the nanocluster mixtures to produce highly pure mono-disperse nanoclusters (figure 5.1).[29,30] The resulting gel contains a impressive 14 species of silver nanoclusters. To obtain a particular species, physical separation of the gel and subsequent resolvation has been the main method for purification.

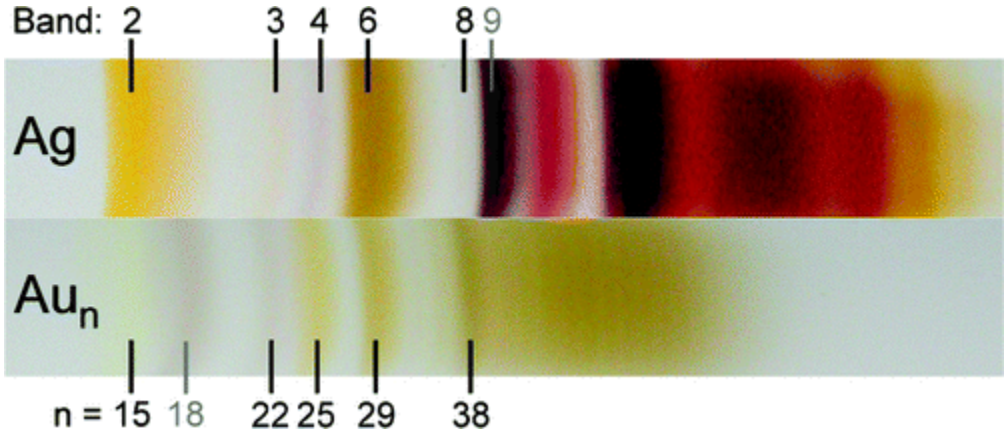

Figure 5.1 Comparison of Au and Ag nanosystems under the same condition of PAGE separation.

The stability of silver nanoclusters was the real main concern in the synthesis and characterization of nanoclusters. Contamination by different sizes dramatically changes the optical properties of these materials, so the purity and stability of these nanoclusters are of the utmost importance. It is interesting to note that the self assemble nature of nanoclusters links purity to stability, where the more stable species will lead to more pure samples.[28,31] A tremendous amounts of time and work during my time at Michigan was devoted to the collaboration with Professor Bigioni to investigate the stability of various silver nanoclusters, in particular under laser excitation. Our initial investigation started with band 2 and band 6 and found that the photo stability of the silver nanoclusters is in the minutes under room condition and seconds under lasers excitation. The stability became our biggest hurdle in our optical studies, particularly in the ultrafast. The work by Professor Bigoni and his students has reached a major turning point in their recent publication studying the temporal stability of nanoclusters by pH control, ion addition and other methods.[28] The result of their work leads to the synthesis of stable silver nanoclusters in high purity, which allows for the identification of silver nanoclusters by mass spectrometry. Due to the very small size of nanocluster and the difficulty in obtaining crystal structures,[12,33,34] mass spectrometry has become essential in the identification of nanocluster formula. One particular silver nanocluster named band 6 in Professor Bigioni's original work has been identified as $Ag_{32}(SG)_{19}$, and it is the major focus of this chapter.[30]

The initial interested in silver based system was not solely based on synthetic exploration. One of the most interesting optical property of gold system is its emission and it has tremendous potential in imagining.[2,9,25,35–38] The possible larger bandgap of silver (compare to gold) in the nanoscale as the number of electron decrease prophets stronger emission, which would further demonstrate the possibility of using nanoclusters as imaging agents on a cellular level. $Ag_{32}(SG)_{19}$ also offers an unexplored area in the ultrafast spectroscopy of nanoclusters.

5.4.1 Sample preparation

The samples used in this publication are produced by the Biogioni group at the University of Toledo. The samples are synthesized and characterized after published procedure.(Guo et al., 2012; Kumar et al., 2010) $AgNO_3$ in water was mix with glutathione in a 1:4 ratio, and a cloudy white suspension of silver thiolate is formed. The mixture was cooled for 30 minutes before excess NaBH4 is added drop wise while stirring at ~1100 rpm. The solution turned to brownish black color after 25 minutes and concentrated to about 10 times less in volume. The silver nanoclusters were precipitated with methanol, and washed with methanol through ultrasonic dispersion-centrifugation. The precipitated was dried under vacuum. The powder silver nanoclusters were purified using a customized polyacrylamide gel electrophoresis procedure.(Kumar et al., 2010) The resulting gel forms bands which contains silver nanoclusters of specific sizes. Band 6 is physically removed from the gel by cutting and is crushed. The crushed gel is submerged in water so that the nanoclusters are diffused out of the gel. The final supernatant was filtered through a 0.22 μm syringe filter, concentrated with a 3 kDa cutoff filter and evaporated to dryness in an Ependorf Vacufuge Concentrator Speed-vac.

The samples were transported in powder form and are stored in a refrigerator. The samples were dissolved in water before the experiment, and their optical densities are adjusted for the experiment.

5.4.2 Steady State Absorption

The steady state absorption for metal nanoclusters has been shown to display important structure details. [13,23] For $Ag_{32}(SG)_{19}$ the absorption spectrum shows a major absorption is observed at 500 nm (figure 5.2) and a shoulder at 480 nm. Since the exact electronic structure of silver nanoclusters has not been calculated, assignments of the transitions are not yet possible. [13,29,32] The peak at 500 nm of the absorption spectrum also resembles the surface plasmon resonance found for larger nanoparticles.[20] However, direct comparison to the absorption spectrum of Ag nanoparticle (figure 5.2) shows that the major absorption at 500 nm is 50 nm away of the surface plasmon resonance (SPR).[2,39] The lack of SPR is a direct evidence of nanocluster formation, an excellent example can be found in pervious publication on gold systems.[40] The absorption features seen at 500 nm and 480 nm supports the idea of nanoclusters as super atoms.[5] The super atom theory uses the gold system as a base model and treats the metal core as a single super atom with distinct electronic transitions, which is vastly different from bulk metal (Mie theory)[41] or nanoparticles. The appearance of fine details in the absorption spectrum is a direct result of the discrete energy level for clusters, or molecular like levels.[13] The absorption spectrum for Ag nanoclusters would further benefit from smaller clusters core sizes or lower temperature measurements, both of which would increase the intensity of the fine details in the absorption spectrum, as demonstrated by the ramakrishina group.[8]

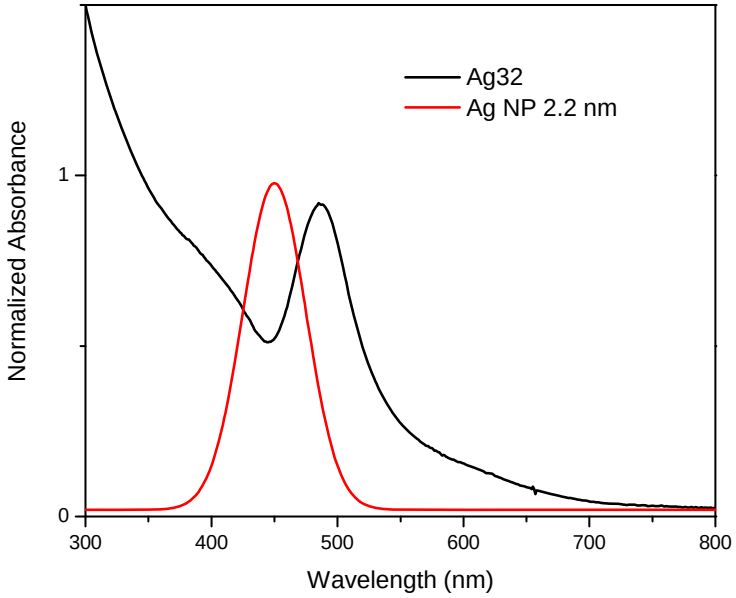

Figure 5.2 Steady state absorption spectrum for $Ag_{32}(SG)_{19}$ and Ag nanoparticle (2.2 nm). The major absorption peak at 500 nm for the nanocluster is not a SPR respond.

5.4.3 Steady State Emission

One of the main attractions of silver nanoclusters compared gold is the proposed increase in the emission efficiency due to the wider of the homo-lumo gap of silver at the nanoscale. For gold nanoclusters, it is well understood that there are two different emissions.[2,22,35,36,42] One of the emissions originates from the metal core and can be found in the visible region, while a second stronger emission is in the near infrared region. The near infrared emission originates from the ligand-metal surface states. The visible emissions of gold nanoclusters are 5 orders of magnitude stronger than bulk gold, with a quantum yield (Q.Y.) on the order of 1 $x10^{-4}$.[2,40] $Ag_{32}(SG)_{19}$ exhibits a very strong emission at 650 nm (figure 5.3) and the maximum emission intensity is measured under 440 nm excitation. The emission wavelength shows no shift under various excitation wavelengths up to 490 nm. A minor shift towards the red is observed at 500 nm. The Q.Y of $Ag_{32}(SG)_{19}$ was calculated using crystal violet as a standard under various concentration. The Q.Y. of the emission at 650 nm was calculated to be $9x10^{-3}$, almost

two orders of magnitude higher than that of gold nanoclusters. The higher Q.Y. suggests that silver is an even better candidate for nanocluster based bio imaging.

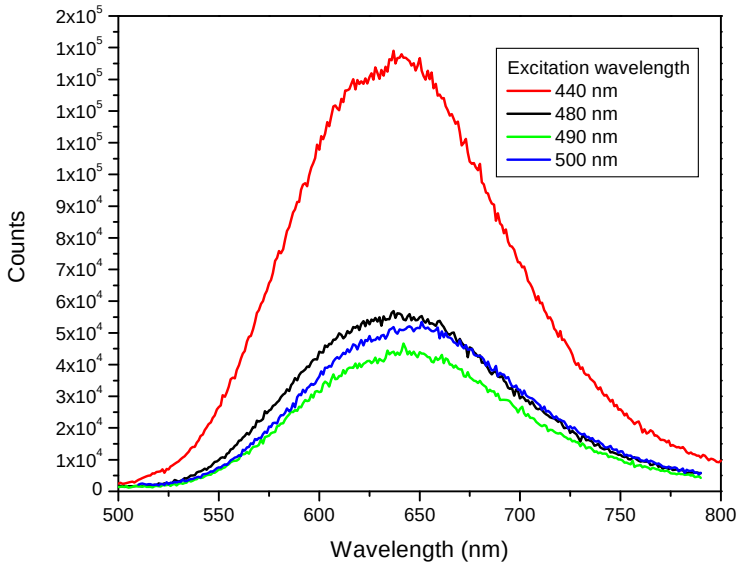

Figure 5.3 Steady state emission spectra of $Ag_{32}(SG)_{19}$ under various excitation wavelength in the visible region. There are no peak shifts up to 490 nm excitation. A minor shift towards the red can be seen under 500 nm excitation. The maximum emission is observed at 440 nm excitation

The excitation spectrum has not been widely use in the filed of nanocluster research, but our pervious investigation of DNA-templated silver nanocluster nano-beacon has reveal fine details about the emission process.[43] In the case of $Ag_{32}(SG)_{19}$, it provided extra information that would be otherwise lost in the steady state emission spectrum (figure 5.2) or the absorption spectrum. The excitation spectrum records the emission intensity as the excitation wavelength changes, and allows for deeper understanding of the major absorptions that contributes to the emission. Using this technique, two different absorption contributes were observed. The two absorption peak directly affects the main emission at 650nm. One of the absorption peaks is at 450 nm while the other peak is at 525 nm (figure 5.4). The over-lay of the absorption spectrum and the excitation spectrum reveals that the emission contribution from the main absorption peak at 500 nm does not contribute to the emission directly and suggests that there are energy transfers from the 500 nm to the emissive states. The two absorption

features also suggest that the emission may not be simple, which prompt us to investigate further into the emission wavelength.

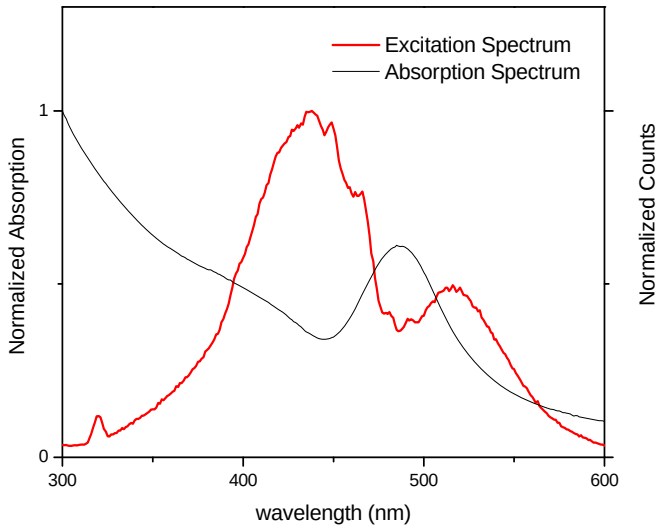

Figure 5.4 Excitation spectrum for $Ag_{32}(SG)_{19}$ compared to the absorption spectrum. Two separate absorption features can be seen that does not relate to the main absorption peak.

A closer inspection of the emission spectrum reveals that the emission spectrum is non-gaussian in nature, to better resolve the exact emission wavelengths a simple Gaussian model was used. Using a simple sum of the gaussian fits, the emission spectrum can be reproduced with two separate emissions at 609 nm and 664 nm (figure 5.5). It has been reported that dual emission can be observed for nanoclusters;[2] however, this is the first report of dual emission from nanoclusters both in the visible region. An additional fit centered at 750 nm is used to reproduce the emission spectrum, but it is not considered as a real observable feature due to the uncertainty of wavelength accuracy of the instrument close to 800 nm. Correlating the excitation spectrum and the dual emission wavelengths, the absorption at 450 nm is more closely related to the emission at 609 nm with energy transfer to the 664 nm. The absorption at 525 nm is closely related to 664 nm but does not couple as strongly to the 609 nm emission, based on the slight wavelength shift under 500 nm excitation in figure 5.2.

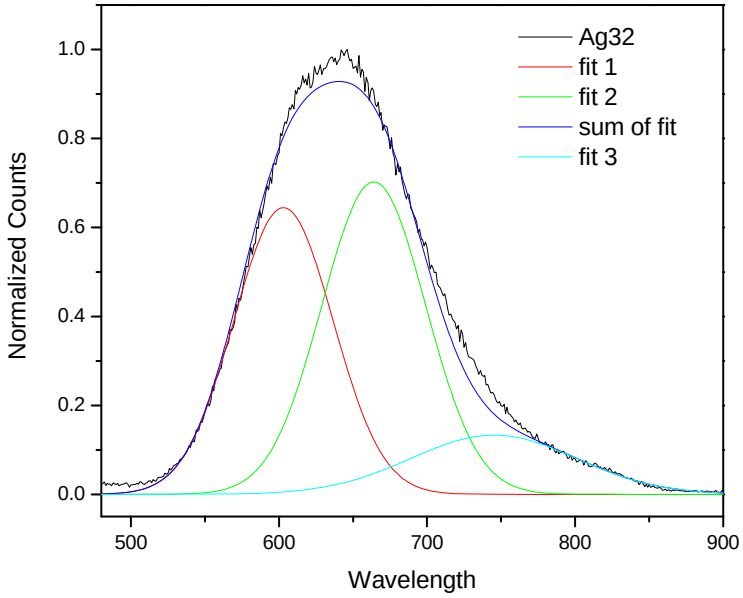

Figure 5.5 Ag_{32} Emission spectrum fitted using simple Gaussian sums. The peak for fit 1 is at 609 nm and the peak for fit 2 is at 664 nm. Fit 3 is sued to reproduce the spectrum, but is not considered in the final fit due to the wavelength accuracy of the instrument at 800 nm.

5.4.4 Mechanism of Emission

To better understand the emission process, fluorescence up-conversion with 60 fs time resolution was used to look at the emission kinetics at 550 nm and 700 nm (figure 5.6, 5.7, 5.8). In theory, if the emission at 650 nm is composed of two different emissions at 609 and 664 nm, the emission processes should be very different, resulting in different kinetics. The fluorescence kinetics at 550 nm shows a life-time of 1.8 ps and 20 ps, (figure 5.6). The kinetics at 700 nm can be fitted with a rise-time of 200 fs, along with two decay times of 400 fs and a very long lived component (figure 5.7). Direct comparison of 550 nm and 700 nm (figure 5.8) should represent the emission at 609 and 664 nm independently (base on our previous gaussian sum in figure 5.5). The emission at 600 nm serves as an intermediate case, closer to the original 650 nm emission (figure 5.8). One of the major differences between the kinetic at 550 nm and 700 nm is the lack of a rise-time component for 500 nm. The lack of a rise-time suggests that the energy transfer processes very fast, on the order of the instrument respond (~60fs). This fast

energy transfer process correlates closely to the core emission, similar to previously reported life-times for gold nanoclusters.[2] The typical life-times for gold nanoclusters are in the 200 – 300 fs range.[2] The emissions life-time for the 609 nm is 1.8 ps, much longer than gold nanoclusters. The longer life-time can be attributed to the increase in Q.Y and can also be explained by the larger homo-lumo gap of silver in the nanoscale. The emission kinetics at 600 nm is combination of the kinetics at 500 nm and 700 nm and confirms the emission at 650 nm can be separated into 609 nm and 664 nm. For the 664 nm emission, the initial rise-time of 200 fs suggested energy transfer into the emissive state, consistent with our excitation spectrum results. Because energy transfer has to occur before this emission process, we believe that this is similar to the "surface state" proposed for gold systems, where the emission comes from a combined ligand and metal state.[22,35] The ligand itself does not emit.[35] The florescence at 664 nm also has a life time of 400 fs and a very long lived component, the long component is beyond our instrument can measure, and could be longer than 1 ns. Since both emissions have a longer life time than gold nanoclusters, we can further attribute the increase in Q.Y to both increases in the core and surface state emissions.

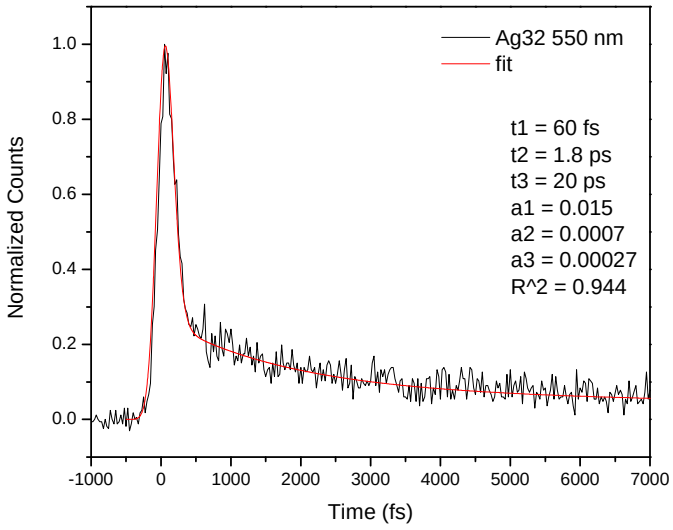

Figure 5.6 Time resolved visible emission for Ag_{32} at 550 nm.

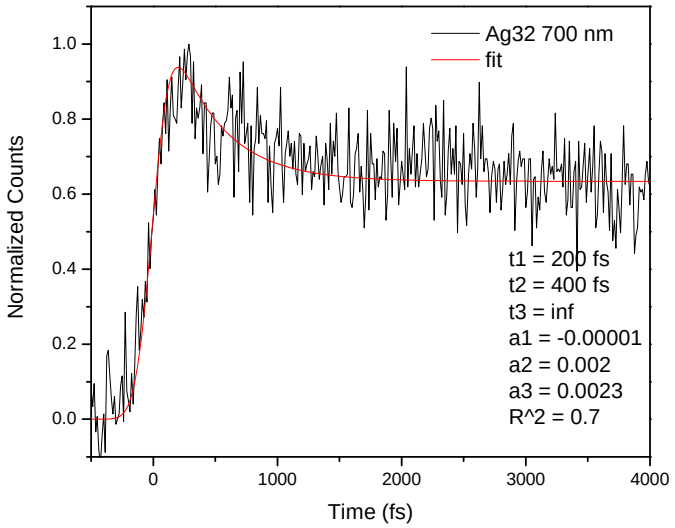

Figure 5.7 Time resolved visible emission for Ag_{32} at 700nm.

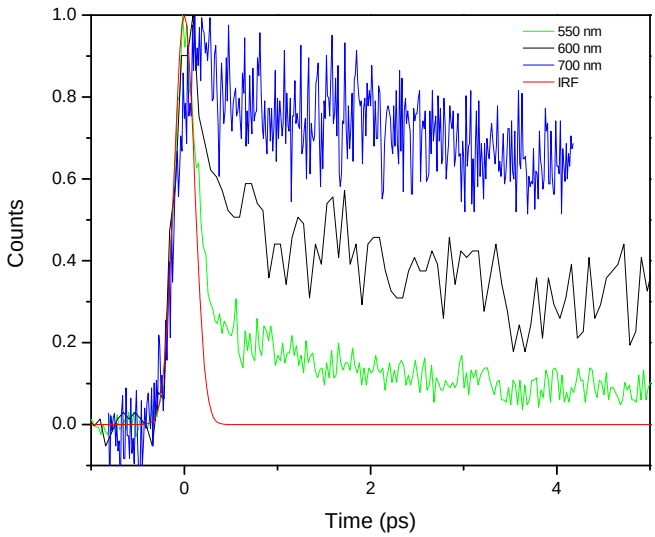

Figure 5.8 Fluorescence kinetics comparison Ag_{32}.

Looking at the fluorescence kinetics and the steady state spectrum, we proposes a possible emission mechanism for $Ag_{32}(SG)_{19}$ (figure 5.9). The emission mechanism suggests that the two different absorption states at 438 nm and 516 nm contribute to the two emissions at 609 and 664 nm respectively. Under excitation at 400 nm, both emission

can be detected and suggests that there are energy transfer between the two absorption states. The emission at 609 nm is fast while the emission at 664 nm is slow. We did not find any experimental result that would indicate and energy transfer between the two emissive states, but there should be some energy transfer between the two absorption states because of the main emission peak at 650 nm is strongest under 440 nm excitation.

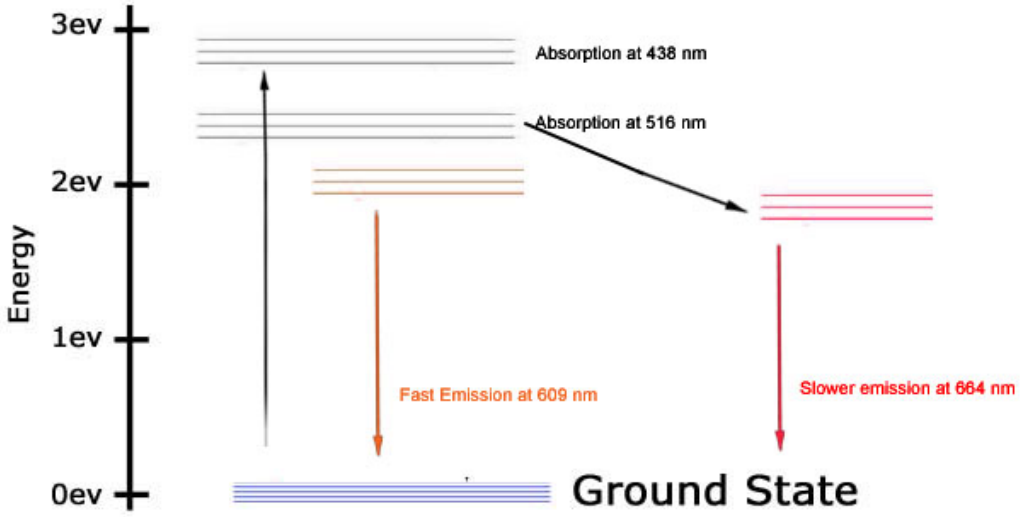

Figure 5.9 Emission mechanism energy diagram for the dual emissions for $Ag_{32}(SG)_{19}$. The fast emission at 609 nm can be assigned to the metal core, while the emission at 664 nm can be assigned to the metal ligand surface states.

5.4.5 Two Photon Excited Emission

One of the strengths of metal nanoclusters is the two-photon excited emission. It has been reported that the two-photon cross-sections for gold nanoclusters are very high and increases with decrease system size.[9] Since we consider gold and silver systems to be similar, two-photon excited emission from $Ag_{32}(SG)_{19}$ is expected. 800 nm excitation of $Ag_{32}(SG)_{19}$ produces emission at 608 nm (figure 5.10). It is very interesting to note that the emission at 664 nm is not observed (with our date collection up to 660 nm), and the emission at 689 nm is a Gaussian peak, unlike the dual emissions observed for the one-photon case. This result would indicate that the absorption at 516 nm and subsequent emission at 664 nm is not a two-photon allowed process, further more, there is no energy transfer into the 664 nm emission from this excitation. This wavelength shift of the

emission under one-photon and two-photon excitation could possibly be used in multi-color imaging. The power dependence of the two-photon excitation shows a slope of two (figure 5.11) and proves that it is a two-photon process. Using the previously calculated Q.Y of $9x10^{-3}$, the cross section of 1000 GM is calculated, similar to typical organic macromolecules. The cross section of Ag_{32} is about half of the reported cross section for the infrared emission of $Au_{25,}$ and 3 orders of magnitude smaller than Au_{25} in the visible.[9]

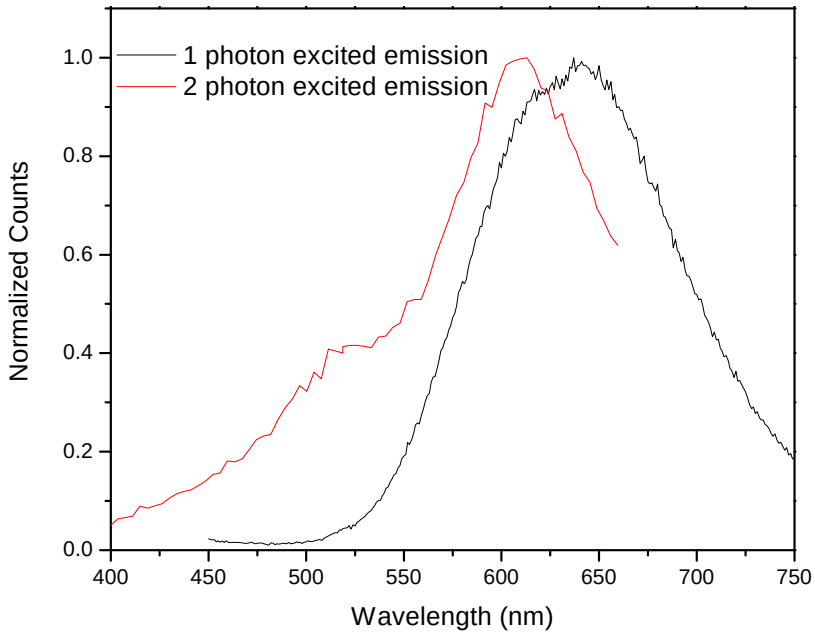

Figure 5.10 Two-photon excited emission wavescan for Ag. The sample is excited with 800 nm source. The emission wavelength under two-photon excitation is very different than the one-photon case. The emission peak is at 609 nm.

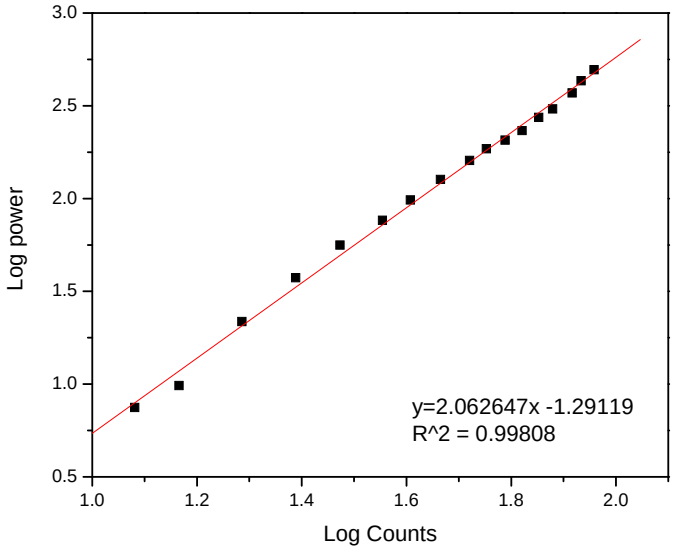

Figure 5.11 Two-photon excited emission power dependence of $Ag_{32}(SG)_{19}$. A slope of two can be fitted and indicates a two-photon absorption process.

5.4.6 Transient Absorption Measurements

Transient absorption measures the change in the absorption spectrum compared to the steady state absorption with 100 fs resolution, and provides excited state dynamics details. Using 400 nm excitations, the transient absorption spectrum was measured with a white light probe from 450 – 750 nm. The spectrum (figure 5.11) shows three interesting features: absorption bleach at 490 nm, two excited state absorption (ESA) at 530 and 702 nm. Comparison to the steady state absorption spectrum reveals that the bleach at 490 nm corresponds to the major absorption in the steady state, and suggests that the absorption at 490 nm is a ground state. The two ESA signals can be assigned to core and surface state excited state based on their wavelengths. The more blue shifted ESA state at 530 nm is of the core, while the 657 nm ESA is related to the lower energy surface states. The core ESA has an initial decay time of about 3 ps and second decay time that is longer than our measurement window. The surface state ESA shows a similar kinetic.

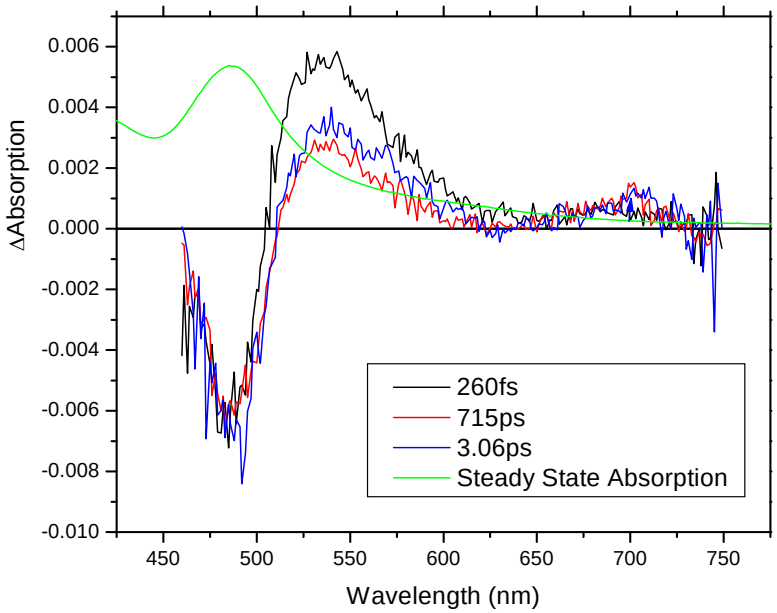

Figure 5.12 *T*ransient absorption for Ag32 at various time delay with steady state absorption. The peak at 470 nm can be assigned to be ground state bleach, and the excited state absorption at 530 nm and 700 nm corresponds to the core and the surface state excited state absorption respectively.

5.4.7 Summary of $Ag_{32}(SG)_{19}$

In this contribution, we investigated the various optical properties of the monolayered protected nanocluster $Ag_{32}(SG)_{19}$. The steady state absorption spectrum reveals that there is a very large ground state at 450 nm, and can be bleached using transient absorption. This ground state is not the surface plasmon found for larger nanoparticles and confirms that $Ag_{32}(SG)_{19}$ is a nanocluster. The absorption spectrum also lacks the distinct features found in gold nanoclusters and suggests that different packing model governs this type of silver nanoclusters. The emission spectrum of $Ag_{32}(SG)_{19}$ reveals two emission peaks in the visible region at 609 nm and 664 nm. The dual emission is confirmed by kinetics measured by fluorescence up-conversion. The main emission peak at 650 nm is a combination of these two emission processes and has a quantum yield of $9x10^{-3}$, two orders of magnitude higher than gold nanoclusters. The emissions at 604 nm and 664 nm have very different life-time kinetics and can be assiged

to the core and surface states respectively. The emission at 609 nm is also two photon active with a cross-section of ~1000 GM, half of that of Au_{25} in the infrared. Transient absorption reveals three different features. A ground state bleach can be observed at 450 nm, and two excited state absorption at 530 nm and 700 nm. The ESA at 530 nm is attributed to the core, while the 700 nm can be attributed to surface states.

$Ag_{32}(SG)_{19}$ exhibits many interesting optical properties, in particular the dual visible emission nature has not been reported. The emission is also two orders of magnitude stronger than gold nanosystems and could surely be used for imaging applications. The two photo cross-section of the $Ag_{32}(SG)_{19}$ is not as high as gold nanoclusters, but the unique wavelength shift could be used in multi-color imaging. The emission mechanism also highlight this unique feature that is similar to gold nanoclusters, but the emissions from $Ag_{32}(SG)_{19}$ are both in the visible. $Ag_{32}(SG)_{19}$ is a new class of nanoclusters that warrant further investigations, in particular silver nanoclusters of various size using this synthetic approach would provide very detailed insight into nanocluster of different metal cores. Further investigation into silver nanoclusters should provide an excellent comparison with gold nanoclusters and address the major question about fundamental properties of metal nanoclusters in general.

5.5 DNA-templated Silver Nanoclusters

In our previous work with gold MPCs Au_{25}, we discovered a number of interesting effects, which are not present in larger gold nanoparticles. In particular, we found that the gold MPCs possessed strong two-photon excited emission, which could lead to applications in imaging and detection areas.[2,9] We also found that as the size of the clusters was reduced from ~5 nm to ~2 nm, the fluorescence lifetime and the excited state lifetimes increased, clear indicators of quantum confinement effects. This change in the lifetime showed a sharp shift when we reached a size of ~2 nm and suggested a change in the mechanism of excitation and emission in the small gold clusters. This was explained by a simple model which relates to a band edge opening and the creation of "molecular-like" states at smaller cluster sizes which was also evident in the steady-state

UV-Vis absorption spectra.[1,2,13,40] An interesting question stems from these results with gold: is this observed shift in mechanism of emission and excitation common for other metal nanoclusters?

Previous section on $Ag_{32}(SG)_{19}$ has showcased the fascination emission properties of silver nanoclusters. In this section we investigate metal nanoclusters that are stabilized by DNA.[43–47] One of the most exciting aspects of these systems is that DNA-based systems give rise to many possible applications in the field of bio-imaging and ultra-sensitive detection of biological agents.[25,45,48,49] DNA-Templated Fluorescence Silver Nanoclusters (DNA/Ag NCs) [43,45,48] are silver nanoclusters nested in single stranded DNA and can be considered as NanoCluster Beacons.[47] DNA/Ag NCs are highly stable systems with tunable fluorescence dependent on the DNA scaffold composition.[43,44,48,49] A new subclass of DNA/AgNCs are NanoCluster Beacons which consist of a poorly emissive Ag NC on a single DNA strand (so called "Ag NCs on ssDNA" in this text), whose fluorescence is greatly enhanced when brought in proximity to a tunable enhancer sequence (the result system is called "Ag NCs on dsDNA" as the enhancer is held in proximity to the AgNC by base pairing).[43,45] The NanoCluster Beacons ("Ag NC on dsDNA") have a quantum yield of approximately 30% per activated cluster, as determined by the gradient method in a fluorimeter with cresyl violet as the standard.[43]

Traditionally, metal MPC systems have been characterized by mass spectrometry and shell substitutions to fully account for the core metal and outer shell ligand number; for DNA AgNC systems, elemental analysis and mass spectrometry have been utilized to estimate the number of atoms.[48,50,51] Unfortunately, these methods report the average number of silver atoms within a DNA strand and not necessarily the number of atoms within a nanocluster. Instead, Ag K-edge Extended X-ray Absorption Fine Structure (EXAFS) has been used to identify DNA/Ag nanocluster size and to demonstrate metal-metal and metal-ligand bonding.[44] From this analysis, AgNCs have been shown to contain Ag-DNA bonds and Ag-Ag bonds at distances consistent with nanoclusters.

Further, the EXAFS analysis estimated the cluster size to be between 8-20 atoms,

depending on the DNA template, [44] although the exact cluster size and geometry is at present unknown. To compare to $Ag_{32}(SG)_{19}$, the characterization using mass spectrometry for DNA- template systems have not yet been reported, due to fact the electro-spray ionization (or other types of ionization) process will destroy the samples. However the folding of simple DNA systems can be modeled extensively, so size estimation of the Ag nanoclusters is reliable. Another major result from the EXAFS study is the proof that there are Ag-Ag bond inside the clusters, eliminating the possibility of Ag network.

In a similar manner to previous section and chapters, we investigate the steady state absorption and emission from nanoclusters templated on ssDNA and the same nanoclusters duplexed into dsDNA. Time-resolved emission was investigated with the aid of ultrafast fluorescence up-conversion. Given the large two-photon response for Au_{25}, we also studied the emission of DNA/Ag NCs from two-photon absorption at 800 nm. Transient absorption was used to probe the excited state dynamics of the system. In this work, we aim to understand the emission mechanism of DNA/Ag NCs.

5.5.1 Sample Preparation

All DNA strands were purchased from Integrated DNA Technologies Incorporated and were purified by desalting. ssDNA (AgNC bearing strand: 5' - CCC TTAAT CCCC TAT AAT AAA TTT TAA ATA TTA TTT ATT AAT) was first dissolved in ultrapure deionized water. Ag NCs were formed by addition of $AgNO_3$ (99.9%, Sigma-Aldrich) to the DNA solution, followed by reduction with $NaBH_4$. Final concentrations were 100 μM DNA, 1.2 mM $AgNO_3$, and 1.2 mM $NaBH_4$ in 20 mM sodium phosphate buffer (pH 6.6). The aqueous solution of $NaBH_4$ was prepared by dissolving $NaBH_4$ powder in water and adding the required volume to the DNA/Ag^+ mixture within 30 seconds, followed by vigorous shaking for 5 seconds. The reaction was kept in the dark at room temperature for 18 hours, filtered, and frozen for transport. dsDNA/Ag NCs were produced at room temperature by mixing of ssDNA/Ag NC with a excess of the complementary strand containing a guanine rich enhancer sequence (5' -

ATT AAT AAA TAA TAT TTA AAA TTT ATT ATA GGGTGGGGTGGGGTGGGG). Absorption spectra were taken 40 min after hybridization. The resultant dsDNA samples were used without further purification or alteration.

5.5.2 Steady State Absorption

The steady state absorption spectra are shown in Figure 5.13 for various Ag nanoparticles (NP). The absorption spectra for Ag NP (2.2 nm) are Gaussian peaks modeled after published results (using wavelength and spectra width) to demonstrate the surface plasmon response for silver nanoparticles.[52] Surface Plasmon Resonance (SPR) is the coherent oscillation of conduction electrons near NP surfaces and can be seen as a strong and board optical absorption near the resonance wavelength. It has been reported that as the nanoparticle size decreases, a red shift is observed.[52] Comparison of the SPR absorption peaks and the absorption spectra for Ag NC on ssDNA reveals a similar absorption peak at ~455 nm, suggesting that the solution of Ag NC on ssDNA may contain larger NPs. Pure ssDNA and dsDNA without Ag NC only absorb in the UV range (200 nm – 300 nm), and does not affect the (visible) absorption of the DNA/Ag systems. Ag NC on dsDNA was formed directly by the hybridization of Ag NC on ssDNA with an excess of complimentary DNA strand with a guanine-rich tail (3'-$G_4(TG_4)_2TG_3$). The absorption peaks for Ag NC on ssDNA is different from the peaks for dsDNA at the same concentration. The weak absorption shoulder at ~455 nm is decreased for Ag NC on dsDNA, possibly resulting from dissolution of solution based NPs after addition of excess compliment DNA strand. The red peak shift for the ~400 nm peak also suggests a decreased system size. Two new absorption peaks emerge at 580 nm and 670 nm for Ag NCs on dsDNA; the appearance of discrete absorption features is a strong evidence for quantum size effects. Quantum size effect is used to describe the change in electronic states as the size of the metal core decreases. From our previous work,[2] we found that as metal nanoparticle size decreases, the metal behaves more like a single molecule or a "super atom". Previous fluorescence reversibility and fluorescence correlation spectroscopy,[47] EXAFS,[44] and the absorption peaks observed in this work are all indicative of Ag NC- DNA nanoclusters.

The absorption spectrum for a hypothetical Ag MPC ($Ag_{25}(SH)_{18}^-$) using Au_{25} geometry and bonding motif has been published.[13] The calculated spectrum shares some similarity to the absorption spectrum of Ag NC on dsDNA suggesting that the DNA system may be electronically similar to MPCs.

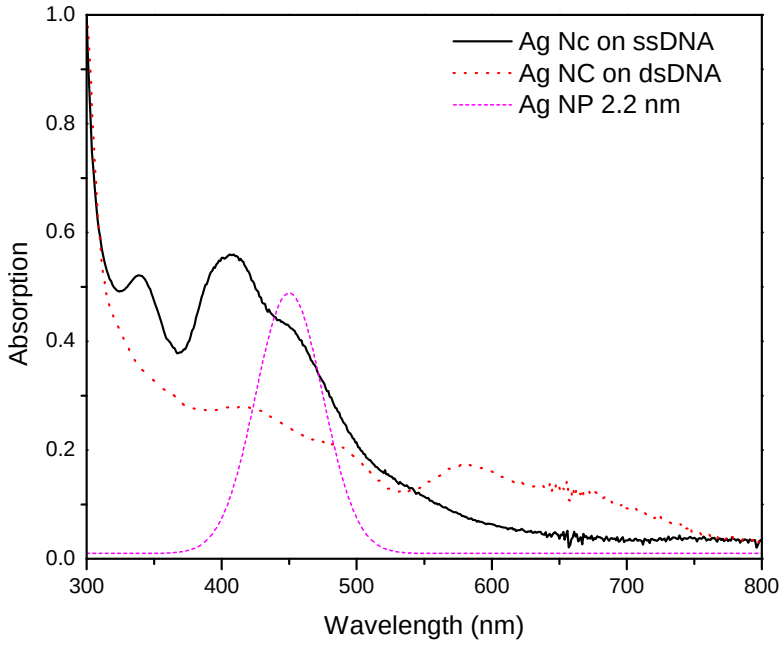

Figure 5.13 Absorption Spectrum for Metal Nanoclusters

5.5.3 Steady State Emission

The normalized steady-state emission for Ag NC on dsDNA (Figure 5.14) was studied with excitation at 400 nm and 580 nm. At 400 nm excitation, the emission spectra for Ag NC on ssDNA showed one peak at 550 nm. The emission spectra for Ag NCs on dsDNA excited at 400 nm shows two peaks at 540 nm (weak) and 650 nm (strong), additional excitation at 580 nm shows the same peak at 650 nm. The peak at 470 nm under 580 nm excitation is the Raman signal from the solvent. The emission at 650 nm was reported to have a bulk enhancement ratio of 500, and from our steady state measurement, it is eight times stronger than the emission at 550 nm. Typically, the emission from bulk metal is only observable under laser excitation with a lower quantum

yield of 10^{-10} (Bulk Au).[48] Emission from other DNA based NC systems has been reported to be as high as 0.64.[47] Quantum efficiency of the activated Ag NC on dsDNA at 650 nm was measured to be 0.30,[48] and the quantum efficiency at 550 nm is estimated to be 0.03. The excitation spectrum for the emission at 650 nm is shown in Figure 5.15. The strong peak in the excitation spectrum is at 590 nm which corresponds to the 580 nm peak in the absorption spectra that emerges upon hybridization.

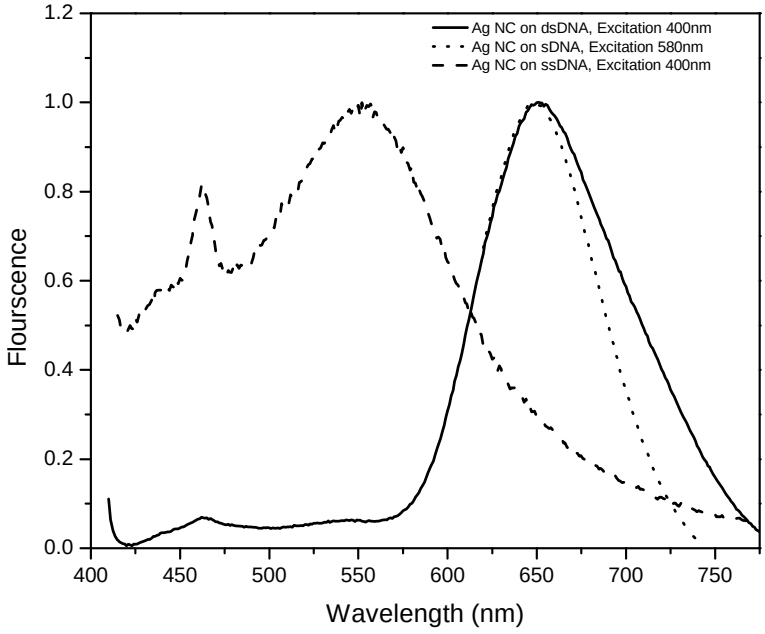

Figure 5.14 Normalized Fluorescence Spectra for Ag NC on ssDNA and dsDNA under 400nm and 580nm excitation

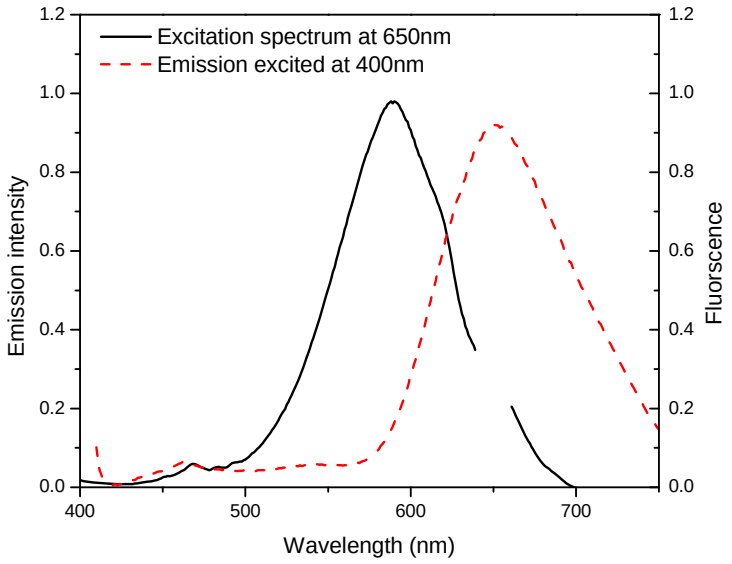

Figure 5.15 Excitation Spectra for dsDNA measuring the emission at 650 nm, and the emission spectrum excited at 400 nm

5.5.4 Time Resolved Fluorescence Up-Conversion

Using time-resolved fluorescence up-conversion, we can study the emission dynamics for DNA/Ag NCs. Based on the result from steady state emission (Figure 5.16), different emission wavelengths were investigated (Figure 5.15a, 5.15b) at 550 nm, 600 nm and 650 nm. Time-resolved emission was detected only for 550 nm and 600 nm (Figure 5.15a), but not for 650 nm. It is reported that time-correlated single photon counting measurements placed the lifetime for the emission at 650 nm at 3.48 ns.[47] The emission at 650 nm was not detected at the time scale measured (up to 4 ps, with 60 fs resolution), suggesting that the emission at 650 nm comes from a later transition, which will be the focus of future studies. The emission measured at 550 nm and 600 nm exhibit very similar dynamics, with rise time of 3.85 ps for 550 nm and 2.49 ps for 600 nm (Figure 5.16a). The fluorescence decay shows a two-component decay with a lifetime of 1 ps and 17 ps. The longer lifetime at 600 nm is potentially contaminated by the long-lived 650 nm emission, with half the amplitude of 550 nm. The similar rise time for the emission at 550 nm and 600 nm leads us to conclude that the fluorescence from these

states originates from the same initial excited state centered. The weak emission feature is common for both Ag NC on dsDNA and ssDNA. Given that the only difference between the two systems is the complementary DNA strand, the emission could be from the common metal core. The observed two-exponential decay (Figure 5.16b) is similar to the three-exponential decay reported for larger dendrimer nanocomposites and very different from the single exponential decay expected of nanoclusters.[2,40,53] However, the lifetime of 1 ps and 17 ps is much longer than the 70 fs, 700 fs and 5.3 ps reported for silver dendrimer nanocompistes.[20] The short lifetime for nanoparticles (and nanocomposites) is reported to be typical for sp-d band hole recombination [20] and the longer lifetime for the DNA/Ag NCs suggests that such recombination is not present. Additionally, the excitation is far from the SPR band, making the emission to be related to the SPR band even less likely. The lifetime analysis suggests that nanoclusters are present but it is possible that other larger nanoparticles can contribute to the bi-exponential decay. Based on the common components of dsDNA and ssDNA and the long lifetime of emission at 550 nm, the emission is from the metal nanoclusters.

The emission from 650 nm could be the result a triplet state, a charge transfer state or surface states. Based on the published work that detail the emission from Au MPCs, [2,20,21] the emission from 650 nm is potentially from a surface state, and it is possible the energy transfer to this state is much later than the time scale investigated. Surface state emission for Au MPCs are reported to be in the NIR region with a quantum yield in the order of 10^{-4},[2,9,22,35,54–56] three orders of magnitudes weaker than the quantum yield of DNA/Ag NCs.

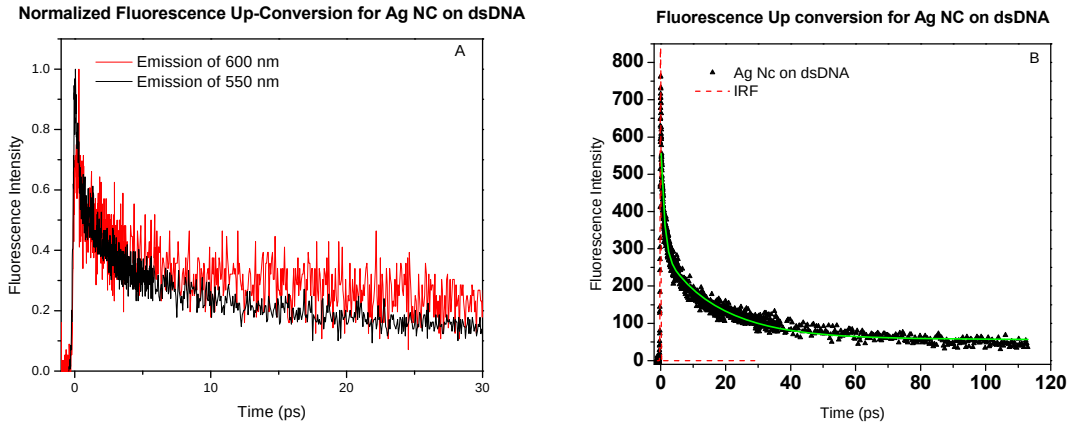

Figure 5.16 A) Normalized Fluorescence Up-conversion lifetime for Ag NC on dsDNA at 550 nm and 600 nm. B) Fluorescence Up conversion for Ag NC on dsDNA at 550 nm, fitted with a bi-exponential decay

5.5.5 Two-Photon Excited Emission

We examined the two-photon absorption (TPA) efficiencies of the DNA/Ag NC at 800 nm excitation (Figure 5.17). The log of pump power dependence against the log of the fluorescence at 630 nm for the Ag NC on dsDNA is shown in Figure 5.18. This data is fitted well by a line of slope two, indicating a two-photon excitation. The method for calculating the TPA cross-section is the comparative two-photon excited fluorescence method with standard reference H2TPP in toluene. The TPA action cross-section at 800 nm for the Ag NC on dsDNA was determined to be ~3000 GM (based upon the measured one photon 30% Quantum Yield for activated clusters). This is a large TPA cross-section value, which promotes the possibility of using the DNA/Ag NCs for multi-photon imaging. The steady state emission at 540 nm is not observed for Ag NC on ssDNA or dsDNA under two-photon excitation. Two-photon excited fluorescence at 630 nm was observed only for Ag NC on dsDNA, detailed at Figure 6. Steady state absorption spectrum (Figure 5.13) shows that at the same concentration, absorption at 400 nm is stronger for Ag NC on ssDNA, yet Ag NC on ssDNA did not possess detectable two-photon excited fluorescence at 650 nm. There are two possible explanations. 1) It is possible that two-photon absorption is stronger for Ag NC on ssDNA, but the transition state for the 650 nm emission is not present, which suggests that the proximity to a

tunable enhancer gives rise to such a state. 2) Ag on ssDNA is not two-photon active and the proximity of the enhancer sequence will cause a geometric or electronic change that gives rise to two-photon allowed transition. However, the excitation spectrum indicates that the emission at 650 nm is strongly related to the transition at 580 nm, suggesting that the lack of an emissive state for Ag on ssDNA is the more likely case.

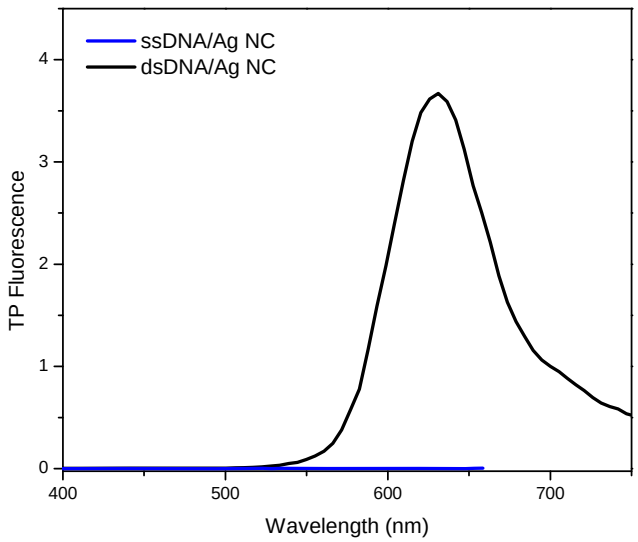

Figure 5.17 Two Photon Fluorescence Emission Spectra for DNA/Ag NCs systems under 800 nm excitation

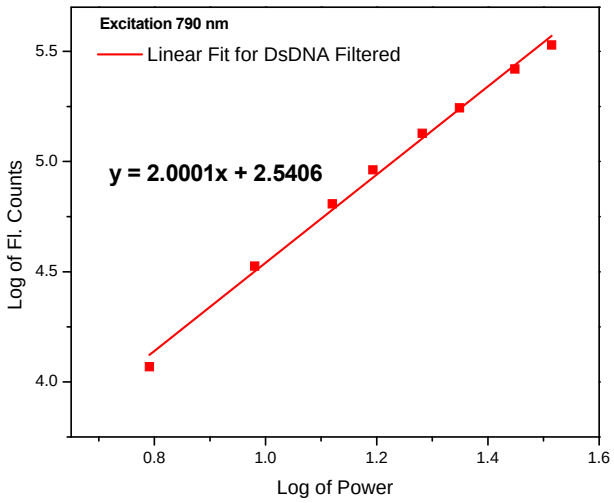

Figure 5.18 Two Photon Power Dependence for DNA/Ag NCs systems

5.5.6 Femtosecond transient absorption

Transient absorption measures the difference between excited state absorption and steady state absorption using pump probe spectroscopy. The change in absorption is measured in the ultrafast time scale of 200 fs to 1600 ps, producing excited state dynamics information at the probe wavelength of 450 nm to 750 nm. Attempts to measure DNA/Ag NCs transient absorption under 350 nm excitation suffered from sample degradation. Excited with a 470 nm pump beam, the transient absorption spectrum (Figure 5.19) displayed a strong excited state absorption (ESA) at ~560 nm for both Ag NCs on ssDNA and dsDNA (Figure 5.20).

We investigated the transient absorption kinetics of Ag NC on both ssDNA and dsDNA (Figure 5.20, 5.21). Kinetics fitting was performed with the Surface Xplorer software supplied by Ultrafast systems. The dynamics of the systems at 565 nm are similar for both Ag NC on ssDNA and dsDNA. The feature at 565 nm has a very short rise time that cannot be resolved by the instrument (~150 fs). It also has a long decay time of a few hundred ps. The long decay time indicates discrete energy levels typical of nanoclusters. The board transient absorption feature suggests a combination of excited states at similar wavelengths. When the enhancer sequence is introduced to form AgNC on dsDNA, an excited state feature is observed at 590 nm (Figure 5.19). The kinetics (Figure 5.22) shows a non-positive value before zero time (excitation) for the peak at 590 nm, indicating that it is a bleached stated that has a longer lifetime than the laser repetition rate (1kHz) of 1 ms or longer. After the zero time, the bleach structure shows a similar rise time compared to the peak at 565 nm (Figure 5.22). However, the ESA peak at 565 nm is very broad (Figure 5.19), covering the bleach state's wavelength at 590 nm. The decay to zero for the 565 nm bleach after excitation is the result of the rising ESA signal, masking the bleach signal; therefore kinetics observed for the bleach is independent of the ESA, suggests that they two excited states are entirely different. Previous investigations done by Moran et al [28] on Au NCs has shown that bleach states in transient absorption can be matched to absorption peaks of the steady absorption spectrum. It is interesting to see that the bleach signal at 590 nm for Ag NC on dsDNA

can be matched to the absorption peak at 590 nm (Figure 5.22), suggesting that they two states are related. The peak at 590 nm also overlaps with the 580 nm peak for the excitation spectrum, so the emission at 650 nm is directly related to the bleached excited state at 590 nm. Therefore, the enhancer sequence creates a new excited state at 590 nm and is directly related to the emission at 650 nm. This is a first report of a emission related excited state for MPCs detected by transience absorption. The enhancer sequence is crucial to the emitting nanoclusters in the AgNC on dsDNA.

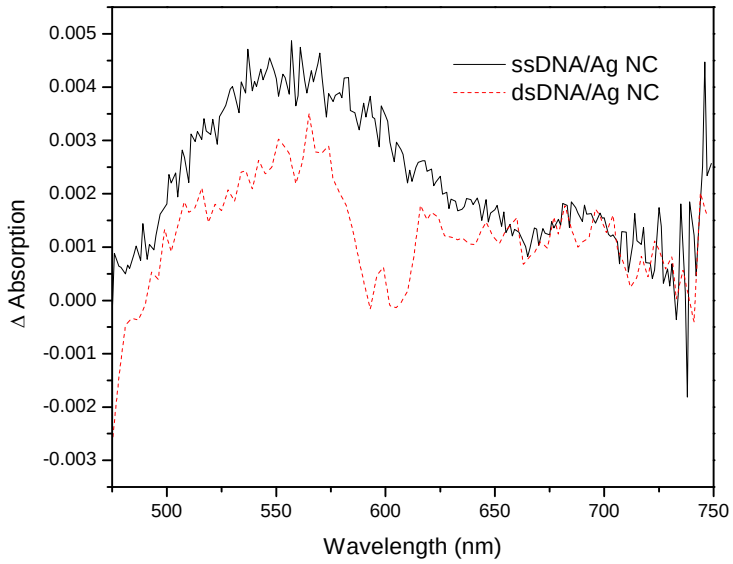

Figure 5.19 Transient Absorption of ssDNA and dsDNA at ~20 ps

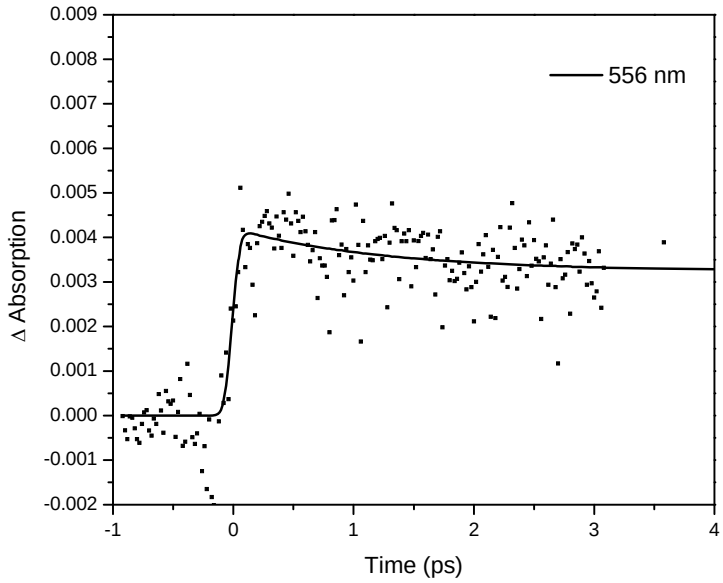

Figure 5.20 Kinetic Fit for Ag NC on ssDNA at 556 nm

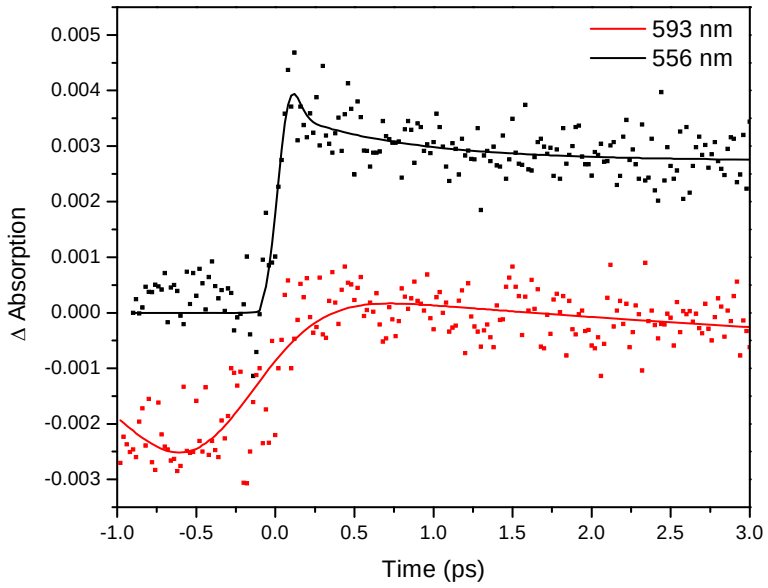

Figure 5.21 Transient absorption kinetic fit for Ag NC on dsDNA at 692 nm and 556 nm

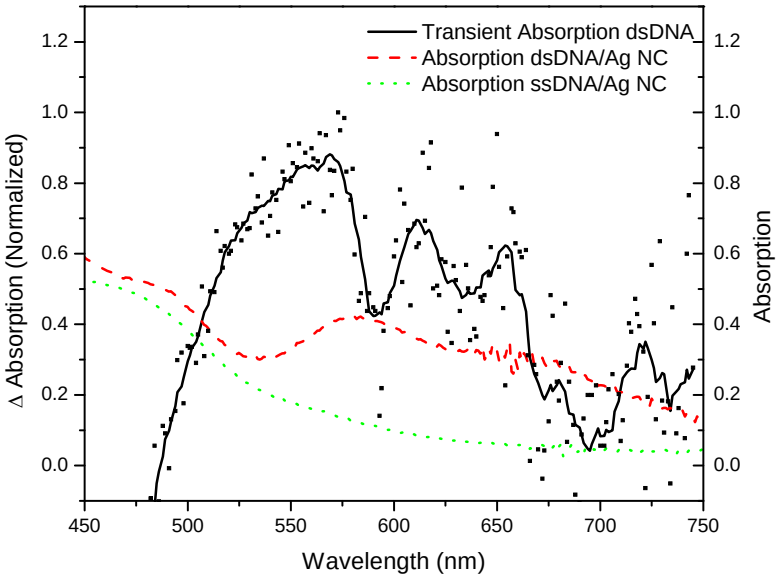

Figure 5.22 Excited bleach observed at 590 nm can corresponds (see text for detail identification of the bleach) to the absorption peak at 590 nm for Ag NC on dsDNA

5.5.7 Mechanism of Emissions

Steady state emission spectrum recorded two different emissions at 540 nm and 650 nm (Figure 5.13). Time-resolved fluorescence experiments indicate that the emission at 650 nm is a single-exponential decay with a lifetime of 4 ns compared to the bi-exponential decay at 540 nm.[47] In our previous investigations,[53] similar dynamics were observed for larger Ag and Au particles, and the bi-exponential decay was assigned to the fluorescence originating from the recombination of electrons in the *s-p* band with holes in the *d* band. However, the long fluorescence lifetime observed for the DNA/Ag NC systems suggests that the dynamics are associated with nanoclusters. The largest amplitude of emission for DNA/Ag NC systems is at 650 nm. Given the strength and long lifetime of the emission, we propose that this emission originates from the surface states of the nanoclusters, similar to NIR emission for Au NCs.[2] From the excitation spectrum, the observed emission at 650 nm is related to the transition at 590 nm. From our analysis, the transition at 590 nm is related to the absorption peak at 580 nm. Hence

the emission at 650 nm is due to the excited state at 590 nm, and the presence of nanoclusters in the system.

The surface state emission for the nanoclusters is attributed to the interaction between the metal core and the outer ligand (thiolate) shell.[13,57] Previous reports have shown that the core and the shell do not interact chemically,[1,22,35] but an increase in the polarization of the ligand shell affects the emission of MPCs.[35] We also suggest that the outer organic layer acts as a field to introduce polarization to the metal core. It is important to treat the metal core as a single "super atom", and therefore can be treated as a system with discrete energy levels. The relatively long lifetime of the energy levels leads to the emission from MPCs. More detailed on modeling of the effect of polarization is needed to further understand this effect. While DNA/Ag NCs do not have a thiolate shell that surrounds the metal cluster, the DNA binds the cluster and could provide a similar polarizing environment to the Ag NC. It was shown that the emission from DNA/Ag NCs is enhanced by the introduction of a guanine-rich tail (3'-$G_4(TG_4)_2TG_3$) on the complementary DNA strand.[47] From previous reports, the emission enhancement for NanoCluster Beacons is the strongest with the guanine-rich tail, while emission from a cytosine-rich tail is much weaker. [47] A comparison of guanine and cytosine reveals that the larger size of guanine could potentially polarize the metal core as a "super atom", even if cytosine has a stronger dipole. The greater enhancement from guanine is consistent with the idea that an induced polarization to the nanoclusters strongly affects their emission properties.

According to the steady state absorption, emission, time-resolved emission and transient absorption data, we propose a two different emission mechanism for Ag NCs on ds DNA detailed in Figure 5.23. The emission at 540 nm may be caused by NPs and NCs in the system, but lifetime analysis suggests that the system is more similar to nanoclusters than nanoparticles. The emission mechanism can be explained by a simple four level system (Figure 5.21). Base on our model, the emission at 540 nm originates from the B state (associated with the metal core) and the emission at 650 nm comes from the surface state. The introduction of the enhancer sequence to the Ag NC creates a new

electronic state C, observed in transient absorption as an excited sate bleach. State C directly relates to the absorption at 590 nm and attributes to the large emission at 650 nm. The large emission observed is due to the highly efficient energy transfer between the 590 nm absorption and the surface state emission. It is possible that the excited state C is itself the emissive state (or state C is the surface state), with the current experiment information available we separate the states to illustrate that state C can be a possible core state, hence different from the surface state. However, we are certain that the large enhanced emission is caused by the new excited state (state C) created by the enhancer sequence upon hybridization.

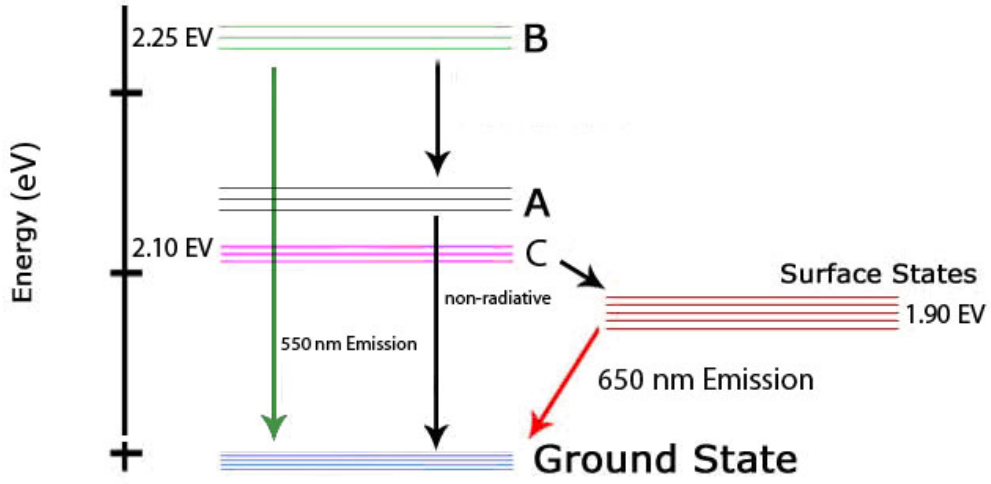

Figure 5.23 Proposed energy structure for dsDNA Ag nanoclusters

5.5.8 Summary on DNA/Ag NCs

In summary, DNA/Ag NCs systems offer many interesting optical properties. Ag NCs on ssDNA have an absorption peak that is similar to the SPR response for nanoparticles (2.2 nm), with the formation of the dsDNA system resulting in a decrease in the absorption. Discrete absorption features are observed for dsDNA which demonstrates the presence of quantum size effect. Emission was measured for DNA/Ag NCs using steady state and time resolved techniques. Two different emission features were recorded: a core emission at 550 nm was shared by both Ag NC on ssDNA and

dsDNA; a stronger surface state emission at 650nm is only observed for Ag NC on dsDNA. An enhancement in emission by the hybridization of the ssDNA by a complementary strand with a guanine-rich tail is observed. Time-resolved fluorescence is observed at 550 nm with a lifetime of 1 ps and 17 ps; the decay lifetime is longer than for nanoparticles. We suggest the polarization of nanoclusters by the enhancer sequence is critical to emission observed at 650 nm. The enhancer sequence also creates a new excited state observed at 590 nm in the transient absorption spectrum. Additionally, the excited state at 590 nm is directly related to the emission. Based on the emission and steady state results, we model the emission mechanism of Ag NCs on dsDNA with a four-level system. Two-photon excited fluorescence with emission at 630 nm was also observed for the first time for DNA-templated metal clusters, and the large cross-section calculated encourages the use of DNA/Ag NC as a bio-imaging tool. We are also excited to report the observation of an excited state in the transient absorption spectrum after 1.5 ps at 590nm that directly related to the emission enhancement of nanoclusters, resulting from the possible polarization of the super atom by enhancer with a guanine-rich tail.

5.6 Summary of silver nanoclusters

This chapter two silver nanoclusters, $Ag_{32}(SG)_{19}$ (Ag MPC) and the DNA Templated Nanoclusters (Ag DNA). The steady state absorption for Ag MPC and Ag DNA showed absorption transition states typical of nanoclusters. The SPR peak at 500 nm, typical of nanoparticles, was not observed. The emission spectrum of the Ag MPC is very unique, and display dual emission in the visible, which a large quantum yield. The emission of Ag DNA has a similar wavelength compared to Ag MPC, but it is not a dual emission. The emission from Ag DNA can be turned on or off base on hybridization. Both emissions can be assigned to a core or surface state based on their ultrafast kinetics. The emission mechanism for both systems are similar, with the exception that Ag DNA's emissive state can be directly correlate to an excited absorption state. Both systems can absorb two-photons and emit at a wavelength that is similar to their one-photon excitation wavelength. Overall, the investigations of silver nanoclusters are successful, providing

many interesting optical details. The optical properties of Ag MPC and Ag DNA are compared to gold nanoclusters in chapter 6.

5.7 Reference

(1) Jin, R. Quantum sized, thiolate-protected gold nanoclusters. *Nanoscale* **2010**, *2*, 343–62.

(2) Yau, S. H.; Varnavski, O.; Goodson, T. An Ultrafast Look at Au Nanoclusters. *Accounts of chemical research* **2013**.

(3) Parker, J. F.; Fields-Zinna, C. A.; Murray, R. W. The story of a monodisperse gold nanoparticle: Au25L18. *Accounts of chemical research* **2010**, *43*, 1289–96.

(4) Sun, D.; Gong, X.; Wang, X.-Q. Soft and hard shells in metallic nanocrystals. *Physical Review B* **2001**, *63*, 193412.

(5) Walter, M.; Akola, J.; Lopez-Acevedo, O.; Jadzinsky, P. D.; Calero, G.; Ackerson, C. J.; Whetten, R. L.; Groenbeck, H.; Hakkinen, H.; Grönbeck, H.; Häkkinen, H. A unified view of ligand-protected gold clusters as superatom complexes. *Proceedings of the National Academy of Sciences of the United States of America* **2008**, *105*, 9157–9162.

(6) Negishi, Y.; Nobusada, K.; Tsukuda, T. Glutathione-protected gold clusters revisited: bridging the gap between gold(I)-thiolate complexes and thiolate-protected gold nanocrystals. *Journal of the American Chemical Society* **2005**, *127*, 5261–70.

(7) Negishi, Y.; Takasugi, Y.; Sato, S.; Yao, H.; Kimura, K.; Tsukuda, T. Magic-numbered Au(n) clusters protected by glutathione monolayers (n = 18, 21, 25, 28, 32, 39): isolation and spectroscopic characterization. *Journal of the American Chemical Society* **2004**, *126*, 6518–9.

(8) Devadas, M. S.; Bairu, S.; Qian, H.; Sinn, E.; Jin, R.; Ramakrishna, G. Temperature-Dependent Optical Absorption Properties of Monolayer-Protected Au 25 and Au 38 Clusters. *The Journal of Physical Chemistry Letters* **2011**, *2*, 2752–2758.

(9) Ramakrishna, G.; Varnavski, O.; Kim, J.; Lee, D.; Goodson, T. Quantum-sized gold clusters as efficient two-photon absorbers. *Journal of the American Chemical Society* **2008**, *130*, 5032–3.

(10) Varnavski, O.; Ramakrishna, G.; Kim, J.; Lee, D.; Goodson, T. Critical size for the observation of quantum confinement in optically excited gold clusters. *Journal of the American Chemical Society* **2010**, *132*, 16–7.

(11) Hicks, J. F.; Miles, D. T.; Murray, R. W. Quantized Double-Layer Charging of Highly Monodisperse Metal Nanoparticles. *Journal of the American Chemical Society* **2002**, *124*, 13322–13328.

(12) Jadzinsky, P. D.; Calero, G.; Ackerson, C. J.; Bushnell, D. A.; Kornberg, R. D. Structure of a thiol monolayer-protected gold nanoparticle at 1.1 A resolution. *Science (New York, N.Y.)* **2007**, *318*, 430–3.

(13) Zhu, M.; Aikens, C. M.; Hollander, F. J.; Schatz, G. C.; Jin, R. Correlating the crystal structure of a thiol-protected Au25 cluster and optical properties. *Journal of the American Chemical Society* **2008**, *130*, 5883–5.

(14) Negishi, Y.; Chaki, N. K.; Shichibu, Y.; Whetten, R. L.; Tsukuda, T. Origin of magic stability of thiolated gold clusters: a case study on Au25(SC6H13)18. *Journal of the American Chemical Society* **2007**, *129*, 11322–3.

(15) Akola, J.; Walter, M.; Whetten, R. L.; Häkkinen, H.; Grönbeck, H. On the structure of thiolate-protected Au25. *Journal of the American Chemical Society* **2008**, *130*, 3756–7.

(16) Schmid, G. The relevance of shape and size of Au55 clusters. *Chemical Society reviews* **2008**, *37*, 1909–30.

(17) Templeton, A. C.; Wuelfing, W. P.; Murray, R. W. Monolayer-Protected Cluster Molecules. *Accounts of Chemical Research* **2000**, *33*, 27–36.

(18) Varnavski, O.; Goodson, T.; Mohamed, M.; El-Sayed, M. Femtosecond excitation dynamics in gold nanospheres and nanorods. *Physical Review B* **2005**, *72*, 235405–.

(19) Miller, S. A.; Womick, J. M.; Parker, J. F.; Murray, R. W.; Moran, A. M. Femtosecond Relaxation Dynamics of Au 25 L 18 − Monolayer-Protected Clusters. *The Journal of Physical Chemistry C* **2009**, *113*, 9440–9444.

(20) Varnavski, O.; Ispasoiu, R. G.; Balogh, L.; Tomalia, D.; Goodson, T. Ultrafast time-resolved photoluminescence from novel metal–dendrimer nanocomposites. *The Journal of Chemical Physics* **2001**, *114*, 1962.

(21) Qian, H.; Y. Sfeir, M.; Jin, R. Ultrafast Relaxation Dynamics of [Au 25 (SR) 18] q Nanoclusters: Effects of Charge State. *The Journal of Physical Chemistry C* **2010**, *114*, 19935–19940.

(22) Devadas, M. S.; Kim, J.; Sinn, E.; Lee, D.; Goodson, T.; Ramakrishna, G. Unique Ultrafast Visible Luminescence in Monolayer-Protected Au 25 Clusters. *The Journal of Physical Chemistry C* **2010**, *114*, 22417–22423.

(23) Aikens, C. M. Origin of Discrete Optical Absorption Spectra of M 25 (SH) 18 − Nanoparticles (M = Au, Ag). *The Journal of Physical Chemistry C* **2008**, *112*, 19797–19800.

(24) Gilbertson, J. D.; Vijayaraghavan, G.; Stevenson, K. J.; Chandler, B. D. Air and water free solid-phase synthesis of thiol stabilized au nanoparticles with anchored, recyclable dendrimer templates. *Langmuir: the ACS journal of surfaces and colloids* **2007**, *23*, 11239–45.

(25) Lin, C.-A. J.; Lee, C.-H.; Hsieh, J.-T.; Wang, H.-H.; Li, J. K.; Shen, J.-L.; Chan, W.-H.; Yeh, H.-I.; Chang, W. H. Synthesis of Fluorescent Metallic Nanoclusters toward Biomedical Application: Recent Progress and Present Challenges. *Journal of Medical and Biological Engineering* **2009**, *29*, 276–283.

(26) Petty, J. T.; Zheng, J.; Hud, N. V; Dickson, R. M. DNA-templated Ag nanocluster formation. *Journal of the American Chemical Society* **2004**, *126*, 5207–5212.

(27) Richards, C. I.; Choi, S.; Hsiang, J.-C.; Antoku, Y.; Vosch, T.; Bongiorno, A.; Tzeng, Y.-L.; Dickson, R. M. Oligonucleotide-stabilized Ag nanocluster fluorophores. *Journal of the American Chemical Society* **2008**, *130*, 5038–+.

(28) Desireddy, A.; Kumar, S.; Guo, J.; Bolan, M. D.; Griffith, W. P.; Bigioni, T. P. Temporal stability of magic-number metal clusters: beyond the shell closing model. *Nanoscale* **2013**, *5*, 2036–44.

(29) Kumar, S.; Bolan, M. D.; Bigioni, T. P. Glutathione-stabilized magic-number silver cluster compounds. *Journal of the American Chemical Society* **2010**, *132*, 13141–3.

(30) Guo, J.; Kumar, S.; Bolan, M.; Desireddy, A.; Bigioni, T. P.; Griffith, W. P. Mass spectrometric identification of silver nanoparticles: the case of $Ag_{32}(SG)_{19}$. *Analytical chemistry* **2012**, *84*, 5304–8.

(31) Wu, Z.; Suhan, J.; Jin, R. One-pot synthesis of atomically monodisperse, thiol-functionalized Au25 nanoclusters. *Journal of Materials Chemistry* **2009**, *19*, 622.

(32) Shichibu, Y.; Negishi, Y.; Tsukuda, T.; Teranishi, T. Large-scale synthesis of thiolated Au25 clusters via ligand exchange reactions of phosphine-stabilized Au11 clusters. *Journal of the American Chemical Society* **2005**, *127*, 13464–5.

(33) Heaven, M. W.; Dass, A.; White, P. S.; Holt, K. M.; Murray, R. W. Crystal structure of the gold nanoparticle [N(C8H17)4][Au25(SCH2CH2Ph)18]. *Journal of the American Chemical Society* **2008**, *130*, 3754–5.

(34) Briant, C. E.; Theobald, B. R. C.; White, J. W.; Bell, L. K.; Mingos, D. M. P.; Welch, A. J. Synthesis and X-ray structural characterization of the centred icosahedral gold cluster compound [Aul3(PMe2Ph)10Cl2](PF6)3; the realization of a theoretical prediction. *Journal of the Chemical Society, Chemical Communications* **1981**, 201.

(35) Wang, G.; Guo, R.; Kalyuzhny, G.; Choi, J.-P.; Murray, R. W. NIR luminescence intensities increase linearly with proportion of polar thiolate ligands in protecting monolayers of Au38 and Au140 quantum dots. *The journal of physical chemistry. B* **2006**, *110*, 20282–9.

(36) Shibu, E. S.; Muhammed, M. A. H.; Tsukuda, T.; Pradeep, T. Ligand Exchange of Au25SG18 Leading to Functionalized Gold Clusters: Spectroscopy, Kinetics, and Luminescence. *Journal of Physical Chemistry C* **2008**, *112*, 12168–12176.

(37) Chevrier, D. M. Properties and applications of protein-stabilized fluorescent gold nanoclusters: short review. *Journal of Nanophotonics* **2012**, *6*, 064504.

(38) Dreaden, E. C.; El-Sayed, M. A. Detecting and destroying cancer cells in more than one way with noble metals and different confinement properties on the nanoscale. *Accounts of chemical research* **2012**, *45*, 1854–65.

(39) Plech, A.; Cerna, R.; Kotaidis, V.; Hudert, F.; Bartels, A.; Dekorsy, T. A surface phase transition of supported gold nanoparticles. *Nano letters* **2007**, *7*, 1026–31.

(40) Yau, S. H.; Varnavski, O.; Gilbertson, J. D.; Chandler, B.; Ramakrishna, G.; Goodson, T. Ultrafast Optical Study of Small Gold Monolayer Protected Clusters: A Closer Look at Emission †. *The Journal of Physical Chemistry C* **2010**, *114*, 15979–15985.

(41) Mie, G. Beiträge zur Optik trüber Medien, speziell kolloidaler Metallösungen. *Annalen der Physik* **1908**, *330*, 377–445.

(42) Wang, G.; Huang, T.; Murray, R. W.; Menard, L.; Nuzzo, R. G. Near-IR luminescence of monolayer-protected metal clusters. *Journal of the American Chemical Society* **2005**, *127*, 812–3.

(43) Yau, S. H.; Abeyasinghe, N.; Orr, M.; Upton, L.; Varnavski, O.; Werner, J. H.; Yeh, H.-C.; Sharma, J.; Shreve, A. P.; Martinez, J. S.; Goodson, T. Bright two-photon emission and ultra-fast relaxation dynamics in a DNA-templated nanocluster investigated by ultra-fast spectroscopy. *Nanoscale* **2012**, *4*, 4247–54.

(44) Neidig, M. L.; Sharma, J.; Yeh, H.-C.; Martinez, J. S.; Conradson, S. D.; Shreve, A. P. Ag K-Edge EXAFS Analysis of DNA-Templated Fluorescent Silver Nanoclusters: Insight into the Structural Origins of Emission Tuning by DNA Sequence Variations. *Journal of the American Chemical Society* **2011**, *133*, 11837–11839.

(45) Sharma, J.; Yeh, H.-C.; Yoo, H.; Werner, J. H.; Martinez, J. S. A complementary palette of fluorescent silver nanoclusters. *Chemical Communications* **2010**, *46*, 3280–3282.

(46) Sharma, J.; Yeh, H.-C.; Yoo, H.; Werner, J. H.; Martinez, J. S. Silver nanocluster aptamers: in situ generation of intrinsically fluorescent recognition ligands for protein detection. *Chemical Communications* **2011**, *47*, 2294–2296.

(47) Yeh, H.-C.; Sharma, J.; Han, J. J.; Martinez, J. S.; Werner, J. H. A DNA-Silver Nanocluster Probe That Fluoresces upon Hybridization. *Nano Letters* **2010**, *10*, 3106–3110.

(48) Petty, J. T.; Fan, C.; Story, S. P.; Sengupta, B.; Iyer, A. S. J.; Prudowsky, Z.; Dickson, R. M. DNA Encapsulation of 10 Silver Atoms Producing a Bright, Modulatable, Near-Infrared-Emitting Cluster. *Journal of Physical Chemistry Letters* **2010**, *1*, 2524–2529.

(49) Vosch, T.; Antoku, Y.; Hsiang, J.-C.; Richards, C. I.; Gonzalez, J. I.; Dickson, R. M. Strongly emissive individual DNA-encapsulated Ag nanoclusters as single-molecule fluorophores. *Proceedings of the National Academy of Sciences of the United States of America* **2007**, *104*, 12616–12621.

(50) O'Neill, P. R.; Velazquez, L. R.; Dunn, D. G.; Gwinn, E. G.; Fygenson, D. K. Hairpins with Poly-C Loops Stabilize Four Types of Fluorescent Ag-n:DNA. *Journal of Physical Chemistry C* **2009**, *113*, 4229–4233.

(51) Gwinn, E. G.; O'Neill, P.; Guerrero, A. J.; Bouwmeester, D.; Fygenson, D. K. Sequence-dependent fluorescence of DNA-hosted silver nanoclusters. *Advanced Materials* **2008**, *20*, 279–+.

(52) Xu, C.; Webb, W. W. Measurement of two-photon excitation cross sections of molecular fluorophores with data from 690 to 1050 nm. *Journal of the Optical Society of America B-Optical Physics* **1996**, *13*, 481–491.

(53) Ispasoiu, R. G.; Balogh, L.; Varnavski, O. P.; Tomalia, D. A.; Goodson, T. Large optical limiting from novel metal-dendrimer nanocomposite materials. *Journal of the American Chemical Society* **2000**, *122*, 11005–11006.

(54) Mooradian, A. Photoluminescence of Metals. *Physical Review Letters* **1969**, *22*, 185–187.

(55) Peng, S.; McMahon, J. M.; Schatz, G. C.; Gray, S. K.; Sun, Y. Reversing the size-dependence of surface plasmon resonances. *Proceedings of the National Academy of Sciences of the United States of America* **2010**, *107*, 14530–14534.

(56) Huang, T.; Murray, R. W. Luminescence of tiopronin monolayer-protected silver clusters changes to that of gold clusters upon galvanic core metal exchange. *Journal of Physical Chemistry B* **2003**, *107*, 7434–7440.

(57) Miller, S. A.; Womick, J. M.; Parker, J. F.; Murray, R. W.; Moran, A. M. Femtosecond Relaxation Dynamics of Au25L18- Monolayer-Protected Clusters. *Journal of Physical Chemistry C* **2009**, *113*, 9440–9444.

Chapter 6

Gold and Silver Nanoclusters

6.1 Original Publication Information

The work in this chapter utilizes data published in two publications:

> **"An Ultrafast Look at Au Nanoclusters"** Sung Hei Yau, Oleg Varnavski, and Theadore Goodson III. *Accounts of Chemical Research*, ***2013*** Article ASAP DOI: 10.1021/ar300280w
>
> **"Ultrafast spectroscopy of $Ag_{32}(SG)_{19}$"** Sung Hei Yau, Oleg Varnavski, and Theadore Goodson III. *Manuscript in Preparation*

In chapter 4 and 5, gold and silver nanosystems are discussed in great lengths. One of the major aims of my work is to understand the effect of changing the metal core on the photo and physical properties of metal nanoclusters. This chapter will compare and contrast various optical properties of gold and silver nanoclusters. A discussion regarding fundamental laws and modeling of these systems will be presented.

6.2 Introduction

In chapter 4, gold nanoclusters of different sizes are presented, and we found a few major optical properties that are unique to these nanoclusters. When the size of metal nanoparticles (5-100 nm) approaches 2 nm and smaller, in accordance's with the free electron model (chapter 1), there is a dramatic change in their optical properties. One of

these optical property is the Surface plasmon resonance (SPR), which is the collective excitation and oscillation of the valence electrons and it is only observed for nanoparticles due to their large system size.[1–3] Absorption spectrums of nanoclusters have distinct features, and as we approach the size of Au_{25}, the absorption fine details correspond to major transitions calculated from the crystal structure.[4] The appearance of these fine features reflects discrete energy levels for nanoclusters, known as quantum size effect.[5–9] Gold nanoclusters also exhibit dual emissions in the visible and in the near infrared (NIR) with quantum yields (Q.Y) that are 5 orders of magnitude stronger than thin film gold.[6,10,11] Using time resolved fluorescence, the life time of the emission of nanoclusters are about 200-300 fs, much faster than the 60 fs of nanoparticles. Finally gold nanoclusters exhibits two-photon excited emission in the visible with very large cross sections.

Gold nanoclusters are very well understood, because of their structural characterization by X-ray crystallography and mass spectrometry.[4,12,13] The research on the optical and physical aspects of gold nanoclusters inspired our group to explore new territories in the area of nanocluster research. Our initial interested was to investigate in-depth the exact relationship between the metal core and the ligand shell. There are two different approaches: changing the ligand shell on the nanocluster or change the metal core. Published results reported on the effect of ligand on the emission of nanoclusters. [10,14] The ligand polarity changes the Q.Y of the emission but not the wavelength, however, the exact relationship between Q.Y and ligand polarity are not clearly defined. Based on the published result we believed that the use of ultrafast techniques may not be able provide new and exciting explanations to the effect of ligand polarity. Instead we turn our attention to metal cores that are similar to gold.[15] Silver was our candidate to study due to its similarity to gold. Silver and gold atoms has the same number of valence electrons, and based on the super atom theory (chapter 1) should have similar packing and shell closing electron numbers, and the silver metal core should have the same structure as gold. Also using the free electron model (chapter 1), gold and silver have the same HOMO-LUMO (Highest Occupied Molecular Orbital to Lowest Unoccupied Molecular Orbital) gap at 5.5 eV and thus the same electron quantization (quantum size

effect) should be observed at ~2 nm at room temperature. The bulk face-center cubic (ffc) packing distance of gold and silver is also the same, giving further support to the structural similarity between to the two systems.

In the search for silver Mono-layer Protected Clusters (MPC), we were fortunate to collaborate with Professor Bigioni at the University, which reported the first synthesis of silver MPCs, using the Brust protocol.[16,17] Additionally, their successful characterization of their silver nanoclusters lead to the structural characterization of $Ag_{32}(SG)_{19}$.[16,18] Detailed discussion about $Ag_{32}(SG)_{19}$ can be found in chapter 5.

In the following sections, we will directly compare Au_{25} to Ag_{32}. The discussion will focus on comparing many different optical properties, both linear and non-liner. Ultimately, we hope to understand if there are common laws for all metal nanoclusters. The discussion in the chapter is based on the data presented in chapter 4 and chapter 5, experimental details are available at the respective chapters and will be omitted in this discussion.

6.3 Steady State Absorption

The steady state absorption spectrum for gold nanoclusters $Au_{25}(SR)_{18}$ has been shown to correlate directly to major transitions calculated from crystal structure (figure 6.1).[4,19] Specifically the peak at 400 nm can be corresponded to the interband (d to sp) transition. Mixed intrabnad (sp to sp) and interband (d to sp) transitions are observed as a peak at 450 nm. Finally the last peak at 670 nm is the Highest Occupied Molecular Orbital to Lowest Unoccupied molecular Orbital (HOMO–LUMO) transition.[4,20] The electronic transitions were calculated based on the crystal structure.[4] Ag_{32} lacks the distinct feature mentioned above, instead a major absorption is observed at 500 nm (figure 1), and an absorption shoulder at 350 nm. The lack of the specific absorption features of $Ag_{32}(SG)_{19}$ strongly suggests that the metal core arrangement are not the same as $Au_{25}(SR)_{18}$. Au_{25} have an icosahedra core, surrounded by gold atoms bonded to the ligand in a “staple” motif.[4,21] The differences in the packing of the metal core can be

further supported by their mass spectrometry characterization. $Ag_{32}(SG)_{19}$, has a different metal to ligand ratio compared to $Au_{25}(SG)_{18,}$ which suggests a different metal to ligand binding motif.[4,16,22] From the results presented above, it should be clear than Ag_{32} does not have a icosahedra core, but the exact core geometry is not yet know. This result is also a major contradiction to the super atom theory, which states the stability of the metal core is a function of the valence electrons.[23] Since gold and silver have the same number of valence electrons, they should have the same shell closing core metal number and the same core packing, which silver obliviously does not. An argument can be made that metal core number is different due to the different ligand binding motif, and the total electronic contribution from the shell (metal-ligand) is different, while the total shell closing electron number could be the same. But without the crystal structure for Ag_{32}, this question remains to be answered.

There are two major absorption feature for $Ag_{32}(SG)_{19}$, a peak at 500 nm and a shoulder at 350 nm. One of the major questions about $Ag_{32}(SG)_{19}$ is the identity of the absorption peak at 500 nm, due to its resemblance to the Surface Plasmon Resonance (SPR) found for larger nanoparticles.[1,24,25] However, direct comparison to the absorption spectrum of a typical 2.2 nm Ag nanoparticle (figure 1) shows that the major absorption at 500 nm does not correspond to the SPR.[7,26] Using the free electron model, an estimate on the size separation between nanoparticles and nanoclusters can be calculated. Silver and gold have the same parameters, thus, the same separation at 2 nm for nanoclusters is expected. The lack of SPR for Ag_{32} agrees with the free electron model quite well, rough size estimation places Ag_{32} to be smaller than 2 nm, and should be considered as a nanocluster. The main absorption peak at 500 nm is further compared to the literature, and reveals that the absorption peak at 500 nm is similar to the absorption peak of 1.3 nm silver nanoclusters at 495 nm.[25] The exact electronic structure of $Ag_{32}(SG)_{19}$ has not been calculated, but using the basic geometry of Au_{25}, the absorption spectrum for $Ag_{25}(SH)_{18}^{-}$ has been calculated.[19,27] The HOMO-LUMO+1 and the HOMO-1-LUMO transitions (2.33eV and 2.49eV, respectively) from literature are similar to the 500 nm absorption recorded (figure 6.2). A similar absorption peak can also be found for Ag_2-Ag_8 systems.[28] There is another absorption feature at ~350 nm, seen as a shoulder (figure 1). This

absorption feature is similar to the HOMO-1-LUMO+1 transition from $Ag_{25}(SH)_{18}$ calculation. However, these peak assignments are only estimates, and with out complete characterization or other silver nanoclusters to compare to, may not be reliable. Nevertheless, a few conclusions can be drawn from the comparison between gold and silver MPCs. First the absorption spectrum for Ag_{32} and Au_{25} indicates that the major absorption corresponds to discrete energy transitions, which is characteristic of "molecular like" nanoclusters. Second, the difference in absorption features between gold and silver MPCs suggests that the metal cores are different, which could be caused by the different ligand-metal binding motif. And finally, the major absorption feature for silver nanoclusters at 500 nm is much stronger than the absorption features for gold nanoclusters, and could be an indication that the energy level spacing are much larger for silver. Overall, it is interesting to see that the free electron model is applicable to silver nanoclusters, but the possible large energy spacing would suggest the use of the bulk HOMO-LUMO gap is insufficient. The super atom theory does not apply to silver nanoclusters, because it fails to predict or explain the stability of Ag_{32}. However, the absorption results strongly support that both Au_{25} and Ag_{32} are nanoclusters, where the metal core is considered a super atom, and the ligand-binded-metal as the shell.

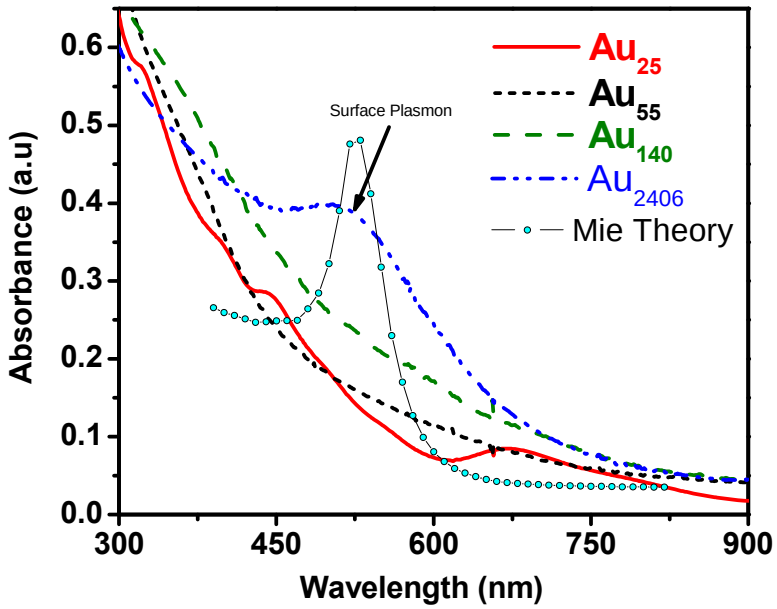

Figure 6.1 Steady state absorption for Au_{25} Au_{55}, Au_{140}, Au_{2406} and Mie theory calculation using parameter similar to Au_{25}.[6]

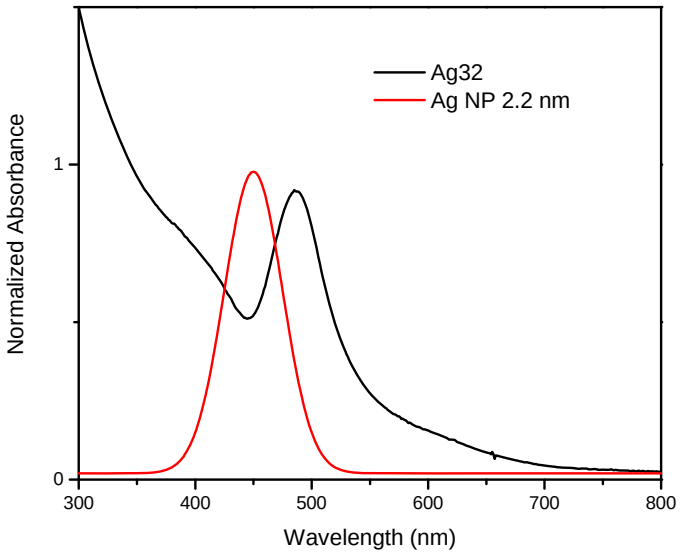

Figure 6.2 Steady state absorption spectrum for $Ag_{32}(SG)_{19}$ and Ag nanoparticle (2.2 nm). The major absorption peak at 500 nm for the nanocluster is not a SPR respond.

6.4 Steady State Fluorescence

For gold nanoclusters, dual emissions have been reported in the literature and is it well understood. [7,10,14,29,30] One of the emissions originates from the metal core and can be found in the visible region. An example of the core emission is the 500 nm emission of Au_{55} (figure 6.3). For gold nanoclusters, a second stronger emission is in the near infrared (NIR) region, and it originates from the ligand-metal "surface states."[14] The visible emissions of gold nanoclusters are 5 orders of magnitude stronger than bulk gold.[6,7] $Ag_{32}(SG)_{19}$ exhibits a very strong emission at 650 nm (figure 5.2) with a quantum yield (Q.Y.) of $9x10^{-3}$ (chapter 5), two orders of magnitude higher than gold nanoclusters. Detail investigation of the emission origin also reveals that the emission at 650 nm can be resolved into two different wavelengths. The dual emission wavelength of silver nanoclusters is very similar to gold nanoclusters, but the emission for Ag_{32} is both in the visible, with peaks at 609 nm and 664 nm. Using the assignment in chapter 5, the emission at 609 nm can be assigned to the metal core, and is red shifted with respect to the gold emission. The red shift in emission and can be explained by the different core structure, which is suggested by the absorption spectrum. The surface state emission is blue shifted for silver nanoclusters and should be a direct result of the different bonding motif between the core and the ligands, evidence in the metal to ligand ratio. The large quantum yield of silver nanoclusters can be explained by possible larger HOMO-LUMO gap of silver nanoclusters in the nanocluster scale. But this assumption may not be correct, due to calculations on $Ag_{25}(SH)_{18}$ shows that the HOMO-LUMO gap for gold and silver systems only differ by 0.01 eV. The quantum yield enhancement is more likely to be the effect of the core packing, which is not yet understood. The widening of the HOMO-LUMO gap for silver is based on the fact that silver is one principle quantum level lower than gold, so the overall number of electrons interacting in the system is less, which can lead to larger HOMO-LUMO gap, especially at the nanometer scale. Regardless of the emission origin, the observed emission is the result of discrete energy transitions, demonstrated by the time-resolve discussion below. For the emission of silver and gold nanoclusters, the dual emission nature of both clusters are interesting and could

be used in imaging applications, but the dual emission in the visible for silver nanoclusters is not expected, considering the large wavelength shift and the increase in strength by two orders of magnitude.

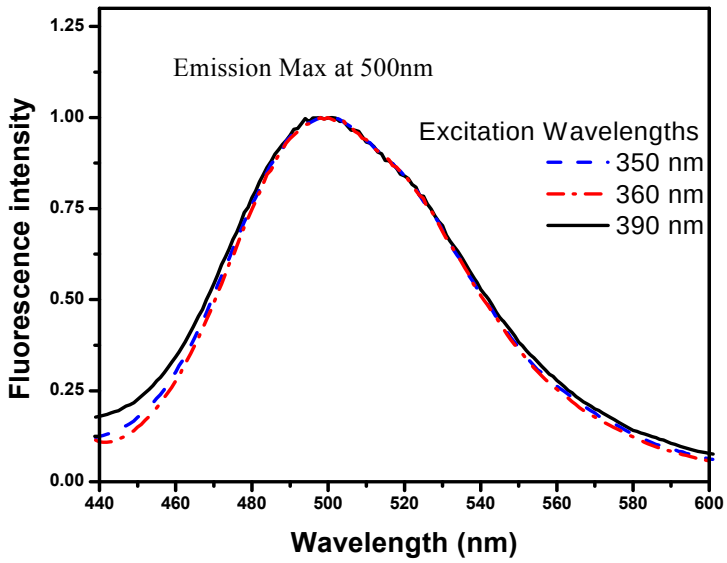

Figure 6.3 Normalized Emission spectra for Au 55, excited at 350, 360 and 390nm. The emission peak is at 500 nm with a quantum yield on the order of $1x10^{-4}$.

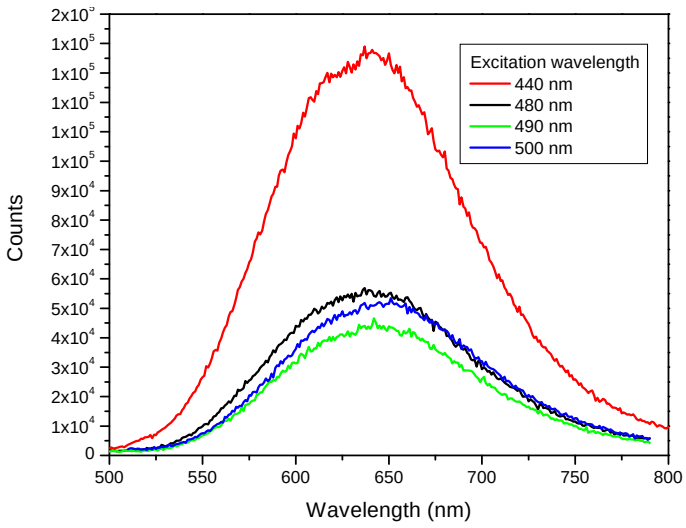

Figure 6.4 Steady state emission spectra of $Ag_{32}(SG)_{19}$ under various excitation wavelength in the visible region. The emission wavelength is at 650 nm with a quantum yield on the order of $1x10^{-3}$. The emission can also be resolved into 609 nm and 664 nm.

6.5 Emission Mechanisms

Using fluorescence up-conversion and steady state spectrum, the emission mechanism of gold (chapter 4) and silver (chapter 5) nanoclusters can be modeled with simple systems. The emission mechanism of gold (figure 6.5) and silver (figure 6.6) nanoclusters shares many similarities, one of the most important is the appearance of surface states which is directly related to the red emission in the NIR for gold and 664 nm for silver. The assignment of the surface state is based on the emission kinetics measured by time resolve fluorescence up-conversion. The emission life time of the metal core (shorter wavelength) for Ag_{32} and gold nanoclusters are also very different. The emission life time for gold nanoclusters are in the 200 – 300 fs range, longer than the well known 60 fs for nanoparticles (figure 6.5). The difference life-time between the nanocluster and the nanoparticle can be explained by the difference in mechanism, which is detailed in chapter 4. For the case for Ag_{32}, the life-time was measured to 1.8 ps, 6 times longer than gold nanoclusters (figure 6.6). The even longer life-time agrees with the super atom idea, and is characteristic of a molecular model. It is interesting to note that both core emissions can be fitted to a single exponential decay. The time-resolved emission for gold nanoclusters is not available for comparison, but it should be similar to that of silver, where a rise time and a long decay should be observed. Although the emission wavelengths for silver and gold nanoclusters are very different, their emission dynamics are similar, this emission decay is perhaps characteristic for all metal nanoclusters.

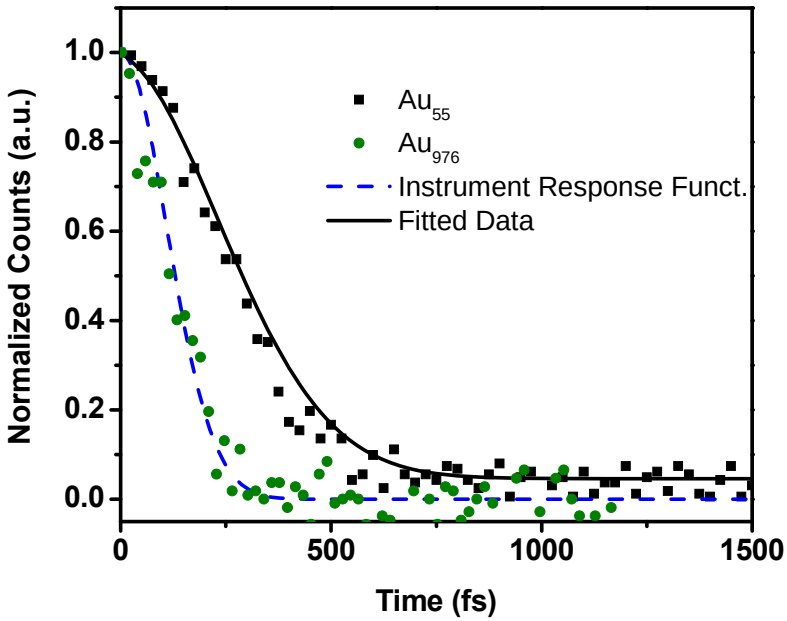

Figure 6.5 Time resolved visible emission for Au_{55} and Au_{976}. The life time of Au_{55} is about ~250fs. The emission from Au_{976} is faster than the instrument response function (blue line).[6]

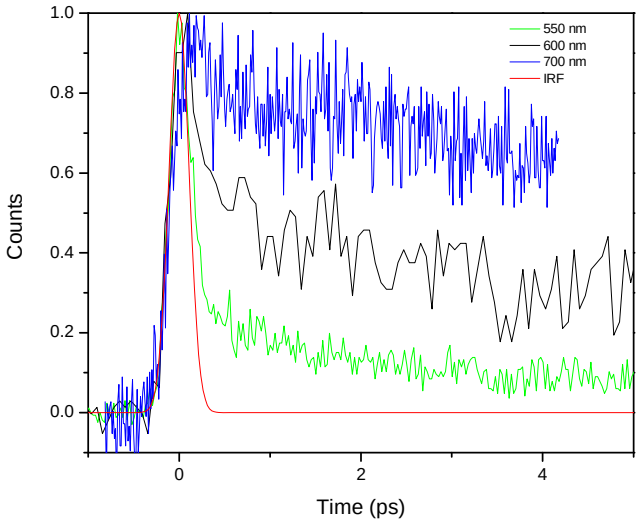

Figure 6.6 Fluorescence kinetics of Ag_{32} at 550, 600 and 700 nm.

The comparison of the emission mechanism proposed for gold (figure 6.7) and silver nanoclusters (figure 6.8) reveals that both emission mechanisms are similar. There are differences in absorption and emission wavelengths as discussed before, but the energy path ways are very similar, and reiterate the idea of "divide and protect". It is also interesting to note that the ligand and metal do not emit by themselves, and emission is only observed when a super atom is formed either with a gold core and a silver core. Overall, the excited state energy levels for silver nanoclusters are higher energy, which could be explained by the lesser electron shielding, leading to a larger energy gaps at the cluster size regimes. However the increase in Q.Y of silver over gold is not yet understood, an educated guess would be the decrease in d-electrons in the case of silver would further weaken non-radiative process, thus increasing the Q.Y. This is based on the weaker e-ph coupling of gold nanoclusters when compared to gold nanoparticles.

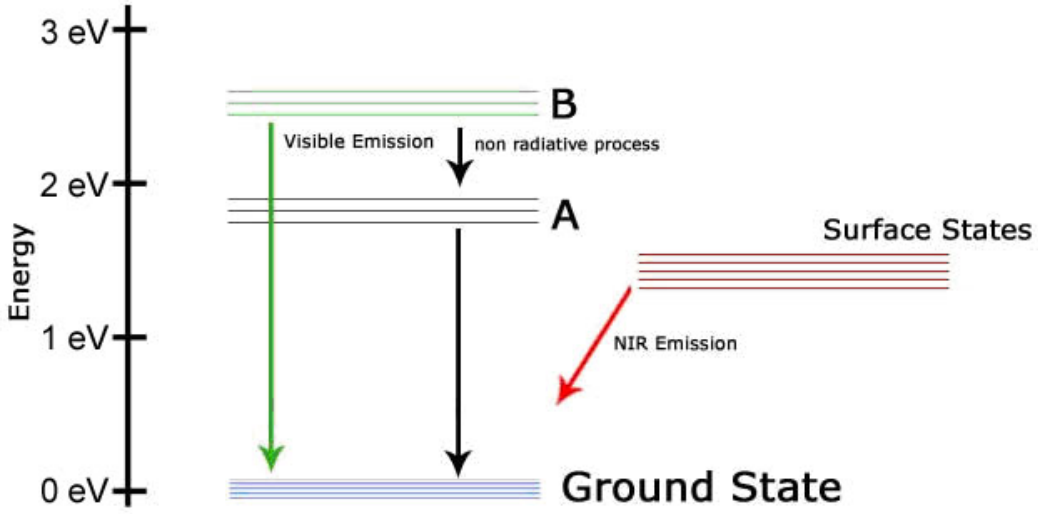

Figure 6.7 Transition energy diagram for the emissions for gold MPCs.[6]

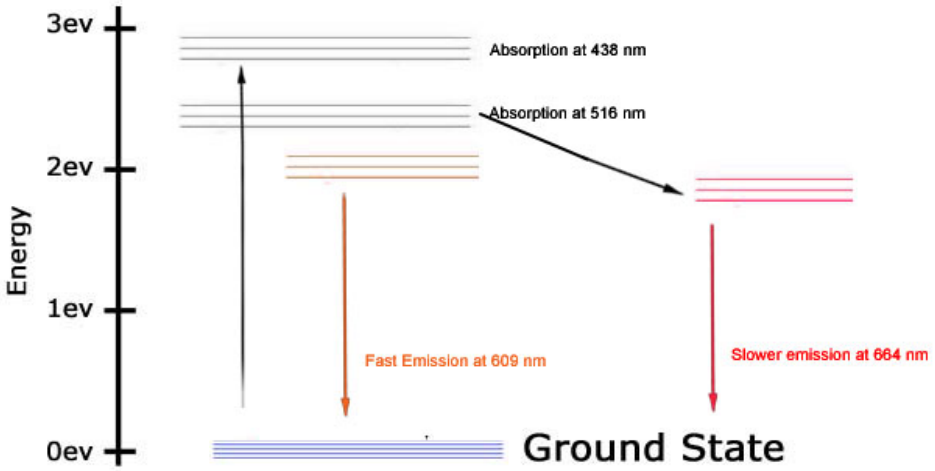

Figure 6.8 Emission mechanism energy diagram $Ag_{32}(SG)_{19}$.

6.6 The Polarization Model

Although the emission mechanism can be explained by the chemical dynamics, there is yet to be a model to account for the complete effects of the metal core or the surface states on emission. Calculations on the electronic structure of gold nanoclusters usually omit the ligands, due to computation limits.[4] We would like to propose a new way to intrepid the emission from the super atom, which we will call the polarization model. Base on the ideas from DNA templated silver nanoclusters (chapter 5), the emissions from the metal core are strongly affected by the local environment.[31–33] In the case of various DNA-based systems, the emission wavelength can be shifted based on the nearby DNA strands. [31–33] Additionally, the emission can be turned on or off based on the addition of specific base pairs.[15,32] Study on the effect of DNA sequences on DNA-templated silver nanoclusters shows that the emission enhancement is strongest using a 15 guanine overhang, which is in direct contact with the nanocluster region. The emission enhancement is not observed for a cytosine rich tail, which has a stronger "point" polarity.[15,31,32] The emission enhancement from the guanine can be attributed to the generation of an excited state that strongly couples to the emissive state.[15] The new excited state could be a result of local field splitting that affects the super atom as a whole. In the case of MPCs, published study on the effects of ligand polarity on the

emission of nanoclusters reported that ligand polarity only changes the Q.Y. of the system but not the wavelength.[10] The result on ligand polarity is very different from the result for DNA systems, and suggests that the ligand does not have a large effect o emission. However, we believe the polarization of the local environment should effect the emission process, as with the case of Plasmon enhancements, it is possible that gold is not as sensitive to silver due to the strong Au-S bonds.

The polarization model proposed herein is very similar to the super atom theory that the metal core as a single atom.[23] The super atom is sensitive to its environment, and the polarization introduced to the super atom could either increase or decrease it energy spacing, similar to electric field effects. However, strong local polarization of the metal core does not cause the emission, such as the case of the cytosine rich silver DNA systems, but the polarization has to be an area effect. The metal core has to be affected over an area or as a whole, such as the case of the guanine system.[31] The metal ligand "surface" (or environment) could cause the polarization of the core states which is similar to the emissive surface states for gold nanoclusters. This model would reflect that wavelength and strength dependence of emission as a function of the metal core energy level spacing, similar to the free electron model. Additionally, the metal core modeling should be expanded to include non-spherical parameters, like the ellipsoidal model, which has not been explored for nanoclusters.[34–36]

A more extensive ligand study of silver nanoclusters could produce more details for this model. A similar model was explored by the Aikens group at Kansas State, and they have recently published the treatment of nanoclusters in a spherical quantum well.[37] Their results reported that perturbation of the metal core as a charged-particle-in-a-sphere shows that ligand fields can cause energy level splitting of the metal core. Additionally, they investigated the effect as a function of metal core distance, and found that metal core electrons should protrude into the ligand space. It would be interesting to adopt their model to investigate the optical properties of $Ag_{32,}$ and revisit the ligand polarity effect on gold nanoclusters. Based on our optical results, silver nanoclusters may be a better candidate to under the fine emission details of the core and the surface state, in particular

the effect of polarization. In general, silver nanoclusters are still in its infancy, and we look forward to the characterization of other nanoclusters, which would provide more detail to the current models.

6.7 Two photon optical response

The two photon respond from gold nanoclusters is one of the most attractive features, especially in imaging and optical limiting applications.[38,39] One of the major differences between the two-photon excited emission of gold and silver nanoclusters is the wavelength. Gold nanoclusters have the same two-photon excited emission wavelength as their one-photon excited emission, with both visible and NIR emissions are two-photon active. Silver nanoclusters only have one detectable wavelength under two-photon excitation, which is the shorter core emission wavelength. The surface state emission for silver nanoclusters is not two-photon active. The lack of two-photon excited emission for silver in the longer wavelength was not expected, and can be related to the different structure. The two-photon absorption cross section for gold and silver nanoclusters are also very different, the absorption cross section of Ag_{32} is about half of the reported cross section for Au_{25} in the infrared. Comparing the cross section for the visible emission, the cross section for Au_{25} is three orders of magnitude higher than Ag_{32}. Comparison of the action cross section (cross section times quantum yield) reveals that gold is only four times larger than silver. . The cross section per atom for gold approaches the theoretical limit.[41] Removing the effects of Q.Y, the action cross-section (product of absolute cross-section and Q.Y) per atom of silver and gold nanoparticles are 15 times apart. The much higher action cross-section per atom for gold could be caused by the abundance d-electrons of gold systems, which could potentially produce the same effect as excited delocalization, similar to organic two-photon active molecules. The decrease in cross section from gold to silver could also be attributed to the change in interband transitions, if the effects are from the d-electrons. However, to fully understand the two-photon respond of silver nanoclusters, a more extensive study into the other size silver nanoclusters is needed.

6.8 Transient absorption measurements

Transient absorption measures the change in the absorption spectrum compared to the steady state absorption and provides excited state dynamics details. To understand transient absorption features, peak assignments are usually made from calculations on the electronic structure. The transient absorption spectrum of gold nanoclusters (figure 6.9) shows quantum size effect and two major excited state absorptions (ESA) at 500 nm and 670 nm. The ESA at 670 nm has been assigned to the HOMO-LUMO transition of the core, and exhibits very molecular dynamics. Silver nanoclusters have a ground state bleach at 490 nm, and two ESA at 530 nm and 702 nm (figure 6.10). The exact transitions of silver nanoclusters is not yet understood, but it is interesting too see that the transient spectrums for silver and gold are similar. The ESA at 500 nm for gold is a very strong, and extends to 600 nm, for silver there is an ESA signal from 550 nm to 600 nm. The ground state bleach at 490 nm dominates the spectrum in this region, masking the ESA state. It is possible that the silver and gold nanoclusters have similar excited state, due to the similarity in the metal core, but the exact assignment is not yet available. Additionally, the ESA at 670 nm for gold and 720 nm for silver are also similar. The 670 nm ESA for gold corresponds to the HOMO-LUMO transition, if we assign the same transition to the 720 nm ESA for silver, it would mean that the HOMO-LUMO gap for silver is actually smaller than that of gold. This assignment would agree with the red shifted core emission for silver nanoclusters, but it disagrees with transient absorption kinetics analysis. The 720 nm ESA has a rise time of about 2 ps and a very long decay life-time. The rise time suggest that energy is transferred into this excited state, consistent with surface states. The lifetime of the ground state bleach has a rise time of about 1.5 ps and a very long life time, which is similar to the bleach at 670 nm for gold nanoclusters. The kinetics at 530 nm, shows a quick initial decay life time of about ~100 fs and a second long life-time, gold nanoclusters shows a similar decay but the lifetime is much longer. The fast life-time of the silver nanoclusters could be related to internal energy conversion processes. Both nanoclusters exhibits very long decay time for the ESA.

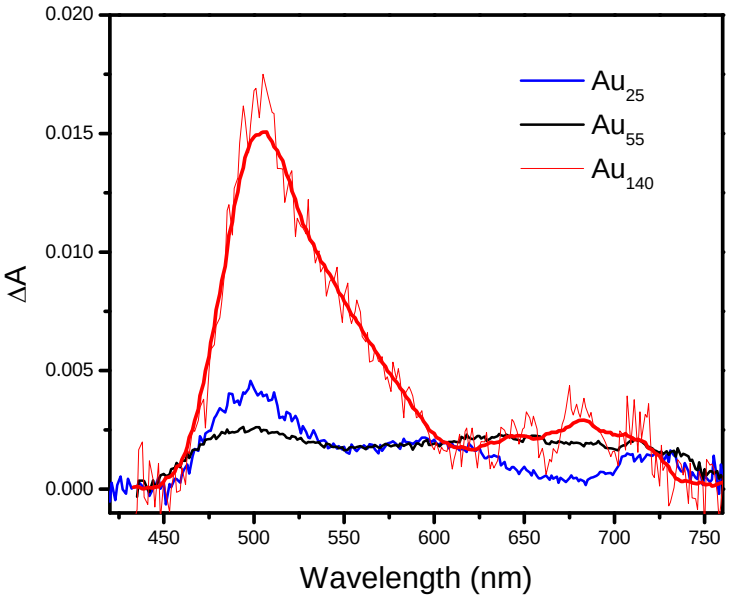

Figure 6.9 Transient absorption for gold MPCs

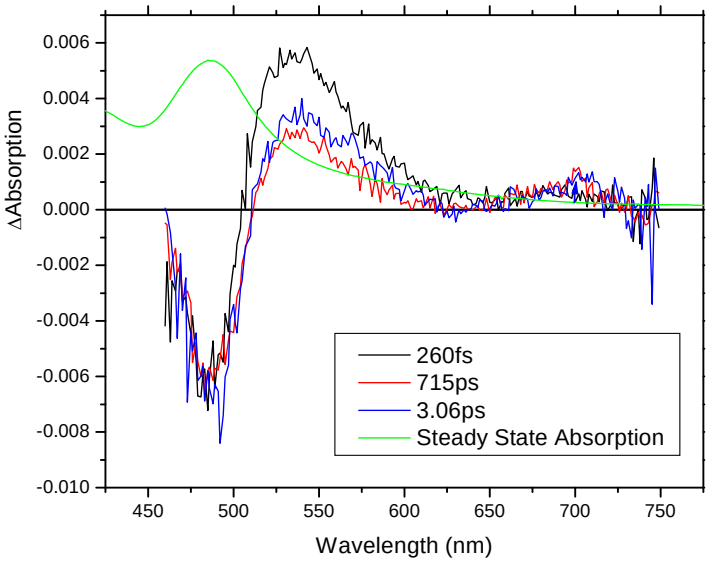

Figure 6.10 Transient absorption for Ag32.

From the transient absorption spectra, gold and silver shares many similarities, most notably the ESA at 550 nm. However, this observation is contradictory to the steady state absorption results. The steady state absorption suggest that metal core structure for silver and gold are very different, but the transient spectra suggests that they have similar excited states. In the end, a complete analysis is not possible without the structure characterization of Ag_{32}, but the similarity in excited states hints at the possibility that there are physical and electronic similarities between gold and silver nanoclusters that are yet to be discovered.

6.9 Summary of silver and gold nanoclusters

Based on the existing theories, namely the super atom theory and the free electron model, gold and silver nanoclusters should share many similarities. Their band gap and packing distances in the bulk are the same, which strongly suggests that they should produce clusters in similar size and structure. Our experimental results show that silver and gold does not share the same metal core packing. However, both gold and silver nanoclusters exhibits molecular like behavior with discrete transitions in their absorption spectrum. The emission spectrum of both nanoclusters exhibit dual emissions. The emissions for the two systems can be assigned to the core (shorter wavelength) and surface state (longer wavelength) based on their wavelengths and dynamics. The stronger emission from the silver system really highlights its potential in bio imaging. The assignment of the core and surface state suggest that both systems can be considered as a super atom. The dynamics of the emission for gold and nanoclusters are different. The emission for silver nanoclusters has a much longer life-time and could be the cause of the increase in Q.Y. The emission mechanism of the two systems reveals that the emission from both nanoclusters can be modeled by a four level system. The shift in the emission wavelength is a result of the change in metal core and the surface state energies. We proposed a new model to consider the emission properties of nanoclusters, based on the polarization of the super atom. The two-photon absorption cross-section for silver nanoclusters is much lower than gold nanoclusters, which is unexpected. The transient absorption comparison revealed excited state similarities. Overall, it is very interesting to

investigate the differences between gold and silver nanoclusters. The optical properties of the two systems are very different. However, the lack of full structural characterization of the silver nanocluster prohibits detail assignments of the electronic transitions. The nanocluster Ag_{32} only presents one nanocluster in the series, so the quantum size effect of silver nanoclusters is not fully known. The lack of characterized silver nanoclusters prohibits investigations into the scaling laws, which is prominent in the gold nanoclusters. Ag_{32} serves as a first step in answering the question regarding fundamental laws for all metal clusters. From the results presented, the super atom theory only accounts for gold nanoclusters with specific packing, and should be extended to include non-spherical systems. The free electron model still holds well for silver nanoclusters, and could be extended to include other metals, such as copper. The question of the existence of a common law that governs all metal nanoclusters remains to be answered. The many interesting insight gain from silver nanoclusters, validates our decision to choose silver as our study candidate. We look forward to developments in the field of silver nanoclusters in the near future.

6.10 Reference

(1) Peng, S.; McMahon, J. M.; Schatz, G. C.; Gray, S. K.; Sun, Y. Reversing the size-dependence of surface plasmon resonances. *Proceedings of the National Academy of Sciences of the United States of America* **2010**, *107*, 14530–14534.

(2) Mohamed, M. B.; Volkov, V.; Link, S.; El-Sayed, M. A. The “lightning” gold nanorods: fluorescence enhancement of over a million compared to the gold metal. *Chemical Physics Letters* **2000**, *317*, 517–523.

(3) Goodson, T.; Varnavski, O.; Wang, Y. Optical properties and applications of dendrimer-metal nanocomposites. *International Reviews in Physical Chemistry* **2004**, *23*, 109–150.

(4) Zhu, M.; Aikens, C. M.; Hollander, F. J.; Schatz, G. C.; Jin, R. Correlating the crystal structure of a thiol-protected Au25 cluster and optical properties. *Journal of the American Chemical Society* **2008**, *130*, 5883–5.

(5) Varnavski, O.; Ramakrishna, G.; Kim, J.; Lee, D.; Goodson, T. Critical size for the observation of quantum confinement in optically excited gold clusters. *Journal of the American Chemical Society* **2010**, *132*, 16–7.

(6) Yau, S. H.; Varnavski, O.; Gilbertson, J. D.; Chandler, B.; Ramakrishna, G.; Goodson, T. Ultrafast Optical Study of Small Gold Monolayer Protected Clusters: A Closer Look at Emission . *The Journal of Physical Chemistry C* **2010**, *114*, 15979–15985.

(7) Yau, S. H.; Varnavski, O.; Goodson, T. An Ultrafast Look at Au Nanoclusters. *Accounts of chemical research* **2013**.

(8) Daniel, M.-C.; Astruc, D. Gold nanoparticles: assembly, supramolecular chemistry, quantum-size-related properties, and applications toward biology, catalysis, and nanotechnology. *Chemical Reviews* **2004**, *104*, 293–346.

(9) Valden, M.; Lai, X.; Goodman, D. W. Onset of catalytic activity of gold clusters on titania with the appearance of nonmetallic properties. *Science* **1998**, *281*, 1647–1650.

(10) Wang, G.; Guo, R.; Kalyuzhny, G.; Choi, J.-P.; Murray, R. W. NIR luminescence intensities increase linearly with proportion of polar thiolate ligands in protecting monolayers of Au38 and Au140 quantum dots. *The journal of physical chemistry. B* **2006**, *110*, 20282–9.

(11) Bigioni, T. P.; Whetten, R. L.; Dag, O. Near-infrared luminescence from small gold nanocrystals. *Journal of Physical Chemistry B* **2000**, *104*, 6983–6986.

(12) Jadzinsky, P. D.; Calero, G.; Ackerson, C. J.; Bushnell, D. A.; Kornberg, R. D. Structure of a thiol monolayer-protected gold nanoparticle at 1.1 A resolution. *Science (New York, N.Y.)* **2007**, *318*, 430–3.

(13) Heaven, M. W.; Dass, A.; White, P. S.; Holt, K. M.; Murray, R. W. Crystal structure of the gold nanoparticle [N(C8H17)4][Au25(SCH2CH2Ph)18]. *Journal of the American Chemical Society* **2008**, *130*, 3754–5.

(14) Wang, G.; Huang, T.; Murray, R. W.; Menard, L.; Nuzzo, R. G. Near-IR luminescence of monolayer-protected metal clusters. *Journal of the American Chemical Society* **2005**, *127*, 812–3.

(15) Yau, S. H.; Abeyasinghe, N.; Orr, M.; Upton, L.; Varnavski, O.; Werner, J. H.; Yeh, H.-C.; Sharma, J.; Shreve, A. P.; Martinez, J. S.; Goodson, T. Bright two-photon emission and ultra-fast relaxation dynamics in a DNA-templated nanocluster investigated by ultra-fast spectroscopy. *Nanoscale* **2012**, *4*, 4247–54.

(16) Kumar, S.; Bolan, M. D.; Bigioni, T. P. Glutathione-stabilized magic-number silver cluster compounds. *Journal of the American Chemical Society* **2010**, *132*, 13141–3.

(17) Brust, M.; Bethell, D.; Schiffrin, D. J.; Kiely, C. J. Novel Gold-dithiol Nano-networks with Nonmetallic Electronic Properties. *Advanced Materials* **1995**, *7*, 795–6.

(18) Guo, J.; Kumar, S.; Bolan, M.; Desireddy, A.; Bigioni, T. P.; Griffith, W. P. Mass spectrometric identification of silver nanoparticles: the case of Ag32(SG)19. *Analytical chemistry* **2012**, *84*, 5304–8.

(19) Aikens, C. M. Origin of Discrete Optical Absorption Spectra of M 25 (SH) 18 − Nanoparticles (M = Au, Ag). *The Journal of Physical Chemistry C* **2008**, *112*, 19797–19800.

(20) Jin, R. Quantum sized, thiolate-protected gold nanoclusters. *Nanoscale* **2010**, *2*, 343–62.

(21) Akola, J.; Walter, M.; Whetten, R. L.; Häkkinen, H.; Grönbeck, H. On the structure of thiolate-protected Au25. *Journal of the American Chemical Society* **2008**, *130*, 3756–7.

(22) Shichibu, Y.; Negishi, Y.; Tsukuda, T.; Teranishi, T. Large-scale synthesis of thiolated Au25 clusters via ligand exchange reactions of phosphine-stabilized Au11 clusters. *Journal of the American Chemical Society* **2005**, *127*, 13464–5.

(23) Walter, M.; Akola, J.; Lopez-Acevedo, O.; Jadzinsky, P. D.; Calero, G.; Ackerson, C. J.; Whetten, R. L.; Groenbeck, H.; Hakkinen, H.; Grönbeck, H.; Häkkinen, H. A unified view of ligand-protected gold clusters as superatom complexes. *Proceedings of the National Academy of Sciences of the United States of America* **2008**, *105*, 9157–9162.

(24) Varnavski, O.; Ispasoiu, R. G.; Balogh, L.; Tomalia, D.; Goodson, T. Ultrafast time-resolved photoluminescence from novel metal–dendrimer nanocomposites. *The Journal of Chemical Physics* **2001**, *114*, 1962.

(25) Muhammed, M. A. H.; Aldeek, F.; Palui, G.; Trapiella-Alfonso, L.; Mattoussi, H. Growth of in situ functionalized luminescent silver nanoclusters by direct reduction and size focusing. *ACS nano* **2012**, *6*, 8950–61.

(26) Plech, A.; Cerna, R.; Kotaidis, V.; Hudert, F.; Bartels, A.; Dekorsy, T. A surface phase transition of supported gold nanoparticles. *Nano letters* **2007**, *7*, 1026–31.

(27) Bakr, O. M.; Amendola, V.; Aikens, C. M.; Wenseleers, W.; Li, R.; Dal Negro, L.; Schatz, G. C.; Stellacci, F. Silver Nanoparticles with Broad Multiband Linear Optical Absorption. *Angewandte Chemie-International Edition* **2009**, *48*, 5921–5926.

(28) Shchukin, D. G.; Radtchenko, I. L.; Sukhorukov, G. B. Photoinduced reduction of silver inside microscale polyelectrolyte capsules. *Chemphyschem: a European journal of chemical physics and physical chemistry* **2003**, *4*, 1101–3.

(29) Shibu, E. S.; Muhammed, M. A. H.; Tsukuda, T.; Pradeep, T. Ligand Exchange of Au25SG18 Leading to Functionalized Gold Clusters: Spectroscopy, Kinetics, and Luminescence. *Journal of Physical Chemistry C* **2008**, *112*, 12168–12176.

(30) Devadas, M. S.; Kim, J.; Sinn, E.; Lee, D.; Goodson, T.; Ramakrishna, G. Unique Ultrafast Visible Luminescence in Monolayer-Protected Au 25 Clusters. *The Journal of Physical Chemistry C* **2010**, *114*, 22417–22423.

(31) Yeh, H.-C.; Sharma, J.; Han, J. J.; Martinez, J. S.; Werner, J. H. A DNA-Silver Nanocluster Probe That Fluoresces upon Hybridization. *Nano Letters* **2010**, *10*, 3106–3110.

(32) Sharma, J.; Yeh, H.-C.; Yoo, H.; Werner, J. H.; Martinez, J. S. A complementary palette of fluorescent silver nanoclusters. *Chemical Communications* **2010**, *46*, 3280–3282.

(33) Sharma, J.; Yeh, H.-C.; Yoo, H.; Werner, J. H.; Martinez, J. S. Silver nanocluster aptamers: in situ generation of intrinsically fluorescent recognition ligands for protein detection. *Chemical Communications* **2011**, *47*, 2294–2296.

(34) De Heer, W. The physics of simple metal clusters: experimental aspects and simple models. *Reviews of Modern Physics* **1993**, *65*, 611–676.

(35) Knight, W.; Clemenger, K.; De Heer, W.; Saunders, W.; Chou, M.; Cohen, M. Electronic Shell Structure and Abundances of Sodium Clusters. *Physical Review Letters* **1984**, *52*, 2141–2143.

(36) De Heer, W.; Selby, K.; Kresin, V.; Masui, J.; Vollmer, M.; Chatelain, A.; Knight, W. Collective dipole oscillations in small sodium clusters. *Physical Review Letters* **1987**, *59*, 1805–1808.

(37) Guidez, E. B.; Aikens, C. M. Development of a charge-perturbed particle-in-a-sphere model for nanoparticle electronic structure. *Physical chemistry chemical physics: PCCP* **2012**, *14*, 4287–95.

(38) Ramakrishna, G.; Varnavski, O.; Kim, J.; Lee, D.; Goodson, T. Quantum-sized gold clusters as efficient two-photon absorbers. *Journal of the American Chemical Society* **2008**, *130*, 5032–3.

(39) Dreaden, E. C.; El-Sayed, M. A. Detecting and destroying cancer cells in more than one way with noble metals and different confinement properties on the nanoscale. *Accounts of chemical research* **2012**, *45*, 1854–65.

(40) Qian, H.; Y. Sfeir, M.; Jin, R. Ultrafast Relaxation Dynamics of [Au 25 (SR) 18] q Nanoclusters: Effects of Charge State. *The Journal of Physical Chemistry C* **2010**, *114*, 19935–19940.

(41) Kuzyk, M. G. Fundamental limits on third-order molecular susceptibilities. *Optics Letters* **2000**, *25*, 1183.

Chapter 7
Summary and Outlook

7.1 Summary

The research into smaller systems produced many interesting insight into the nano-meter world. Materials in nano-meter scale can be divided into nanoparticles and nanoclusters, and they can be divided by size. The 2 nm distinction for the two systems is a direct result of the quantum confinement, which can be calculated by the free electron model or the kubo model. The quantum confinement observed for nanoclusters lead to many interesting optical properties. Beside the optical effects, nanoclusters in this size also offer new ideas to the fundamental properties of nanomaterials. In particular, metal cores in this size regime are considered as “super atom”: a self assembled group of atoms that are stable due to electronic shell closing, and their share electronic states are similar to one single molecular unit. The high stability of these close shell metal cores are only observed at certain sizes, giving an almost finite set of samples. The fine details of the cluster formations and the prediction of cluster formations are extremely complex. In addition to the electron shell closing, new consideration for the geometry should be added to existing models. The nanocluster itself can be divided into the metal core and single ligand shell, and can be explained by the super atom theory. The super atom nature of the nanoclusters gives rise to emission that can be excited by one-photon or two-photons. The size and arrangement of the metal core has a direct effect on these optical properties, it is the adjustable optical effects that attracts of attention of the community. The various models presented in this work only answer part of the observations. The fact is, the field of nanoclusters is still young and recent progress in the identification and characterization of nanoclusters finally give the scientific community a firm ground to build new ideas.

New discoveries are being made everyday which brings new ideas and understanding into the modeling of the super atom, and new types of super atom. Of all the variations of metal nanoclusters, one major theme persists. Quantum size effect can be observed for a large variety of different metal nanoclusters, and serves as a basic explanation of the molecular like nature of the super atom.

My work on the various nanoclusters focused on the optical properties in both the steady state and ultrafast. The use of steady state techniques allows us to investigate the overall properties of nanoclusters. Although steady state spectroscopy is a simple tool, careful analysis and experimentation can reveal a wealth of information, like the work on silver nanoclusters in chapter 5. Ultrafast spectroscopy reveals the chemical dynamics of the systems, and really allows us to study optical affects that would be otherwise not observable. In the case of nanoclusters, ultrafast spectroscopy provided direct evidence for the separation from nanoparticles; moreover it provides details about the electronic processes. Our optical studies really aim to understand the fundamental physics behind these nanoclusters, and it is our hope that our physical investigation can lead to the development to new and more exciting materials.

Gold nanoclusters serve as a foundation in many investigations and modeling, especially Au_{25} and Au_{102}. In chapter 4 there are a few really exciting results. Emission from metal nanoclusters that is much stronger than their bulk counter part has tremendous potential in bio-imaging. In particular nanoclusters can be used to expand the nano-toolbox, giving scientist and engineers systems from hundreds of nanometers to one nanometers. Nanocluster also have the added benefit to be dye free and perhaps the addition of dye to these systems can result in multicolor imaging agents. It is also worthy to note that the emission of Au_{55} was long debated, and our work was the first publication that confirms the emission with time-resolved fluorescence up-conversion along with the steady state. Quantum size effect can be clearly observed in the absorption spectrum and most importantly serves as a clear distinction between nanoclusters and nanoparticles. The fluorescence life-time of nanoclusters and nanoparticles was one of the feature art works on the cover of the Journal of Physical Chemistry C at time of publication. The

impressive two-photon absorption cross section was not expected, but to this day, Au_{25} has one of the highest two-photon absorption cross section. Not only metal nanocluster can be used as an optical limiting material, the two-photon excited emission allows for use in biological systems with reduced photo damage. The discovery of acoustic vibration in gold nanoclusters is very exciting and could serves as an identification tool for future nanoclusters. The emission mechanism for gold nanoclusters can be modeled using a simple 4 state systems, the implication of this modeling is the super atom idea of "divide and protect". The metal core is separated as the ligand as the super atom, while, the liganded bounded metal serves as a protect shell. While surface state is the current explanation for the longer wavelength emission, it is not yet completely understood. Using silver nanoclusters as a comparison model, we propose the idea of the polarization model, where the super atom can be affect by its environment as a whole, and can be adjusted the desired wavelength or quantum efficiency. The major impact of the work on gold has to be the clarification of nanocluster and nanoparticles, the very fine seperatoin at 2 nm that can be modeled and observed. Gold nanocluster was the starting point of my work and it is silver nanoclusters that really caught my attention.

The investigation of silver nanoclusters started from a simple question: Is there a common law that governs all metal nanoclusters? A similar question was addressed in the super atom theory and has been used as a major model of this work. But the super atom theory only considers gold nanoclusters, and it is my interest to expand the idea of super atom across different metals. The work on silver nanocluster was fought with many difficulties. The early year of work on silver nanoclusters was plagued by sample instability and impurity, and it is through collaboration with Professor Bigioni that we were finally able to obtain insightful optical results from Ag_{32}. It remains a large hurdle for researcher to identify nanoclusters, and our optical study would be meaningless without proper characterization (which in the case of Ag_{32} took more than 2 years of work). Ag_{32} serves as a excellent starting point of the foray into silver nanoclusters, its steady state optical property already disagree with what we know about the super atom theory, and shows us that there could be many different stable packing of the metal core. It is still unsure if the packing is related to the metal used, because only Ag_{32} is the only

silver nanocluster identified by mass-spectrometry. The emission of Ag_{32} also shows that dual emission is not unique to gold nanoclusters, and perhaps can be expected for all metal nanoclusters. The dual emission of silver nanocluster was both in the visible, which was not expected, but was successful resolved by our time-resolved fluorescence up-conversion. The publication of the emission result would be the first ever report on the emission of silver nanoclusters. The quantum yield of Ag_{32} is two orders of magnitude higher than gold nanoclusters, making it a stronger candidate in imaging. The two-photon excited result was truly astonishing, with only the shorter emission wavelength detected. Ag_{32} could be a new type of imaging agent, where there is a measurable (50 nm) wavelength shift from one-photon to two-photon excitation. It is possible that Ag_{32} can be used to achieve ultrahigh resolution imaging, epsically in the case of near field microscopy. The emission mechanism of Ag_{32} serves as a excellent comparison to the gold systems, with both system exhibits a separate core and surface state emission which is characterized by their life times.

Beside the Ag_{32} system, DNA-templated Ag nanocluster was also investigated in chapter 5. DNA-templated Ag nanoclusters have a unique emission mechanism, and it is the first ever report of a creation of an emissive state due to polarization. The activation of the emission process by hybridization is also very different from silver nanoclusters. For DNA templated Ag nanocluster the biggest challenge remains to be the complete identification of the metal core, but the evidence published and discussed in chapter 5 strongest suggest a 8-20 metal core. The DNA silver nanoclusters can also be made into bio imaging agents easily, making it a ideal system for practical imaging applications. The biggest impact of the DNA Ag system is the mission change based on the hybridization pair used. It is the observation made by our collaborator that the emission is strongest when guanine is used instead of cytosine that gives me the idea of the polarization model.

7.2 Future Work and Outlook

The field on nanocluster research is only in its beginning stages, the various physical optical observation offered in this thesis is only a small part of the puzzle. Even as we speak, there are new nanoclusters being identified, and new ideas are emerging. From what I learned about gold and nanoclusters there are a few clear ideas that is worth developing and exploring. I divide these ideas into three board areas of research, metal nanosystem modeling, biological applications and the new idea of nano metal alloys.

Metal Nanosystem Modeling. While gold nanoclusters that we investigated can be explained by the super atom model, there is still much confusion in the field regarding the how each nanocluster should be modeled. Currently there are a few metal clusters that have been discovered, such as Au_{38} or Au_{60} that does not fit into the super atom model, more over they seems to exhibit different packing based on their assignment. While their exact structure many not be known without crystallization and x-ray analysis, it is an excellent opportunity to reexamine the super atom theory to includes the factor of geometry along with electro shell closing. Additionally, these systems can be benefited from ultrafast optical investigation, and should be a coordinated effort by the community as a whole. The bigger quest of a unified theory for metal nanoclusters of different metal can be and should be addressed by the development of new types of metal nanoclusters beyond gold and silver, perhaps the yet smaller copper would be a good candidate. It should be obvious that silver nanoclusters will be the center of investigation in the next decade. Professor Bigioni has demonstrated that a series of silver nanocluster can be made, however, the devil lies in the stability and characterization. Nerveless we look forward to the challenge ahead in the area of silver nanoclusters (Mono-layered Protected).

Biological Applications. Currently, the field of bio-imaging is dominated by the use of nanoparticles, in particular, the manipulation of the Plasmon Resonance to enhance emission or surface effects. While dye loaded nanoparticles have been used in cellular imaging, we hope to see more bio imaging using nanoclusters. The very small size of nanoclusters offers the opportunity to penetrate the nucleus, and could potentially be used in DNA level imaging, not to mention the already DNA templated Ag nanoclusters.

Additionally the use of two-photon excitation could offer deeper penetration depth for cellular imaging. Overall, the use of nanoclusters in the bio imaging is not yet wide spread, but as researchers look for higher resolution in their image, it is logical that they should consider nanoclusters for such applications.

Metal Alloy Nanoclusters. The lack of surface plasmon for nanocluster has been a major physical property for nanoclusters, but it is also a reason while nanoclusters are not used in the field of plasmonics. Very recently work by Professor Dass at the University of Mississippi has demonstrated the synthesis of gold silver mixed alloy based on the Au_{144} systems; with more groups joining in the synthesis of these allow systems. The basic structure based on calculation is built on a gold core and a silver shell, with the total system size less that 2 nm. The real interest is in the published absorption spectrum, where the silver plasmon can be observed with as few as 52 silver atoms. Moreover there is a trace of the gold plasmon peak. This is currently being investigated in our group, with emphasis on emission enhancement. A boarder question can be asked of the nature of the metal alloy nanoclusters and the reappearance of the plasmon. The observation of plasmon in this scale also opens up new ideas in the field of plasmonics, where the systems sizes are the 100 nm. The use of nanoclusters could provide never seen before resolution in surface plasmonic imaging.